CHEMILUMINESCENCE AND PHOTOLUMINESCENCE OF RUTHENIUM CHELATES

by

Fred Edward Lytle

B.S., Juniata College
(1964)

Submitted in Partial Fulfillment
of the Requirements for the
Degree of
DOCTOR OF PHILOSOPHY

at the

MASSACHUSETTS INSTITUTE OF TECHNOLOGY

August, 1968

Signature of Author____
Department of Chemistry, August 27, 1968

Certified by____
Thesis Supervisor

Accepted by____
Chairman, Departmental Committee on Graduate Students

This doctoral thesis has been examined by a Committee of the Department of Chemistry as follows:

Professor Kerry W. Bowers _____ (Chairman)

Professor David M. Hercules _____ (Thesis Supervisor)

Professor Richard C. Lord _____

CHEMILUMINESCENCE AND PHOTOLUMINESCENCE

OF

RUTHENIUM CHELATES

by

Fred Edward Lytle

Submitted to the Department of Chemistry
on August 27, 1968, in partial fulfillment of the
requirements for the degree of
Doctor of Philosophy

ABSTRACT

Chemiluminescence-Most solution chemiluminescence that has been reported, to date, can be placed into one of three categories: reactions involving molecular oxygen or peroxides, oxidation of anion radicals, and alternating current electrolysis of aromatic hydrocarbons.

Earlier work in our laboratory prompted a closer look at possibilities for producing chemiluminescence by electron transfer to a potential emitter, i.e. by reducing a compound to a luminescent species by a one electron reduction process.

The over-all reaction for the first type of system studied can be written as

$$RNH_2^{+m} + \text{reductant} \rightarrow RNH_2 + h\nu$$

The radical-cation of 1, 6-diaminopyrene proved to be an example of a chemiluminescent electron acceptor fitting this general type of reaction. For the case where hydrazine was the reducing agent, it was shown that the emitting species was the parent diamine. And for the case where the naphthalene radical-anion was the reducing agent, it was shown that enough energy is available to produce an excited state of 1, 6-diamino-

pyrene by a simple one-electron reduction reaction.

The over-all reaction for the second type of system studied can be written as

$$ML_x^{+(n+1)} + \text{reductant} \rightarrow ML_x^{+n} + h\nu$$

where M represents a metal ion and L a suitable ligand. The complexes successfully used in the present study all had ruthenium as the central metal ion (n=2). The ligands were 2,2'-bipyridine, 5-methyl-1,10 phenanthroline, 5,6-dimethyl-1,10-phenanthroline, and 3,5,6,8-tetramethyl-1,10-phenanthroline (all having x=3). For the case where 2,2'-bipyridine was the ligand, it was shown that the emitting species was the ruthenium (II) chelate when either hydrazine or hydroxyl ion were used as the reducing agent. It was also shown that the published mechanism for hydrazine oxidation does not completely describe all of the reactions occuring in the $Ru(III)(bipyr)_3Cl_2$-hydrazine chemiluminescent system.

The results of this research, combined with the earlier studies, indicate that electron-transfer reactions involving a potentially luminescent acceptor show great promise for discovering new chemiluminescent reactions.

Photoluminescence-No previously published explanation of the luminescence of tris-(2,2'-bipyridine) ruthenium (II) dichloride has been completely adequate in explaining all of the experimental data. Evidence is presented in this thesis that supports assignment of the emission as charge-transfer, spin-forbidden luminescence. Spin-orbit coupling existing in the complex enhances the probability of singlet-triplet transitions and yields an abnormally short-lived phosphorescence.

In an EPA solvent, the rate constants for phosphorescence, triplet internal conversion, singlet internal conversion, fluorescence and intersystem crossing have been determined as:
$k_p = 2.9 \times 10^5\ sec^{-1}$; $k_{ic}^3 = 3.1 \times 10^5\ sec^{-1}$; $k_{ic}^1 = 5 \times 10^8\ sec^{-1}$; $k_f = 4 \times 10^5\ sec^{-1}$; and $k_{ix} \geq 5 \times 10^{10}\ sec^{-1}$ respectively.

Thesis Supervisor: David M. Hercules

Title: Associate Professor

I go,

I went,

I have gone;

Leaving my

Footprints

In the sands

Of time.

But, alas;

They end not

With a man,

But a

Hole.

ACKNOWLEDGEMENTS

The author would like to express his appreciation to Professor David M. Hercules for the suggestion of the problem. The patience and encouragement sustained during the course of the research at M.I.T., in addition to the beginning years at Juniata College, amply demonstrate his ability as a fine teacher. Appreciation is also due Professor Kerry W. Bowers for helpful suggestions and criticisms during the course of the work and in reading the manuscript.

The author wishes to thank the following individuals, outside of the laboratory, whose help concerning various facits of the research was invaluable; Professor W. E. Ohnesorge of Lehigh University for a general understanding of transition-metal-complex luminescence; Dr. Jack Chang of Eastman Kodak for electrochemical measurements and teaching the author a systematic approach to experimentation; Mr. George K. Turner of G. K. Turner Associates for a lengthy discussion concerning fluorometer calibration; and Mr. E. T. Meserve of TRW for helpful discussions concerning the Nanosecond Spectral Source.

The author wishes to thank his colleagues for many interesting and enlightening discussions. Tony Vaudo should be mentioned for aid in constructing the constant temperature cryostat. Steve Carlson should also be mentioned for doing all of the "dirty work" connected with the NMR studies.

The author is indebted to his parents for the extreme financial hardships that they had to endure to guarantee him an undergraduate education.

And finally, the author is indebted to his wife, Marsha, for often boosting his morale and for enduring hardships beyond the call of duty.

TABLE OF CONTENTS

INDEX OF FIGURES

INDEX OF TABLES

COMMONLY OCCURRING STRUCTURES

Structure	Name
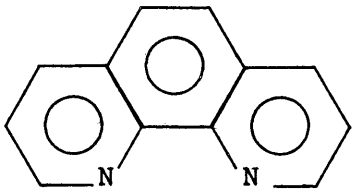	1,10-phenanthroline
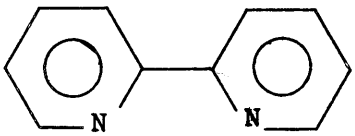	2,2'-bipyridine
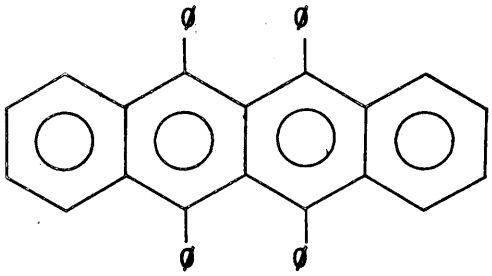	rubrene
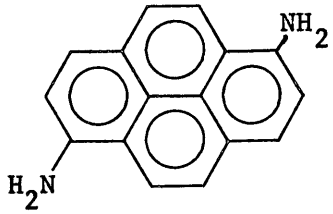	1,6-diaminopyrene

I. Chemiluminescence Introduction

Chemiluminescence can be defined, simply, as the production of light by a chemical reaction. The phenomenon is not new and has been recognized since 1877, when Radziszewski demonstrated that lophine reacted with oxygen in alcholic potassium hydroxide producing light (38). Two well known examples of chemiluminescent compounds are luminol (1) and luciginin (14). The general subject has been reviewed recently by McCapra (29). Most solution chemiluminescence that has been reported, to date, can be placed into one of three categories; reactions involving molecular oxygen or peroxides (15), oxidation of anion radicals (7, 8), and alternating current electrolysis of aromatic hydrocarbons (51, 44, 18).

In the course of Lansbury's (19) work on the alternating current electrolysis of rubrene, it was discovered that the radical-cation reacted with electron donors to produce chemiluminescence. These results prompted a close look at other possibilities for producing chemiluminescence by electron transfer to a potential emitter, i. e. by reducing a compound to a luminescent species by a one electron reduction process.

The general scheme for an electron-transfer reaction can be written as

$$A^+ + D \rightarrow A + D^+ \qquad \text{I-1}$$

where A is the electron acceptor and D is the electron donor. Generally, chemiluminescence should result from this type of reaction

if three criteria are met. First, sufficient energy must be available from electron-transfer to produce an excited state of the reduced species. Second, the reduced species must be capable either of emitting or energy transfering to a potential emitter. Third, the kinetics of the reaction must be sufficiently rapid so that the rate of photon production is detectable.

When initially investigating the general electron-transfer reaction shown in Equation I-1, two possibilities came to mind: the reduction of aromatic hydrocarbon radical cations and the reduction of metal chelates. Instead of experimenting with the unstable radical-cation of rubrene, it seemed more advantageous to utilize Wurster's salts, which are stable radical-cations derived from aromatic diamines. For this family of compounds the overall reaction can be written as

$$RNH_2^{+m} + \text{reductant} \rightarrow RNH_2 + h\nu$$

The radical-cation of 1,6-diaminopyrene proved to be an example of a chemiluminescent electron acceptor fitting this general type of reaction.

The over-all reaction for the second type of system studied can be written as

$$ML_x^{+(n+1)} + \text{reductant} \rightarrow ML_x^{+n} + h\nu$$

where M represents a metal ion and L a suitable ligand. The complexes successfully used in the present study all had ruthenium as the central metal ion (n=2). The ligands were 2,2'-bipyridine, 5-methyl-1, 10-phenanthroline, 5,6-dimethyl-1,10-phenanthroline and 3,5,6,8-tetramethyl-

1,10-phenanthroline (all having x=3).†

The aim of the present chemiluminescence research was the elucidation of the mechanism with respect to chemical reactions, electron-transfer processes and the characteristics of the resultant excited molecular electronic states involved in the emission process. The chemiluminescence of Ru(II)(bipyr)$_3$Cl$_2$-hydrazine solutions was chosen as a representative reduction reaction and is considered in detail.

The results of this research, combined with the earlier studies (19), indicate that electron-transfer reactions involving a potentially luminescent acceptor show great promise for discovering new chemiluminescence systems.

---

† Chemiluminescence from a ruthernium chelate has also been observed by J. P. Paris (unpublished studies, Juniata Colleg, Huntingdon, Pa., 1962).

II. Photoluminescence Introduction

Because the origin of the luminescence of $Ru(bipyr)_3Cl_2$ was not clearly established, an extensive investigation was undertaken to elucidate the emission mechanism. Ruthenium is a group VIII second-row transition element having a [Kr] $4d^6$ electronic configuration in the dipositive oxidation state. 2,2' Bipyridine is a well know chelating agent and is fully discussed in the review by Brandt, et al. (3). Of the group VIII elements, cobalt, ruthenium, rhodium, osmium, iridium and platinum have been reported to form luminescent complexes (9,55,32).

The first published account discussing the origin of the luminescence of $Ru(bipyr)_3Cl_2$ was by Paris and Brandt (35). These authors used arguments similar to those of Jørgenson (23) to assign intense bands in the chelate absorption spectrum to d→ π* charge-transfer transitions. Since the long wavelength band was attributed to a d→ π* transition, they treated the emission as π*→d charge-transfer fluorescence. In his Ph.D. thesis, however, Paris (34) described the process as phosphorescence. An attempt to measure the emission lifetime yielded an upper limit of 100 microseconds. Paris assumed that the lifetime was abnormally short because spin-orbit coupling made the spin-forbidden transition more allowed. He also suggested that the tail on the long wavelength charge-transfer absorption band could be due to a singlet-triplet transition.

Porter and Schläfer (37) referred to the emission as a d* → d phosphorescence and Crosby et al.(10) concurred with the d* → d transition type but concluded that the emission was fluorescence. The basis for Crosby's assignment was two low intensity long wavelength absorption bands. One of these bands was assigned to a d → d* spin-allowed transition, and the other to the corresponding spin-forbidden transition. However, Palmer and Piper(33) pointed out that the spin-allowed d → d* transition for $Ru(bipyr)_3Cl_2$ would lie to the blue of the long wavelength charge-transfer band and could not possibly account for the observed absorption. In a personal communication to Palmer and Piper, Crosby stated that the absorption band attributed to the spin-forbidden d → d* transition was due to an impurity in their chelate preparation.

Subsequently, Crosby and Klassen(25) presented new evidence indicating a charge-transfer assignment for the luminescence. They synthesised a series of bis-(bipyridine) ruthenium complexes having widely different values of 10 Dq. In every case the emission started at the long wavelength end of the charge-transfer absorption band. Consequently, the energy of the emission did not follow the value of 10 Dq as would be expected for a d → d* transition. The long wavelength tail in the absorption spectrum was assumed to be a vibronic component of the charge-transfer transition. They did not suggest an emitting state multiplicity. However, Crosby and Demas(11) did propose phosphorescence on the basis of the four micro-second emission lifetime at 77°K.

The purpose of the photoluminescence investigation is to clarify the reported data and to establish the luminescence mechanism. A charge-transfer spin-forbidden transition adequately explains all of the experimental observations.

III. Experimental

A. Chemicals

All inorganic and common organic chemicals were reagent grade or better and were used without further purification, unless otherwise noted.

All solvents were either Eastman "Spectro-grade" solvents or Matheson, Coleman and Bell "Spectroquality" solvents and were used without further purification.

1,10 -Phenanthroline and its 5-methyl, 5-phenyl, 5,6-dimethyl and 3,5,6,8-tetramethyl derivatives were purchased from G. Frederick Smith Chemical Company and were used without further purification.

2,2' -Bipyridine was purchased from Eastman Organic Chemicals and was twice recrystallized from ethanol (m.p. 68-69°C, uncorrected, reported 70°C).

Pyrene was purchased from K and K Laboratories and was twice recrystallized from ethanol (m.p. 151-152°C, uncorrected, reported 70°C).

Rubrene was purchased from Aldrich Chemical Company and was vacuum sublimed several times. The resultant product was pure as indicated by thin layer chromatography.

Ruthenium trichloride hydrate was purchased from Alfa Inorganic Company and was used without further purification.

Tris-(2,2'-bipyridine) ruthenium dichloride was purchased from G. Frederick Smith Chemical Company and was twice recrystallized from

water. The final product was identified by Nuclear Magnetic Resonance (NMR) with respect to ligand type and number of ligands.

Tris-(1,10-phenanthroline) ruthenium dichloride and the corresponding complexes of the 5-methyl, 5-phenyl, 5,6-dimethyl and 3,5,6,8-tetramethyl derivatives were prepared by a modification of the method of Veening and Brandt(49). 200 ml of water containing 0.2gm of $RuCl_3 \cdot H_2O$, 0.5 gm of appropriate ligand and 2.5 gms of hydroxylamine sulfate was refluxed for two hours. The resultant mixture was cooled and extracted several times with benzene. The volume of the aqueous layer was reduced to about 50 ml by boiling. The solution was filtered hot and then cooled in an ice bath. The resultant precipitate was recrystallized from water.

1.6-Diaminopyrene was prepared by a modified method of Vollman, et al. (52). 10 gms of pyrene in 100 ml of glacial acetic acid, at 90°C, was mixed with stirring to 75 ml of nitric acid. A mixture of 1,4 - and 1,6-dinitropyrene immediately precipitated. This mixture was stirred for one-half hour at 100°C, cooled, and filtered. The precipitate was thoroughly washed with ethanol. To separate the two isomers, the above precipitate was added to 100 ml of pyridine, stirred for several minutes, filtered and washed. The pyridine insoluble 1,6-dinitropyrene was dried in a vacuum desiccator (m.p. 294-296°C, uncorrected, reported 309°C)..

1 gm of the purified 1,6-dinitropyrene was added to 20 ml of alcohol. This solution was brought to a boil and 10 ml of an aqueous

60% sodium sulfide solution was slowly added. The mixture was refluxed for a few hours until it definitely turned a dark green color. After cooling, the solution was vacuum filtered in the absence of oxygen. The precipitate was washed twice with deoxygenated water and twice with deoxygenated alcohol. The resultant 1,6-diaminopyrene was dried in a vacuum desiccator (m.p. 218-220°C, uncorrected, reported 232°C).

1,6-diaminopyrene radical-salt was prepared by a modified method of Scott, et al.(42) 0.12 gms of 1,6-diaminopyrene were dissolved in 1000 ml of xylene by stirring overnight. This solution was continually bubbled with nitrogen to prevent the oxidation of the diamine. A solution of 0.05 gms of bromine in 5 ml of carbon tetrachloride was dropwise added to the xylene solution until the diamine fluorescence disappeared. The precipitate was vacuum filtered and washed with xylene. The radical salt was dried in a vacuum desiccator.

B. Solutions

$Ru(bipyr)_3Cl_2$ is slowly air oxidized to the tripositive state when it is in a 50% sulfuric acid solution. Thus, all such solutions were prepared using previously deoxygenated solvents.

$Ru(bipyr)_3Cl_2$ decomposes over a period of several days in an EPA solvent (5 parts diethyl ether; 5 parts iso-pentane; 2 parts ethyl alcohol by volume). The product was not identified. All measurements with this solvent were made within 24 hours of preparation; no decomposition was evident.

The 1,6-diaminopyrene radical salt slowly reacted with water to form an unidentified product. All solutions containing this salt were kept as dry as possible, and all measurements were taken within an hour of solution preparation.

C. Spectral Instrumentation

Spectrophotometer - Absorption spectra were recorded using a Cary Model 14 spectrophotometer.

Fluorometer - Emission spectra were recorded with a fluorometer constructed from Aminco-Building Blocks. Figure III-1 shows the component configuration and optical path. The monochromators are Aminco Grating Monochromators (4-8401) equipped with variable slits (D42-61041) and mounted on an optical bench (D65-61041). The excitation monochromator is blazed for 300mu while the emission monochromator is blazed for 500mu. The sample chamber has provisions for right angle excitation (C111-61041), front surface excitation (C66-62140) and phosphorescence (C195-61041).

The detector is an E.M.I. 9558 QA photomultiplier. The photocathode is of a tri-alkali type (S20) which in conjunction with the quartz window yields a spectral range of 165 to 850mu. The applied voltage is 1250 volts across the dynode chain, which for the particular tube employed yields a sensitivity of 300 amps/lumen. The dynode chain is a linear configuration with all of the resistors being 200 K ohm except for a 470 K resistor between the tenth and the eleventh

FIGURE III-1

Fluorometer Constructed from Aminco Building Blocks

Top View

Key

B - Optical bench.

C - Thermoelectric cooler.

D - Detector.

E - Emission monochromator.

F - Fluorescence cell.

G - Grating.

L - Lamp.

M - Front surface mirrors.

S - Slit mechanism.

X - Excitation monochromator.

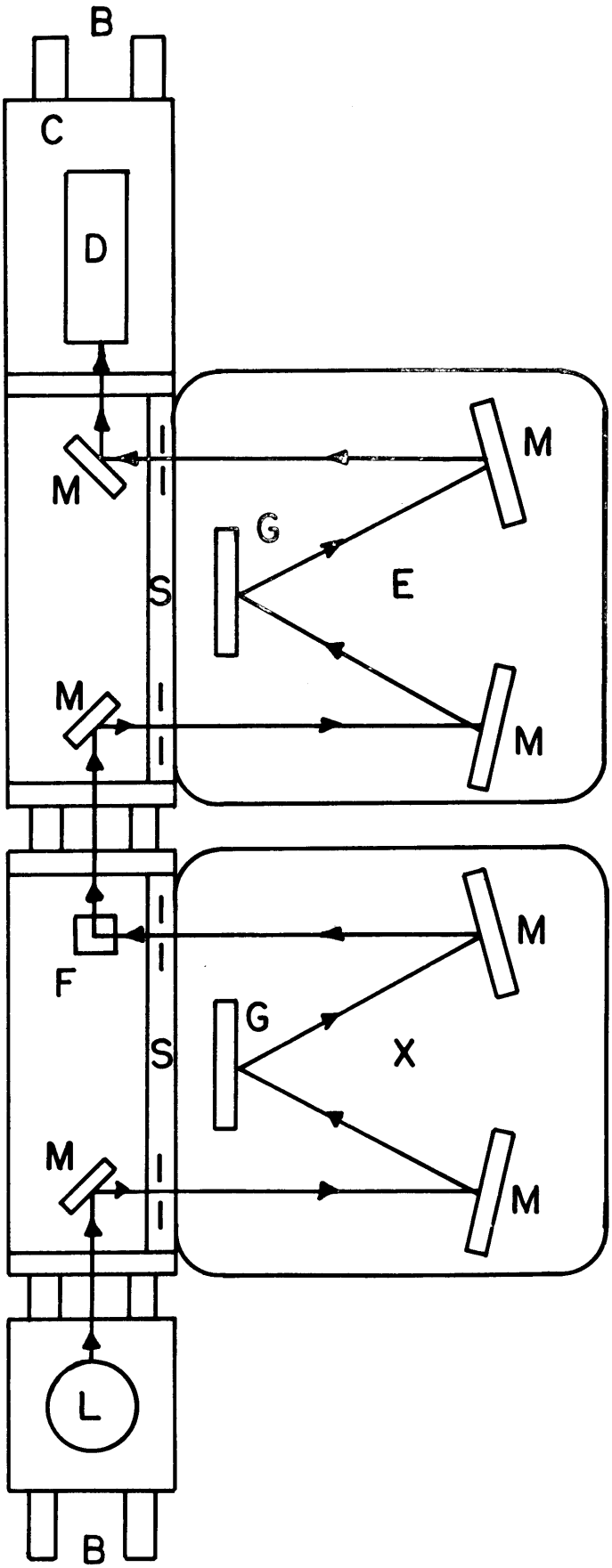
B
C
D
M
M
G
E
S
M
M
M
F
G
X
S
M
M
L
B

dynodes. Instead of a resistor, a 150 volt Zener diode is used between the photocathode and the first dynode. No capacitors were used in the dynode wiring.

The photomultiplier is powered by a Kepco regulated d.c. supply, Model ABC 2500M. At 1000 volts the a.c. ripple is about 20 millivolts. This is a sufficiently low a.c. component for this particular application. The supply is connected for negative high voltage per the manual and was modified by replacing the provided banana plug outlets with chassis BNC connectors.

The photomultiplier temperature is held at -30°C by a thermoelectric junction. The particular cooling chamber used is a Products for Research Model TE-104. The dynode assembly mentioned above is designed to mate with the cooler and was purchased from the same corporation. The chamber was mounted directly to the optical bench and alligned with the light beam exciting the emission monochromator.

The output from the photomultiplier anode was filtered by the LRC network shown below:

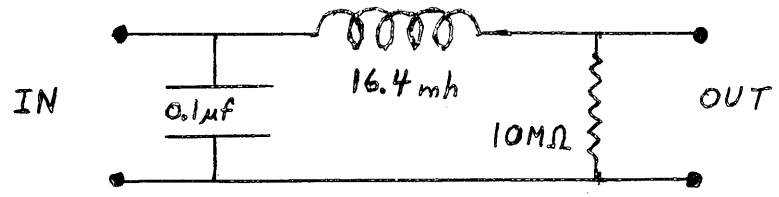

The amplifier used is a Hewlett Packard Model 412-A-VTVM. The input impedance was utilized as the load resistor. The amplifier output, connected to the recorder, was one volt full-scale regardless

of the range setting.

The noise level of the fluorometer is quite low. With an input impedance of 10 megohms the photomultiplier dark voltage is usually about fifty microvolts.

The wavelength driving and monitoring systems are modifications of those used by Aminco. The electrical schematic for the wavelength driving system is shown in Figure III-2A. The scan switch allows the motor to be driven clockwise (increasing the wavelength), counter-clockwise (decreasing the wavelength) or to be turned off. The speed adjustment controls the rate (in mu/sec) that the spectrum is scanned. The jog switch bypasses the speed adjustment and operates the motor at its fastest rate. The electrical schematic for the wavelength monitoring system is shown in Figure III-2B. The grating is mechanically coupled to the 30 K ohm variable resistor. The zero adjust is a ten-turn variable resistor. The voltage output to the recorder is the potential difference between the two variable resistors. The gain (mu/in) adjustment is made with the recorder.

The recorder is a Hewlett Packard Model 7005B. The input impedance is one megohm on both channels (x and y) for the ranges in use.

Three lamps are currently available for use with the fluorometer; Xenon, Mercury-Xenon, and Quartz-Iodine. The Xenon and

FIGURE III-2

A - Wavelength Driving System

B - Wavelength Monotoring System

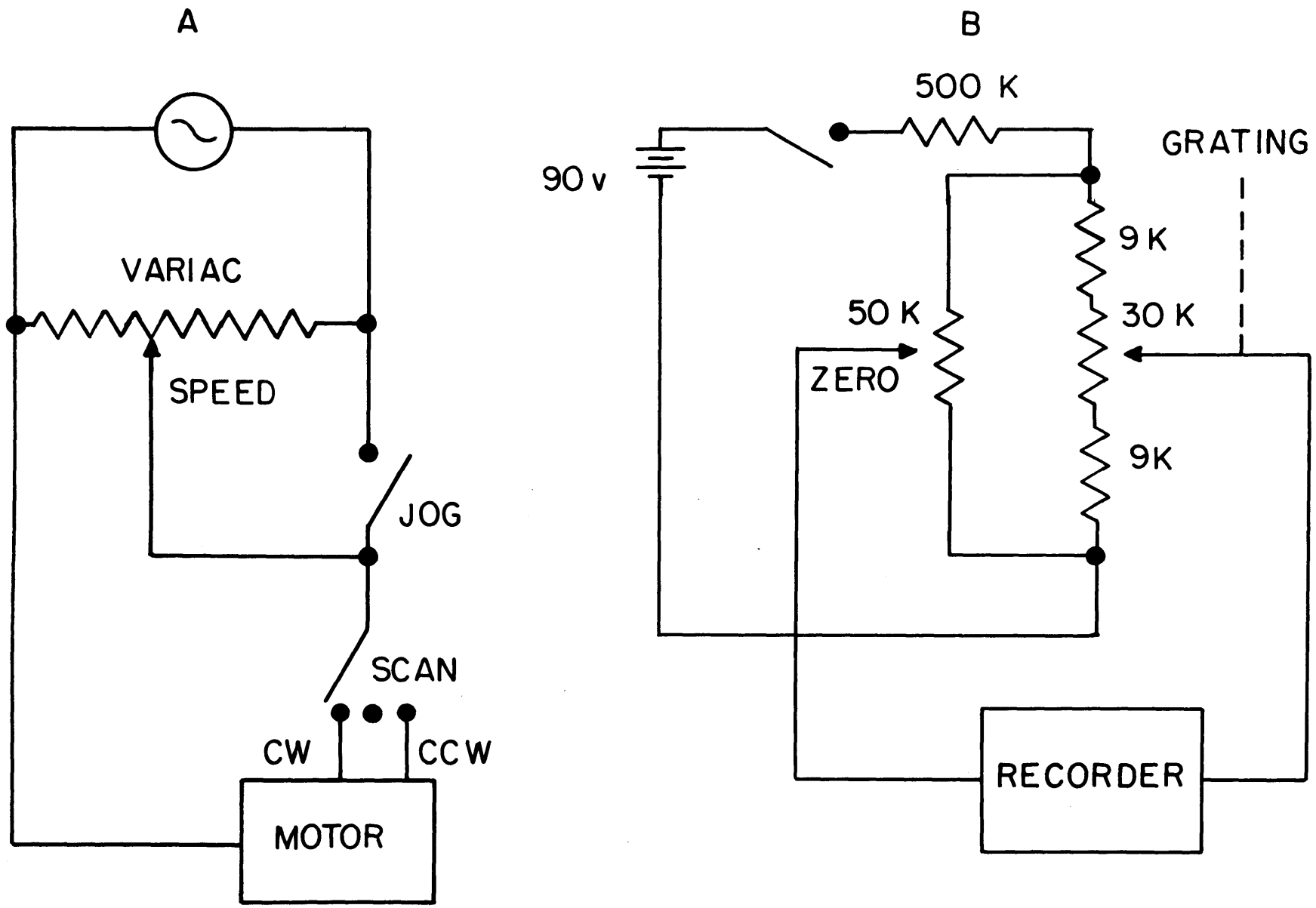
A
VARIAC
SPEED
JOG
SCAN
CW
CCW
MOTOR
B
500 K
90 v
GRATING
9 K
50 K
30 K
ZERO
9K
RECORDER

Mercury-Xenon lamps are those supplied by Aminco (416-992 and 416-993 respectively). The lamp housing (C188-61041) and the lamp power supply (D2-62000) are also supplied by Aminco. The Quartz-Iodine lamp is a 400 watt Sylvania product (400 T4Q/CL/F). The power supply for this lamp is an 8 amp Variac connected to the house line through an 8 amp Sola constant voltage transformer. The lamp is operated at 110 volts. Both sets of lamps are cooled with forced air when operating.

Lifetimes-Fluorescence and phosphorescence lifetimes were measured on a spectrometer constructed from a TRW Nanosecond Spectral Source System. The system is comprised of a Model 31A Nanosecond Spectral Source, Model 32A Decay Time Computer, Model 33A Photomultiplier Unit, Model 34A Fluorescence Excitation Chamber, and two Model 35A Relay Lens Assemblies. The signal, measured across a 50 ohm load resistor, is pre-amplified with a Tektronix Model 1A1 vertical plug-in and displayed on the upper beam of a Model 556 Oscilloscope. The Decay Time Computer output is pre-amplified with a Tektronix Model B vertical plug-in and displayed on the lower beam of the same oscilloscope . Fluorescence lifetimes as short as 1.7 nanoseconds can be obtained directly from the Decay Time Computer.

A phosphorescence attachment was made to fit into the Model 34A Fluorescence Excitation Chamber. To facilitate this modification, the Model 35A Fluorescence Sample Holder was removed and replaced with a piece of sheet metal so constructed as to hold the Aminco phosphorimeter dewar assembly. When measuring phosphorescence lifetimes of

compounds emitting above 500mu, an RCA 7265 photomultiplier was used to detect the emission. The photocathode of this tube is of the tri-alkali type (S20). This tube was held in a Pacific Photometric Instruments potted cryogenic housing Model 77. The detector assembly could then be cooled to dry ice temperatures, reducing the dark current. The photomultipler was powered by a Kepco regulated d.c. supply, Model ABC 2500M.

When measuring phosphorescence lifetimes longer than 100 nanoseconds, the Decay Time Computer was not used. In this case, the photomultiplier output was displayed on the Model 556 oscilloscope and recorded with a Tektronic Model C-12 camera and Polaroid Type 107 film. The pulsewidth of the source was insignificant in comparison to such phosphorescence decays, and simple log intensity-versus-time plots were used to calculate the lifetimes.

Chemiluminescence-Since the chemiluminescence of interest is short lived its spectral distribution must be measured under flow conditions. The reactants were placed into two 200 ml syringes which were mounted on a Harvard Appartus Model 600-2-200 syringe pump. The outlets of the syringes were connected with teflon tubing to a special mixer. Figure III-3 shows the "T" mixer used to introduce the chemiluminescing solution into the fluorometer cell compartment. The mixer is constructed from 8 mm glass tubing having a 2 mm bore. The special feature of the mixer is the platinum gauze which is glass blown directly into the capillary. The gauze produced a turbulent flow

FIGURE III-3

"T" Mixer - Side View

Key

A - Input for reagent A.

B - Input for reagent B.

G - Platinum gauze.

O - Output for reaction products.

V - Cross section of mixer viewed by the fluorometer.

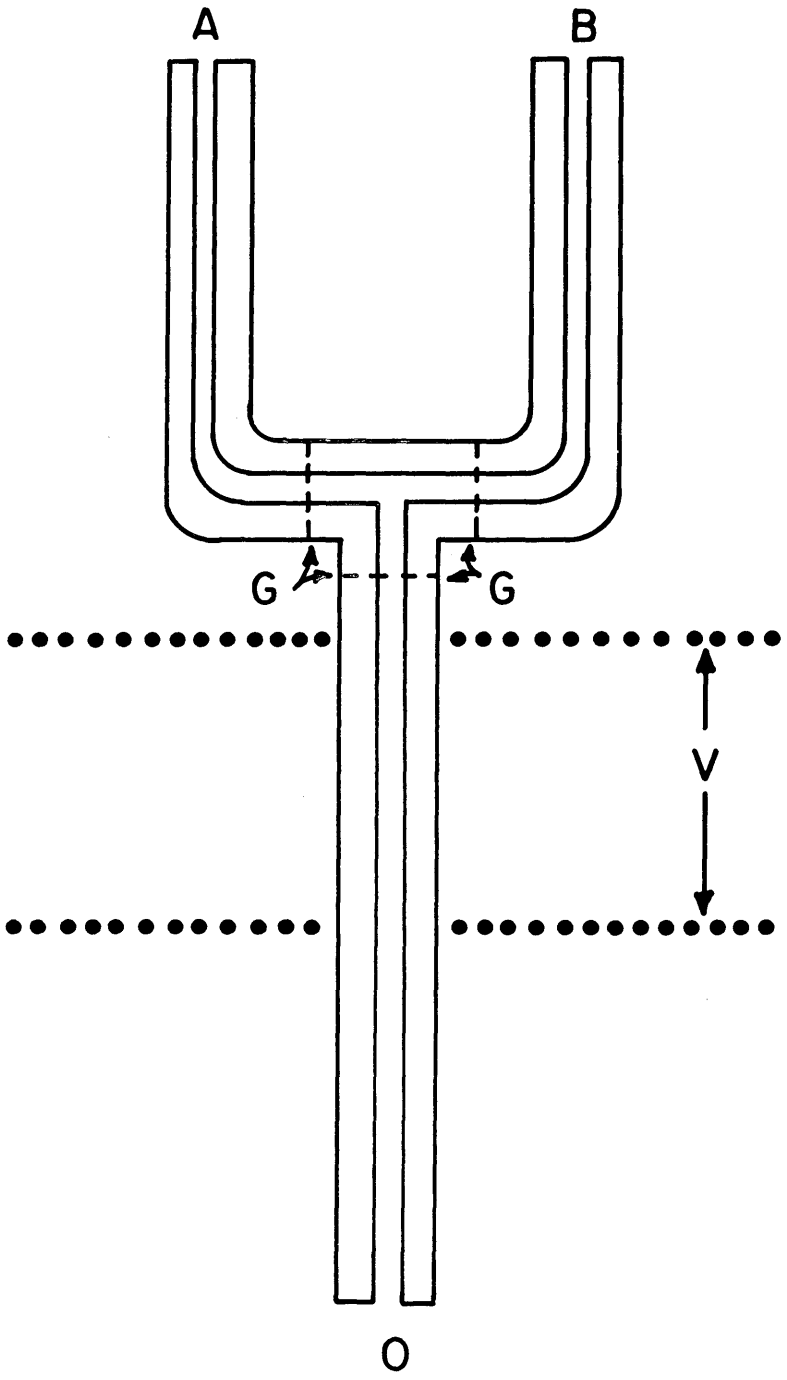
A
B
G
G
V
O

which greatly enhanced the mixing. While the solution was flowing, an emission spectrum was recorded on the fluorometer. Since flow artifacts are frequently observed, the true spectrum was determined from a composite of several runs.

D. Temperature Control

Above ambient-For spectral measurements above ambient, the cell shown in Figure III-4 was employed. Temperature control of the thermostating liquid was achieved with an Instrumentation Laboratory, Constant Temperature Bath Model 127. Temperatures were measured with a mercury thermometer placed in the thermostating bath.

Below ambient-a cryostat capable of maintaining constant temperatures from 300° to 68°K was constructed. The entire unit, shown in Figure III-5, is mobil, and the cryostat can be operated in the spectrophotometer, fluorometer and the nanosecond spectral source system.

An Air Products Cryo-tip nitrogen refrigerator Model AC-1-110 is utilized having a Spectroscopy Shroud WMX-1 modified to accomodate one-centimeter square Beckman cells (described in Section III G.3). The cell holder is specially made for our application and is shown in Figure III-6. The shroud windows are Thermal American Spectrosil A optically flat quartz discs, 1 3/4 inches in diameter and 1/8 inch in thickness.

Gas flow through the refrigerator is controlled with an Air

FIGURE III-4

Thermostating Cell

Key

C - Beckman cell.

I - Thermostating liquid inlet.

M - Mercury thermometer.

O - Thermostating liquid outlet.

R - Rubber stopper.

T - Test tube.

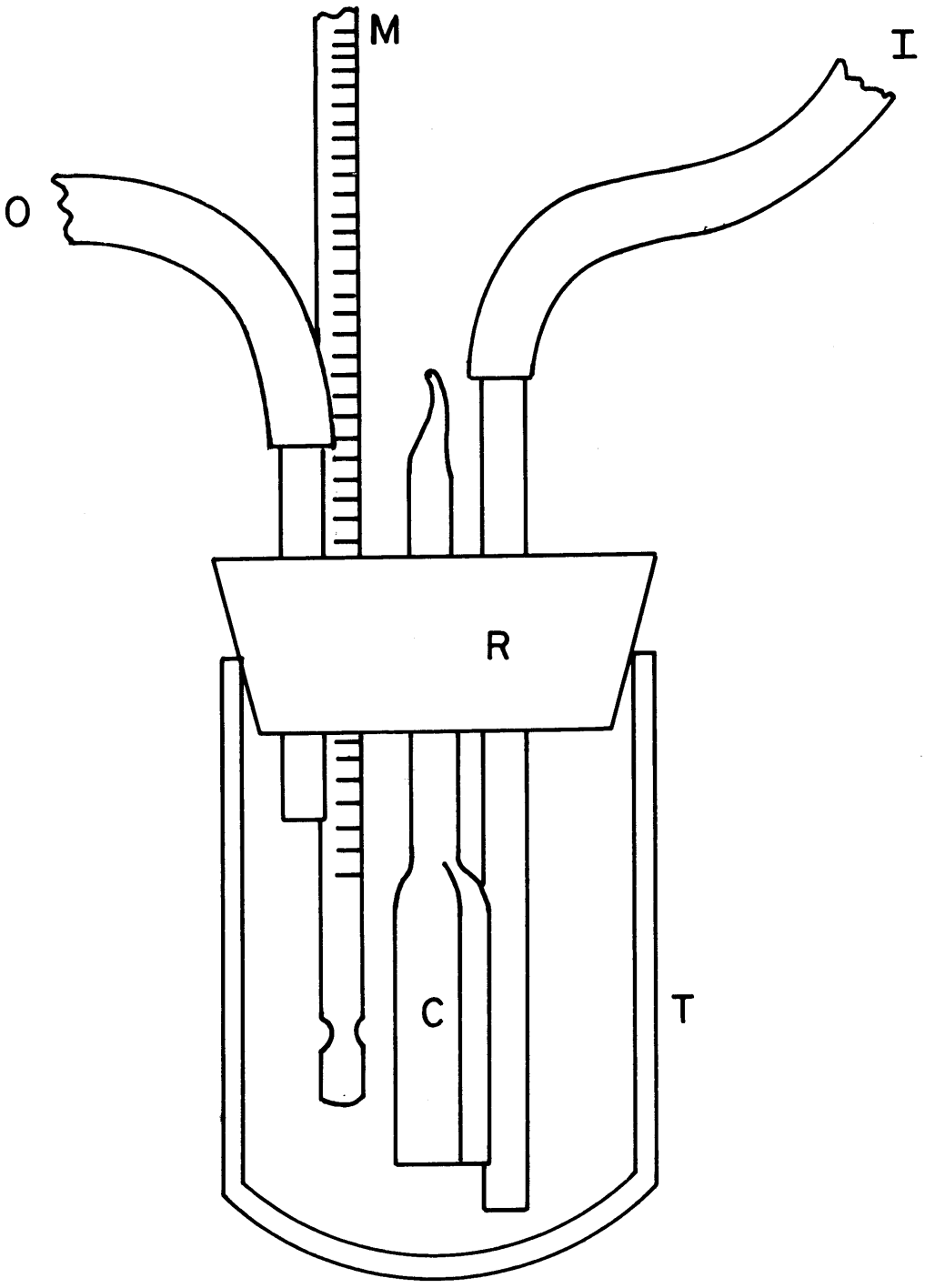
M
I
O
R
C
T

FIGURE III-5

Constant Temperature Cryostat

Key

C - Cryostat with the spectroscopy shroud.

D - Diffusion pump.

E - Electrical control panel.

F - Forepumps.

G - Gas control panel.

H - High pressure flexible nitrogen lines.

J - Lab jack.

M - Medium pressure flexible nitrogen lines.

R - Recorder.

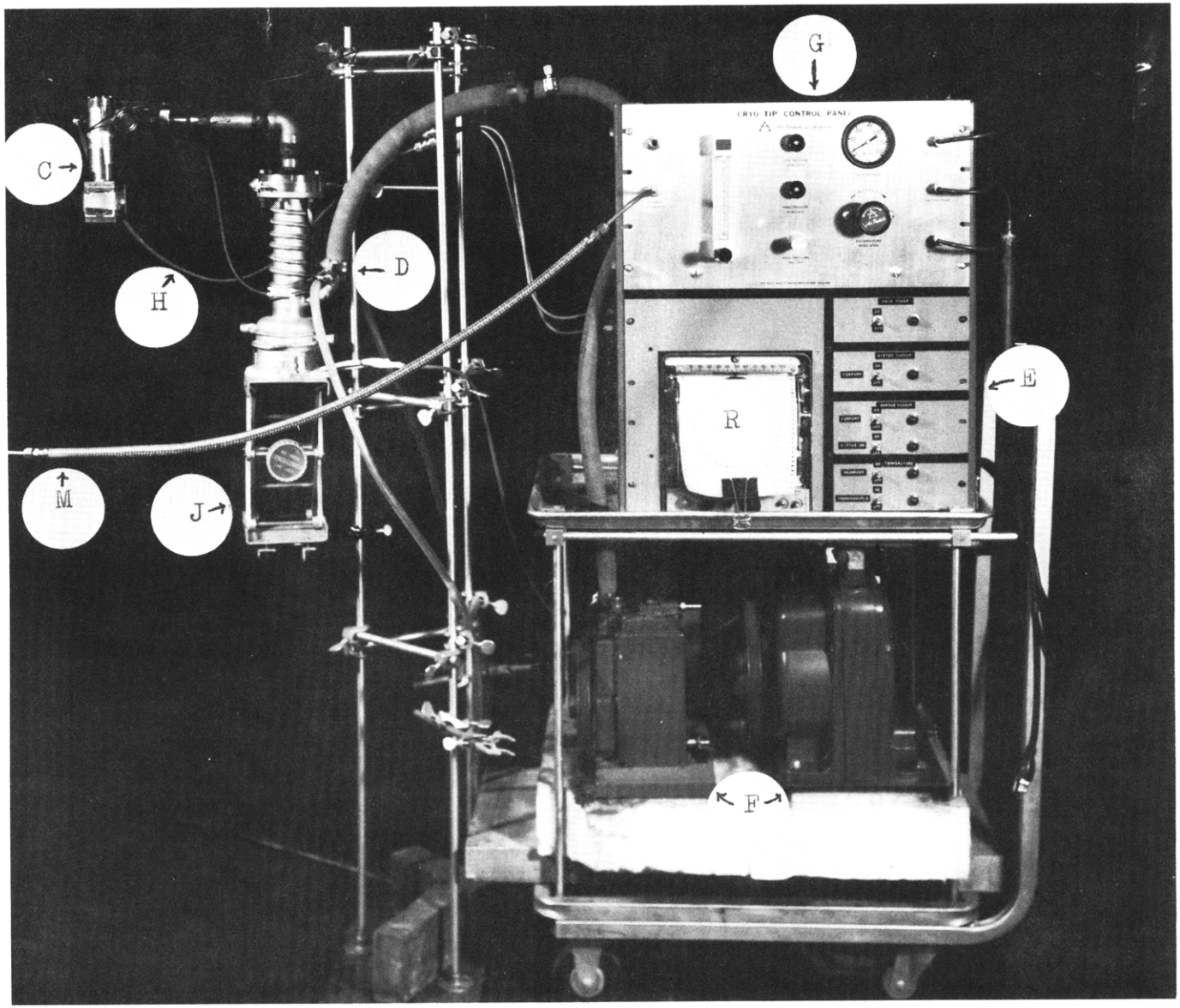
G
C
D
H
E
R
M
J
F

FIGURE III-6

Cryostat Cell Holder

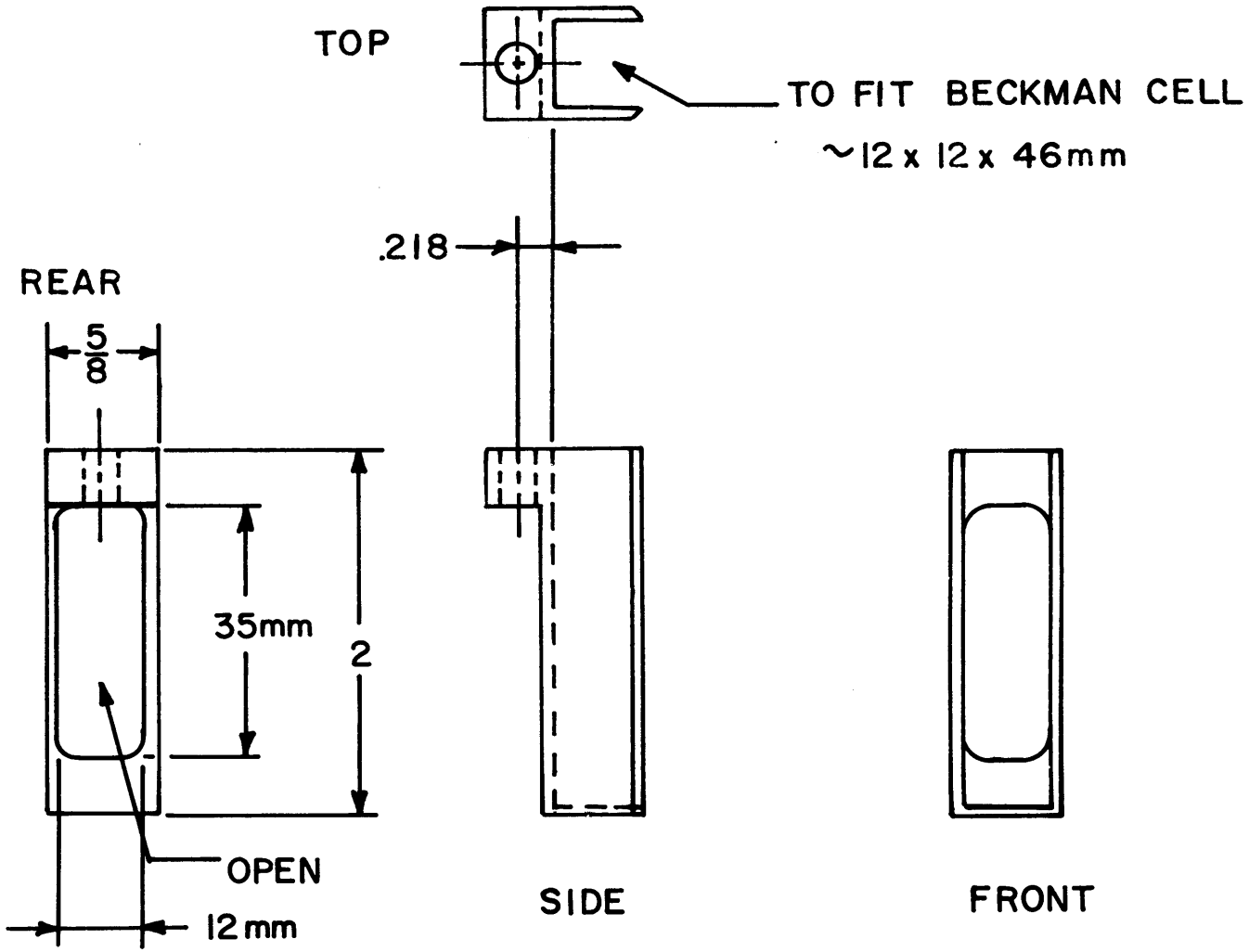
TOP
TO FIT BECKMAN CELL
~12 x 12 x 46mm
.218
REAR
5/8
35mm
2
OPEN
12mm
SIDE
FRONT

Products Model OC-11 Gas Control Panel, which is connected to the cryostat by flexible gas lines. This panel is modified by the replacement of the provided high pressure shut-off valve with a Whitey microregulation valve Model 22-R54-A. The source of gas is a high pressure manifold connected to four tanks of prepurified nitrogen. The output of this manifold is attached directly to a high pressure regulator, which drops the nitrogen to 200-1500 pounds per square inch. The medium pressure nitrogen is carried in 1/4 inch copper tubing to several convenient locations in the laboratory. The gas is then transferred to the Control Panel by a Swagelok flexible metal hose.

The shroud vacuum is maintained by a Welch Duo-seal vacuum pump #1405B and a Consolidated Vacuum Corporation MCF-60 two inch water cooled diffusion pump #8419. Since the volume of the space to be evacuated is small, the shroud can be slowly "roughed" through the operating diffusion pump. A Vactron Lab Equipment Bellows Valve CVB-50L-Q separates the cryostat from the vacuum system, facilitating sample changes.

A second vacuum pump, Welch Duo-seal high capacity #1397B, is used to evacuate the nitrogen lines. It also provides a vacuum for the low pressure side of the refrigerator when operation below 80°K is desired.

Temperatures are determined by use of a calibrated thermocouple which is wrapped around the cold tip of the netrogen refrigerator.

The voltage from this device, if measured with a Leeds and Northrup Type K-3 Universal Potentiometer, is accurate enough to determine the temperature to within one degree. Qualitative observation of temperature changes is possible when the thermocouple output is displayed on a Varian Model 10-A strip chart recorder.

E. Kinetic Measurements

1. Slow reactions

For slow reactions the reagents were mixed by stirring and then transferred to spectrophotometer cell. The Cary 14 was utilized by operating the instrument so that it displayed the absorption at a particular wavelength as a function of time. Attempts to monitor solution emission as a function of time failed.

2. Fast reactions

Basic Instrumentation-The basic instrumentation used for studying fast reactions was the Durrum-Gibson Stopped-Flow Spectrophotometer. The principles of operation of this instrument are set forth elsewhere.(6) Zero offset, filtering and triggering networks were constructed per the Durrum Manual.

Output-For very fast reactions the signal from the photomultiplier is amplified by a Tektronix Type 2A63 differential plug-in and is displayed on a 564 Storage Oscilloscope equipped with a Type 3B3 time base. The data are then recorded with a Tektronix Model C-12 camera and Polaroid Type 107 film.

For moderately fast reactions the signal from the photomultiplier is amplified by a Hewlett Packard Model 17501A Input Module and displayed on a Model 7100B strip chart recorder.

Chemiluminescence Mode-To measure chemiluminescence intensity, the input to the Durrum Mirror Box must be taped shut so that room light is not detected. The output is the photomultiplier signal as a function of time.

Absorption Mode-The light source for the absorption mode is the 400 watt Sylvania Quartz-Iodine lamp described in conjunction with the fluorometer. The lamp, operated at 100 volts d.c., is powered by a series connection of Technipower Model L80-12M and L20-L2M regulated power supplies. The monochromator is a Jarrel Ash 0.25 Meter Ebert, Model 82-40. The monochromated light is adjusted so that it properly enters the Durrum Mirror Box. With no absorption, the voltage applied to the photomultiplier is adjusted for a full-scale deflection of the recording device. The output is the photomultiplier signal as a function of time.

F. Miscellaneous Instrumentation

Electrochemical-Current-voltage curves were measured by use of Heath Kit Model EUA-19A operational amplitiers and a Model EUA-19-2 polarography module. The results were displayed on a Houston Model HR-100 x-y recorder.

The reference electrode was a saturated calomel electrode,

unless otherwise mentioned. It was separated from the sample solution by means of a vycor plug. For aqueous solutions, the indicator electrode was contructed from a wax impregnated graphite rod. For non-aqueous solutions a platinum electrode was employed. The counter electrode was platinum and was separated from the bulk of the solution by a glass frit.

Nuclear Magnetic Resonance-All nuclear magnetic resonance spectra were recorded on a Varian Model A-60 NMR spectrometer.

Infrared-All infrared spectra were recorded on a Perkin Elmer Model 237B infrared spectrometer.

Electron Paramagnetic Resonance-All electron paramagnetic resonance spectra were recorded on a Varian Model 4502 EPR spectrometer equipped with a 9 inch magnet.

Absolute Fluorescence Spectra-The absolute emission spectra for compounds emitting at wavelengths lower than 600mμ were recorded on a Turner Spectro Model 210.

G. Procedures

1. Fluorometer calibration

Wavelength-The emission monochromator can be calibrated for wavelength accuracy by placing a mercury pen lamp in the sample chamber and measuring its emission spectrum. The excitation monochromator can be calibrated by placing a fluorescent solution in the sample

chamber and running an excitation spectrum using the Mercury-Xenon lamp.

Bandpass-The bandpass of the monochromators can be identified with the half-width of any spectral line. Such results must be corrected for other wavelengths since the bandpass is a cosine function of the grating angle. The table below simmarizes the results for the 3650Å mercury line.

Slitwidth(mm)	Bandpass(Å)	Slitwidth(mm)	Bandpass(Å)
1/8	~10	3/4	50
1/4	30	1	80
1/2	40	2	140

Emission-The response of a fluorometer to emitted light varies considerably as a function of wavelength. The intensity of fluorescence, as measured, can be computed by the following equation.

$$F(\lambda,\lambda') = k \cdot s(\lambda) \cdot \phi \cdot I(\lambda') \cdot [1-T(\lambda')] \qquad \text{III-1}$$

where $F(\lambda,\lambda')$ is the measured fluorescence intensity; $S(\lambda)$ is the wavelength dependent instrumental sensitivity; ϕ is the quantum yield of fluorescence; $I(\lambda')$ is the intensity of the exciting wavelength of light; $T(\lambda')$ is the transmission of the fluorescing solution at the exciting wavelength; and k is a wavelength independent quantity that depends upon the fraction of the total emitted quanta that arrive at the detector.

If the total quanta emitted from a fluorescent substance are denoted Q, then the spectral distribution will be $dQ/d\lambda$ if the instrument output is linear in wavelength. If the instrument output

is linear in frequency, the spectral distribution is then $dQ/d\lambda$, which is equivalent to $(dQ/d\lambda) \cdot \lambda^2$ (36).

To determine the wavelength dependancy of $S(\lambda)$, the photomultiplier-monochromator combination must be calibrated. One of the easiest methods employs a U.S. National Bureau of Standards lamp, which when properly operated emits energy according to Planck's Blackbody equation (24,45).

The output of the lamp, from 380 to 770 mμ can be calculated by the equation,

$$E(\lambda) = \frac{(0.56)^5(\exp[c_2/0.56\ T_c]-1)}{\lambda^5(\exp[c_2/\lambda T_c]-1)} \qquad \text{III-2}$$

where c_2 is a constant provided with the lamp; T_c is the color temperature at which the lamp is operated; and 0.56 is the normalizing wavelength in microns. To convert this energy output to quanta, it is necessary to multiply by the wavelength since,

$$E_{total} = (\text{number of quanta}) \cdot hc/\lambda$$

Once the spectral response of the fluorometer to the standard lamp has been measured, the sensitivity can be calculated. Since the instrument is operated at finite bandpass, it is usual to express the response as $dR/d\lambda$. The calculated lamp output then becomes $dQ/d\lambda$, and the sensitivity and fluorescence intensity are likewise modified. $S(\lambda)$ is then calculated in a straightforward fashion,

$$S(\lambda) = \frac{dR/d\lambda}{dQ/d\lambda} \qquad \text{III-3}$$

Operationally, the light from the NBS lamp is allowed to illuminate a microscope slide coated with magnesium oxide(48). This slide is placed at 45° in the sample chamber and a spectrum is recorded from the reflected light. Several experimental details must be taken into account.

a) The light is very intense and the voltage on the photomultiplier will have to be reduced so that the signal can be recorded. As indicated in the Section III-C Fluorometer discussion, a Zener diode should be placed between the photocathode and the first dynode. This assumes that the characteristics of the tube do not change as the supply voltage is lowered.

b) The magnesium oxide layer is formed by burning a strip of magnesium metal and allowing the smoke to deposit on a clean glass surface. First, treat the strip with acetone to remove any rolling oil that may be present. Then ignite the strip with burning ethanol, since this will not contaminate the smoke or strip. Put two separate layers on the glass plate, one on top of the other.

c) The reflectivity of the magnesium oxide is as follows:

λ	% REFLECTED	λ	% REFLECTED
240	96	400	97.4
260	94	420	97.7
280	91	440	97.9
300	92	460	98.2
320	93	480	98.4
340	93+	500	98.6
360	94	600	99.4
380	95	700	99.7

d) For any instrument where polarization is important, use two reflective surfaces. Let the NBS lamp illuminate one surface which in turn illuminates the second surface. The instrument will then monitor the light reflected from the second surface.

e) Be positive that any area the photomultiplier "sees" is flat black, excepting the illuminated magnesium oxide surface.

f) A check should always be made to see how valid corrections made with one slit width are for another slit setting. Remember that $dR/d\lambda$ implies a finite slit width.

g) Also remember that the bandpass of a grating monochromator varies as a function of the cosine of the grating angle. If the standard lamp varies as a function of bandpass, this affect probably should be taken into account.

Figure III-7 shows the NBS lamp output in units of energy and quanta, the measured response curve and the calculated sensitivity. All of the data are normalized to unity at 560mμ. It is to be noted that the value of $dR/d\lambda$ did not change upon going from 1/8 mm slitwidth to a 1 mm slitwidth. Therefore, no correction was made for bandpass or grating angle. No correction was deemed necessary for the wavelength dependence of the magnesium oxide reflection. Figure III-7 also shows the calculated monochromator efficiency curve. These latter data were determined by dividing the calculated sensitivity by the published response curve for the photomultiplier (13). The result agrees with Aminco's data for their 500mμ blazed grating.

Excitation-The intensity of an excitation source varies

FIGURE III-7

Detector Calibration Curves

Key

E - NBS lamp output in energy.

M - Monochromator efficiency.

Q - NBS lamp output in quanta.

R - Measured response.

S - Sensitivity.

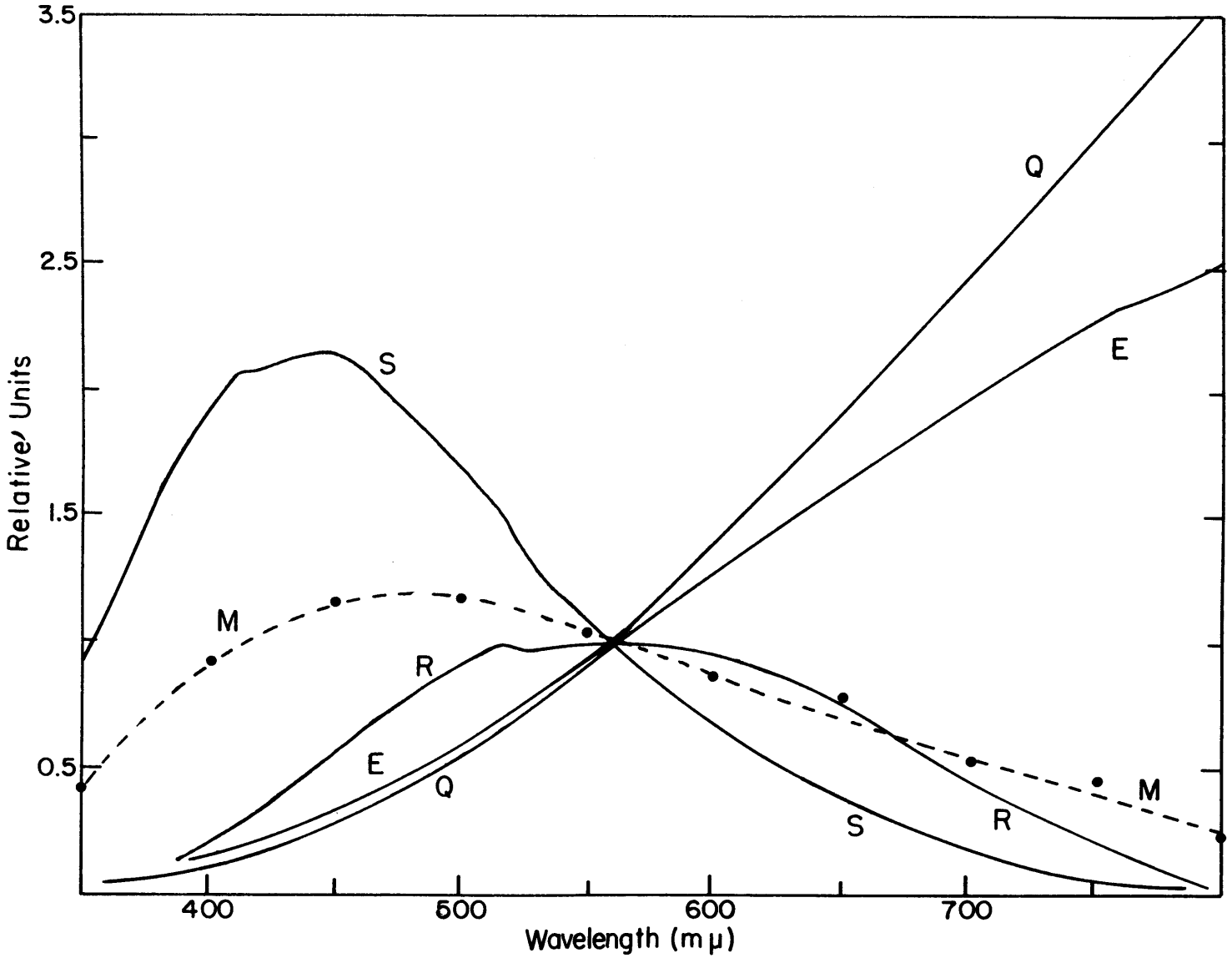
3.5
2.5
1.5
0.5
Relative Units
400
500
600
700
Wavelength (mμ)
S
Q
E
M
R
E
Q
S
R
M

considerably as a function of wavelength. The source output can be determined by use of the following consideration.

For the case of a fluorescent substance having a wavelength independent quantum yield in solutions where $T(\lambda') < 1\%$ the intensity of fluorescence, as measured, can be computed by the following equation.

$$F(\lambda,\lambda'') = k \cdot s(\lambda) \cdot \phi \cdot I(\lambda'') \qquad \text{III-4}$$

If an excitation spectrum is measured for such a case, the fluorescence intensity at any fixed emission wavelength then becomes,

$$F_{\lambda}(\lambda'') = k \cdot I(\lambda') \qquad \text{III-5}$$

It is then possible to directly determine $I(\lambda')$ since it is related only by a constant to the measurable $F_{\lambda}(\lambda')$.

Operationally, a 2×10^{-2}M solution of Rhodamine-B in ethylene glycol is utilized (53,47,54). This solution has a quantum yield independent of λ'. In a 1 mm cell such a solution will absorb above 2.0 at all wavelengths lower than 600mu.

A front surface excitation spectrum is used to measure $F_{\lambda}(\lambda')$ and a 640mu high-pass filter is inserted before the emission monochromator to insure that no scattered source output reaches the photomultiplier.

Figure III-8 shows the measured output of both the Xenon and Quartz-Iodine lamps. It is to be noted that the Xenon lamp output did change upon going from 1 to 1/2 mm slitwidth. However the Quartz-Iodine lamp output did not change. No correction was made for the

FIGURE III-8

Spectral Distribution of Lamps

Key

X - Xenon lamp, 1mm slitwidth.

Q - Quartz-iodine lamp.

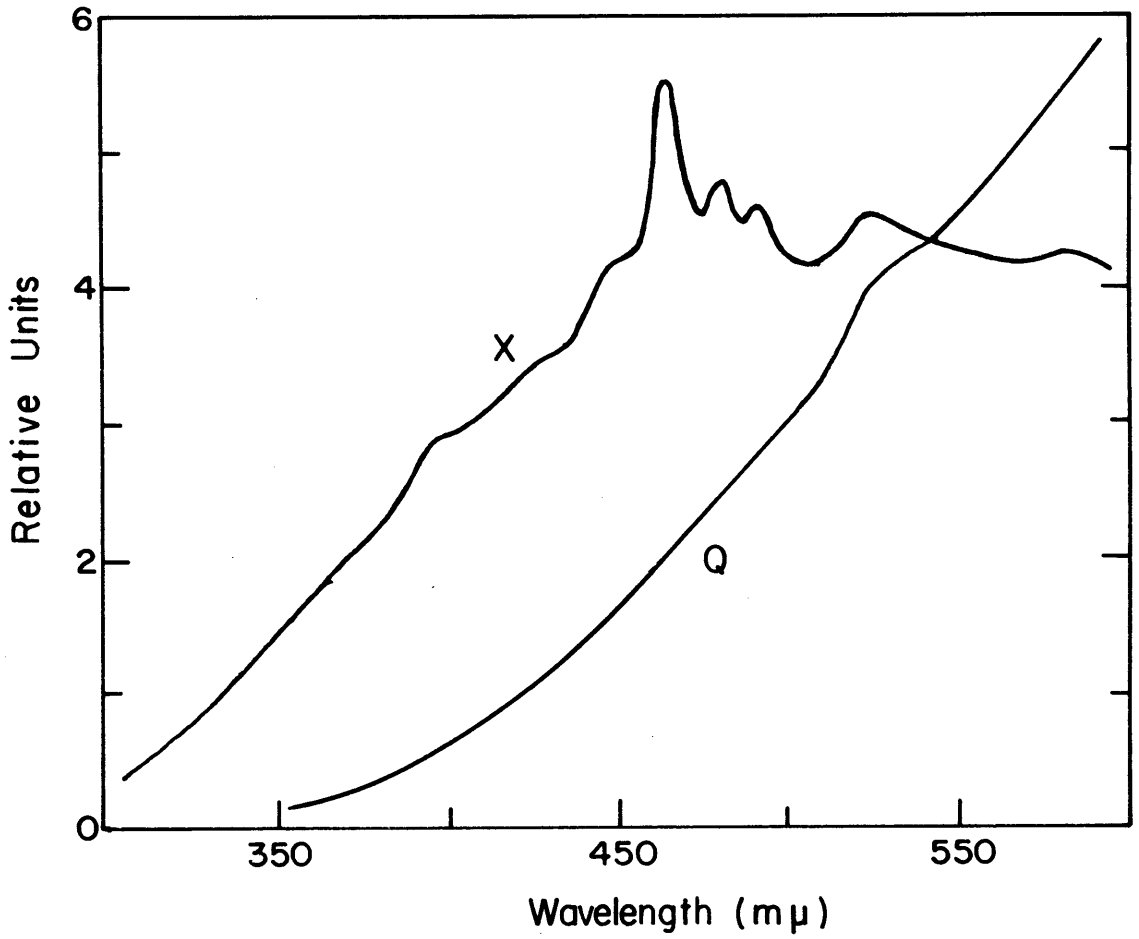
6
4
2
0
Relative Units
X
Q
350
450
550
Wavelength (mμ)

presence of the front surface mirror in the measuring configuration.

Calibration check-The fluorescence spectrum of a dilute solution of fluorescein was measured, at the same excitation wavelength, on both the Aminco and the Turner Spectro Model 210. The Aminco data were corrected for instrumental sensitivity and normalized to match the Turned spectrum at the emission maximum. Both curves are shown in Figure III-9. The match is very good except at long wavelengths where the Turner is known to overcompensate. It is thus shown that the calculated Aminco sensitivities are correct.

2. Quantum Yield

Wavelength Independent-By integrating the combinations of Equations III-1 and III-3 the following expression for relating the area under the corrected emission curve to the quantum yield can be derived.

$$A \equiv \int \frac{dq}{d\lambda} = \int \frac{dF/d\lambda}{ds/d\lambda} = k \cdot \phi \cdot I(\lambda') \cdot [1-T(\lambda')] \qquad \text{III-6}$$

This equation is true as long as ϕ and k are independent of λ.

If the same excitation wavelength is used for both the unknown, u, and the standard, s, the following equation can be derived from Equation III-6.

$$\frac{A_u}{A_s} = \frac{\phi_u \cdot [1-T_u]}{\phi_s \cdot [1-T_s]} \qquad \text{III-7}$$

For all the quantum yields measured, rubrene was used as the standard. In dilute ($T(\lambda') > 99\%$) n-hexane solutions, this compound

FIGURE III-9

Fluorometer Calibration Check

Key

——— - Turner fluorescein spectrum.

oooo - Corrected Aminco fluorescein spectrum.

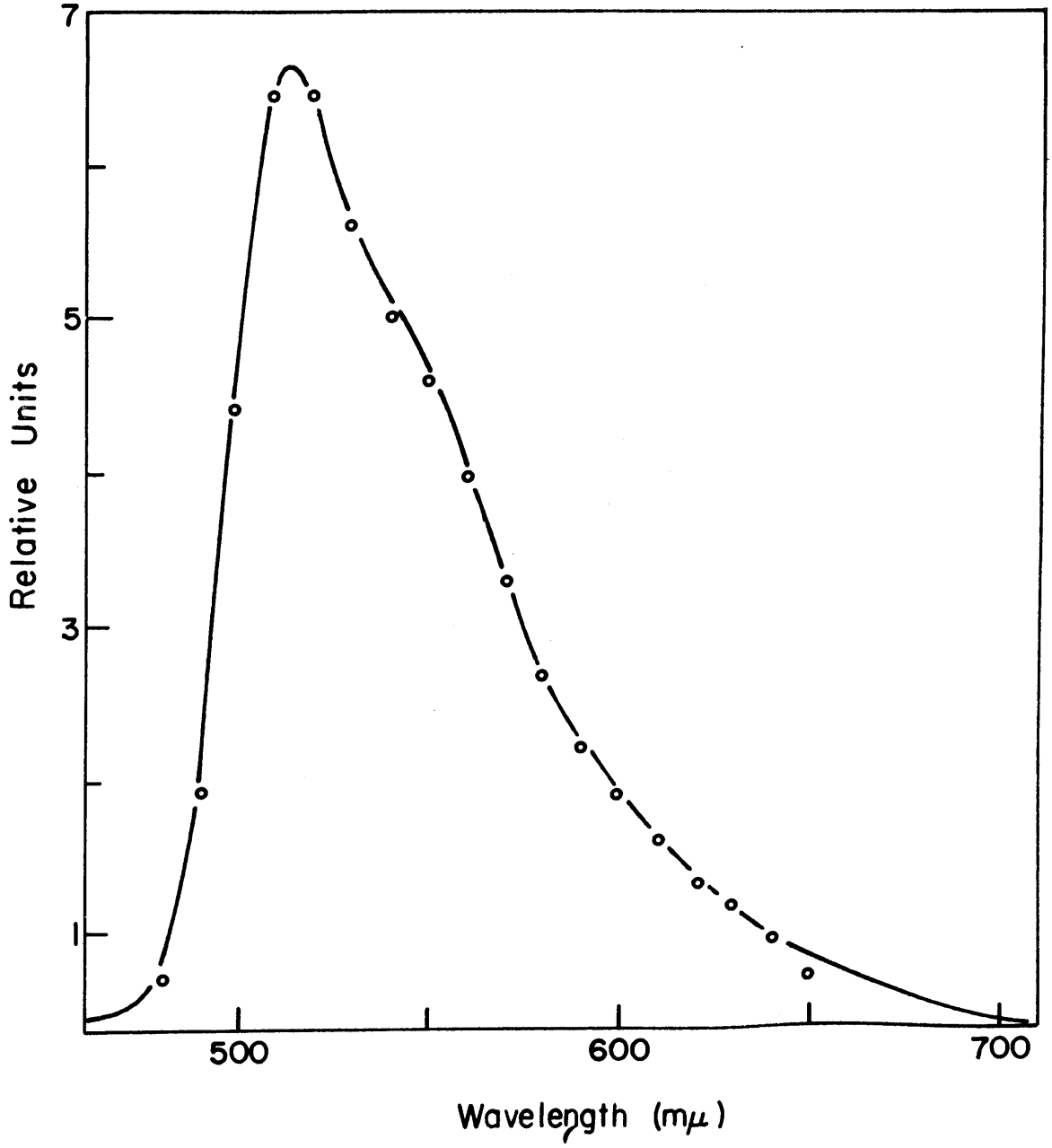
7
5
3
1
Relative Units
500
600
700
Wavelength (mμ)

has a quantum yield of unity. Equation III-7 then simplifies to

$$\phi_u = \frac{A_u \cdot [1-T_S]}{A_S \cdot [1-T_u]} \qquad \text{III-8}$$

When $T(\lambda') < 80\%$, it is best to account for the change in the intensity of the exciting light as it traverses the sample cell(17). The equation for the quantum yields, so corrected, becomes

$$\phi_u = \frac{A_u \cdot [1-T_S] \cdot F_S}{A_S \cdot [1-T_u] \cdot F_u} \qquad \text{III-9}$$

where F = exp (-abc), and "a" is the molar absorptivity, b is the distance between the front of the cell and the point of observation, and c is the molar concentration.

For all solutions requiring this correction, a 1 mm mask was placed in front of the sample cell so that b=1/2 and F=exp(-1/2· absorption).

Wavelength Dependent-Equation III-4 can be used to determine the quantum yield as a function of exciting wavelength. By monitoring the fluorescence at a fixed wavelength, for a solution where $T(\lambda') < 1\%$ over all of the wavelengths of interest, Equation III-4 is reduced to

$$\phi(\lambda') = k \cdot \frac{F_\lambda(\lambda')}{I(\lambda')} \qquad \text{III-10}$$

where $F(\lambda')$ is the measured excitation spectrum and $I(\lambda')$ is the lamp intensity.

3. Deoxygenation and cells

All spectral measurements, except those in the ultraviolet, were performed using Beckman one-centimeter square pyrex

cells modified by the addition of 8 mm pyrex 10/30 outer ground glass joints. All solutions were deoxygenated in these cells by bubbling with nitrogen. The apparatus used is shown in Figure III-10. The nitrogen, pre-saturated with solvent, is rapidly flowed for several minutes to flush the system free of oxygen. Then the bubbling capillary is lowered through stopcock S1 into the sample solution. All solutions are bubbled for 15 minutes. The capillary is removed through stopcock S1, which is then closed. The solution is frozen solid with liquid nitrogen and stopcock S2 is opened to the house vacuum. The stems on the Beckman cells are then sealed by heating and collapsing the tubing.†

†A comparison with vacuum degassing demonstrated that the deoxygenation method described above was adequate for all of the measurements of interest.

FIGURE III-10

Deoxygenation Apparatus

Key

B - Capillary bubbler.

C - Beckman cell.

J - 10/30 ground glass joint.

N - Nitrogen inlets, from solvent bubblers.

S - Sealed section of the stem.

S1 - Two-way stopcock.

S2 - Three-way stopcock.

V - Vacuum inlet.

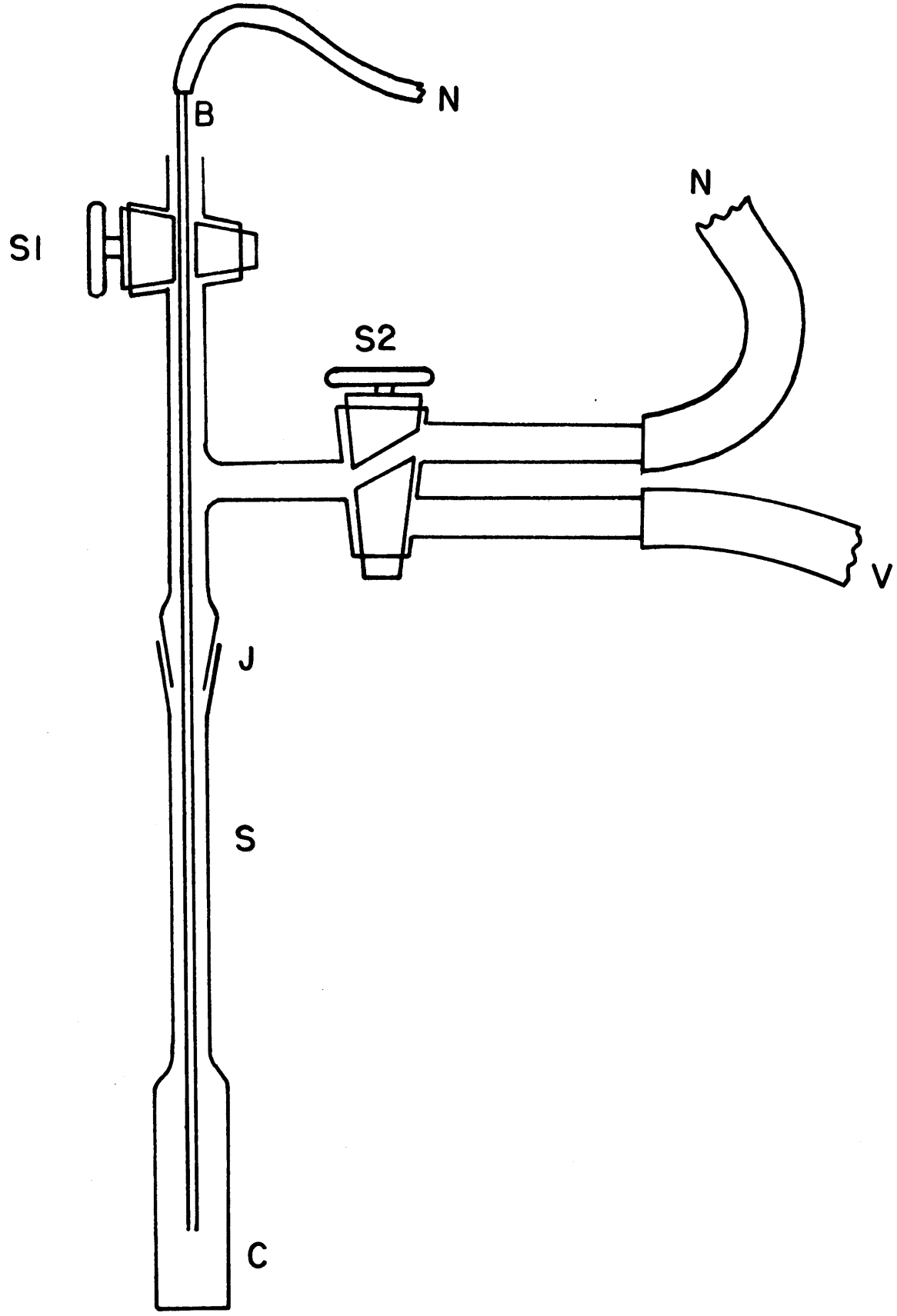
N
B
N
S1
S2
V
J
S
C

IV. PHOTOLUMINESCENCE STUDIES

A. Results

1. Absorption and Emission Spectra

Chelate spectra-The room temperature absorption and emission spectra of the $Ru(bipyr)_3Cl_2$ complex in water are shown in Figure IV-1. Absorption bands appear at 5.40, 4.80, 4.20, 4.00, 3.50, 3.10, 2.90, 2.55, 2.37 and 2.20μ^{-1}. The emission maximum appears at 1.60μ^{-1}. No large solvent effects were observed on either the locations of the maxima or the intensities of the bands. The spectral data for several solvents are summarized in Table IV-1.

Low temperature absorption and emission spectra of the chelate in an ethanol: methanol (5:1) glass are shown in Figure IV-2. The most intense absorption band appears at 2.20 $^{-1}$ while that for emission appears at 1.70μ^{-1}. Both the emission and absorption bands exhibit a regular vibronic progression; the spacing of the absorption band is ca. 0.17μ^{-1} while that of the emission band is ca. 0.13μ^{-1}.

2,2'-Bipyridine spectra-Figure IV-3 shows the absorption and emission spectra of 2,2'-bipyridine in 50% sulfuric acid. In this medium, both nitrogens are protonated and the electrical properties will be similar to those found in the coordinated compound. Absorption bands appear at 5.10, 4.40 and 3.45μ^{-1}. The fluorescence maximum appears at 3.00μ^{-1} and the phosphorescence maxima appear at 2.25 and 2.13μ^{-1}.

TABLE IV-1

Band Maxima and Intensities

Solvent	1	2	3	4	5	6	7	8
H_2O	2.20[a]	2.37	2.55	2.90	3.10	3.50	4.00	4.12
	1.42[b]	1.19	0.53	0.59	1.04	8.35	2.33	2.72
50% H_2SO_4	2.21	2.33	2.54	2.86	3.15	3.50	3.97	4.12
	1.34	1.10	0.50	0.58	1.04	8.40	2.40	2.60
DMSO:H_2O 2:1	2.20	2.32	2.54	2.86	3.08	----	----	----
	1.46	1.23	0.56	0.60	1.06	----	----	----
EtOH:MeOH 5:1	2.22	2.35	2.54	2.86	3.15	3.48	3.95	4.10
	1.46	1.20	0.54	0.57	1.06	8.80	2.50	2.80
EPA	2.21	2.32	2.53	2.80	3.08	3.48	3.95	4.11
	1.35	1.21	0.58	0.62	1.07	7.23	2.10	2.40

a) Band maxima in μ^{-1}
b) Band intensities in liter/mole-cm

FIGURE IV-1

Absorption and Emission Spectra of $Ru(bipyr)_3Cl_2$

Key

A - ——— Absorption, $1x10^{-4}$M in H_2O, 1cm path length.

B - ——— Absorption, $5x10^{-4}$M in H_2O, 1cm path length.

----- Emission, $5x10^{-4}$M in H_2O.

Emission is corrected for photomultiplier-monochromator response, and is in relative units.

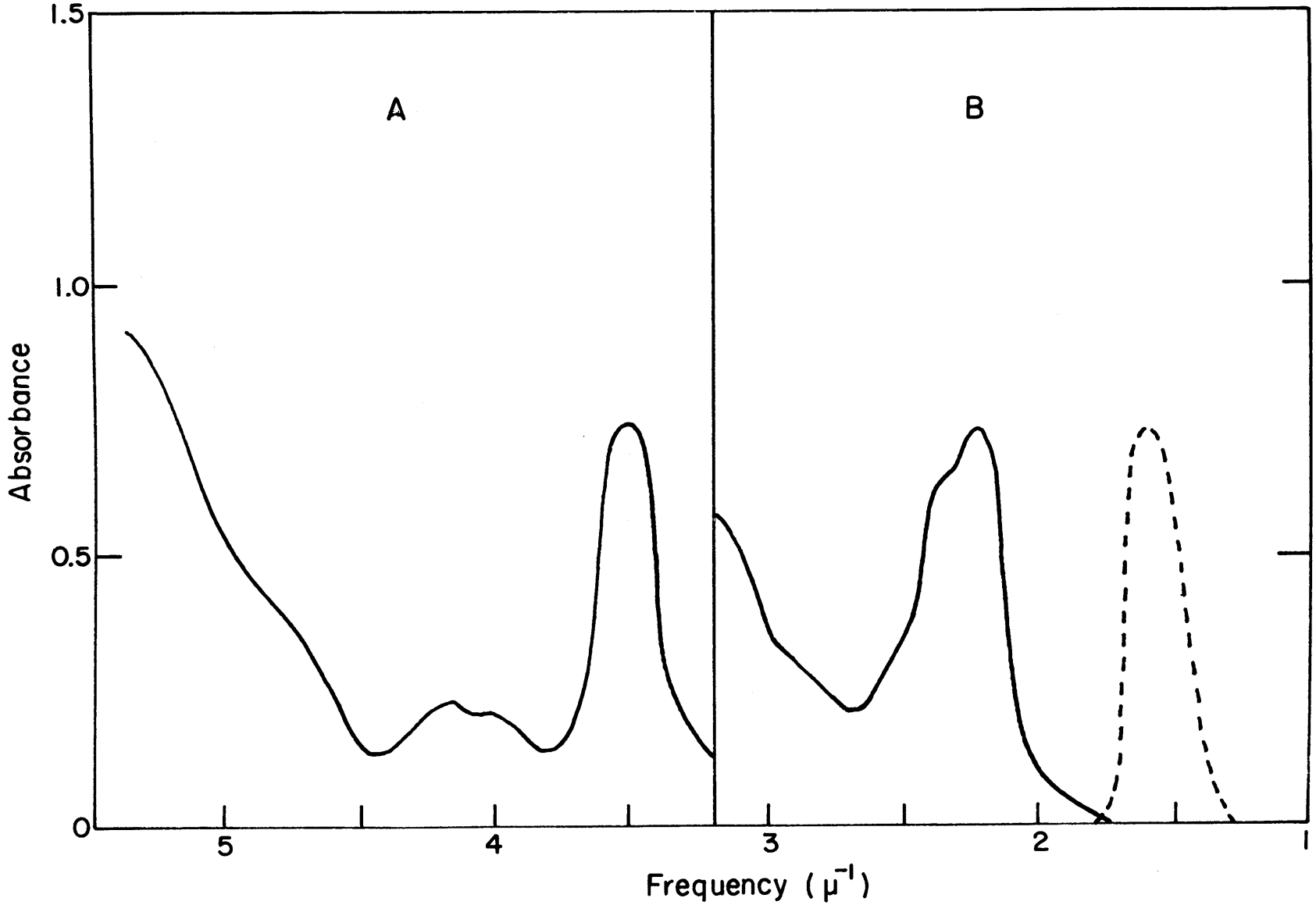
1.5
1.0
0.5
0
Absorbance
A
B
5
4
3
2
1
Frequency (μ⁻¹)

FIGURE IV-2

Low Temperature Absorption and Emission Spectra

of $Ru(bipyr)_3Cl_2$

Key

——— Absorption and ----- emission spectra of $Ru(bipyr)_3Cl_2$ in an ethanol:methanol (5:1) glass at 77°K. The luminescence is corrected for detector-monochromator response, and is in relative units.

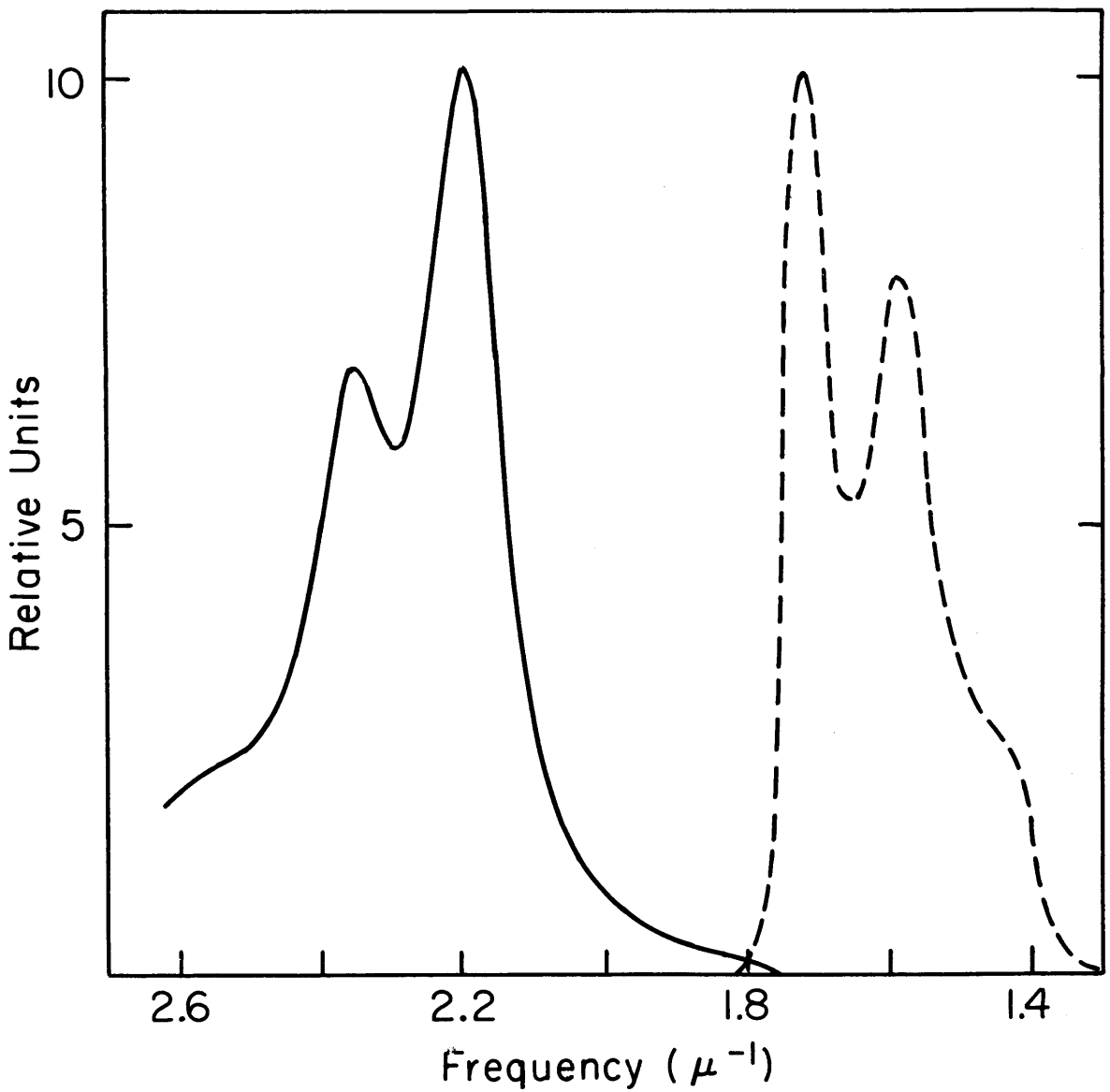
10
5
Relative Units
2.6
2.2
1.8
1.4
Frequency (μ^{-1})

FIGURE IV-3

Absorption and Emission Spectra of 2,2'-Bipyridine in 50% H_2SO_4

Key

——— Absorption, 2.5×10^{-5}M, 1cm path length, room temperature.

----- Fluorescence, 2.5×10^{-5}M, 77°K.

°°°°° Phosphorescence, 2.5×10^{-5}M, 77°K.

Both emission spectra are corrected for detector-monochromator response, and are in relative units.

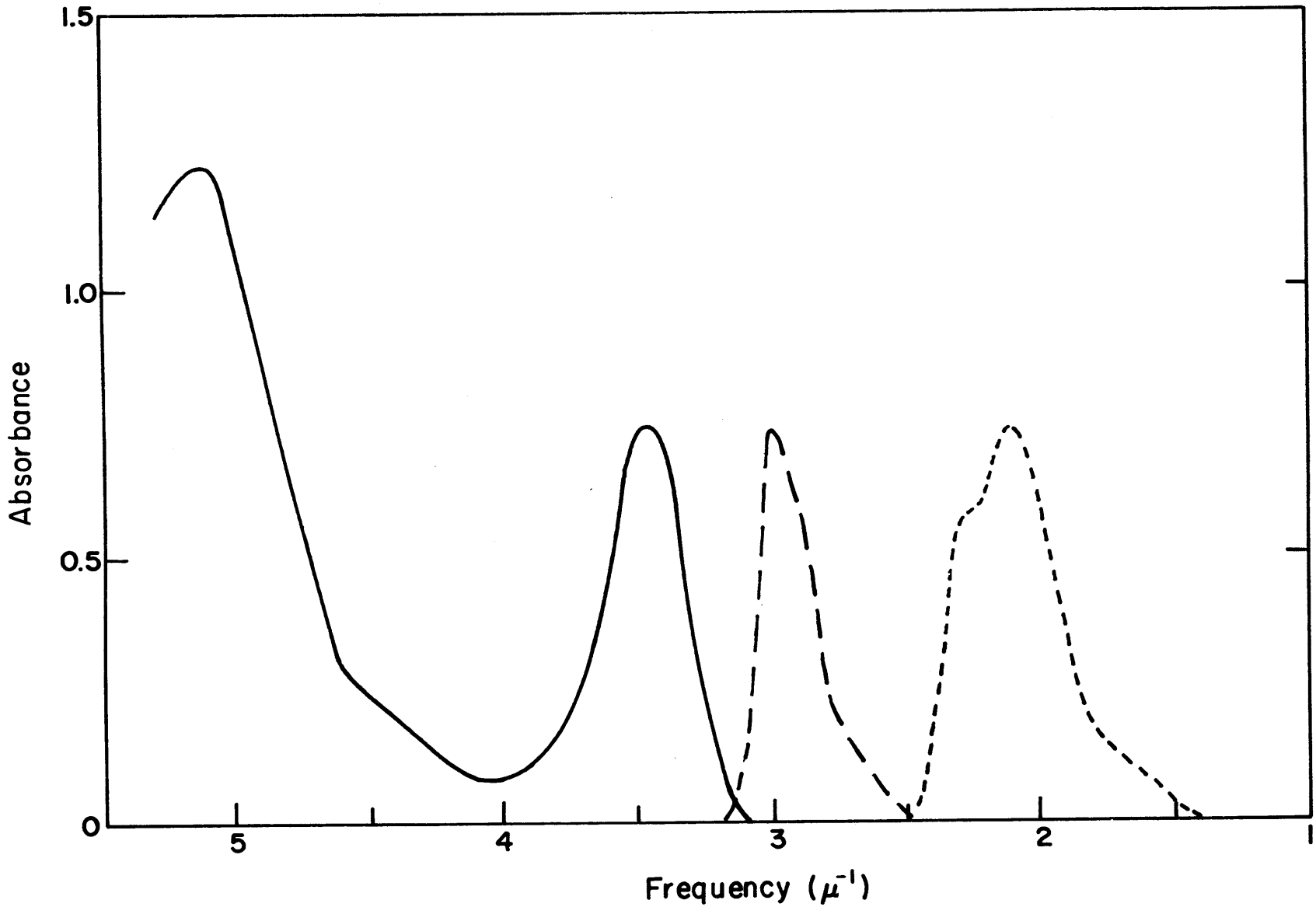
1.5
1.0
0.5
0
Absorbance
5
4
3
2
1
Frequency (μ^{-1})

It was found that the half-width of the ligand band at $3.45\mu^{-1}$ is temperature dependent. Figure IV-4 shows this band measured at both room temperature and 77°K. The half-width was $0.17\mu^{-1}$ at room temperature and $0.13\mu^{-1}$ at 77°K.

Infrared spectra-The infrared spectra of 2,2'-bipyridine and the chloride salt of its ruthenium(II) chelate are shown in Figures IV-5 and IV-6, respectively. Both spectra were recorded utilizing potassium bromide pellets. A comparison of the two curves indicates a one-to-one correspondence between most of the ligand and chelate bands. However, at least two new bands are evident in the chelate spectrum that are not in the ligand spectrum. They are located at 1450 cm^{-1} and 1310 cm^{-1}.

2. Temperature Dependent Spectral Properties

Spectral Data-Both the luminescence quantum yield and lifetime of $Ru(bipyr)_3Cl_2$ are strongly temperature dependent. Figure IV-7 shows the lifetime as a function of temperature in two different glass forming solvent mixtures - ethanol: methanol and 50% H_2SO_4. The temperature at which the large increase in lifetime occurs corresponds visually to glass formation. A comparable increase does not occur in the quantum yield, which remains essentially the same before and after glass formation. This result is shown in Figure IV-8 for an EPA solvent.

FIGURE IV-4

Temperature Dependence of the Half-width of the Protonated Ligand 3.45 μ^{-1} Band

Key

——— Absorption at room temperature.

----- Absorption at 77°K.

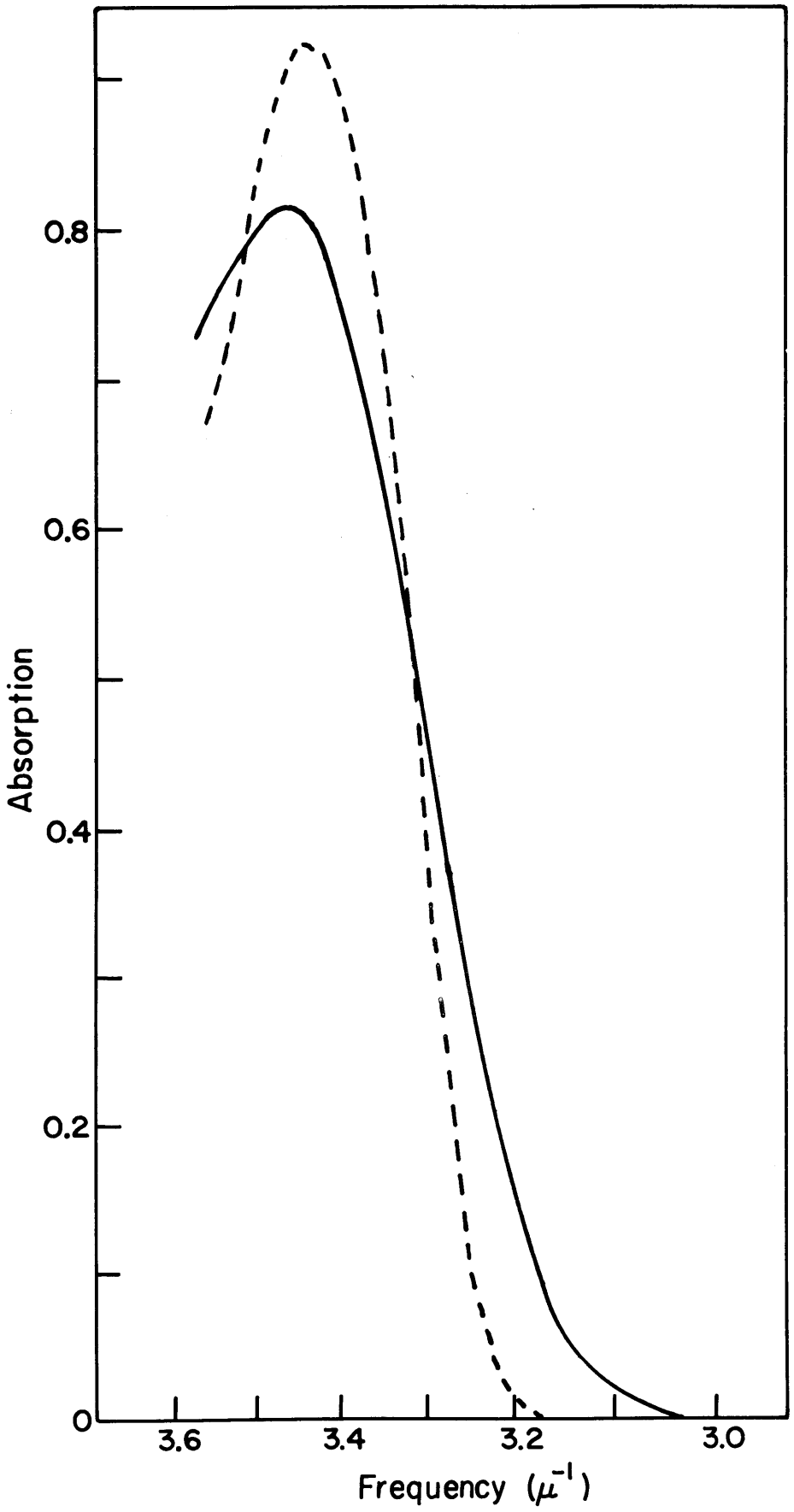
0.8
0.6
0.4
0.2
0
Absorption
3.6
3.4
3.2
3.0
Frequency (μ^{-1})

FIGURE IV-5

Infrared Spectrum of 2,2'-Bipyridine

KBr Pellet

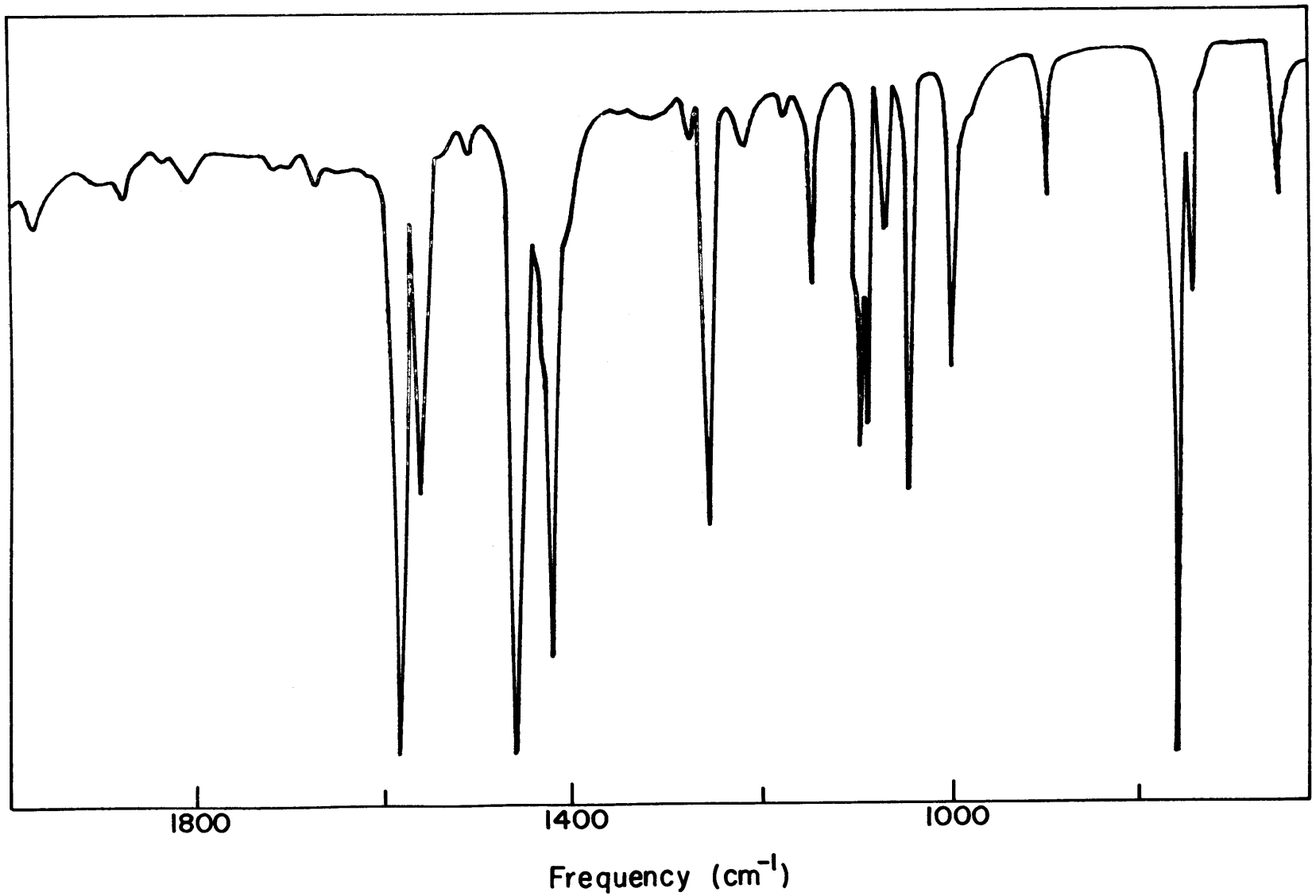
1800
1400
1000
Frequency (cm⁻¹)

FIGURE IV-6

Infrared Spectrum of $Ru(bipyr)_3Cl_2$

KBr Pellet

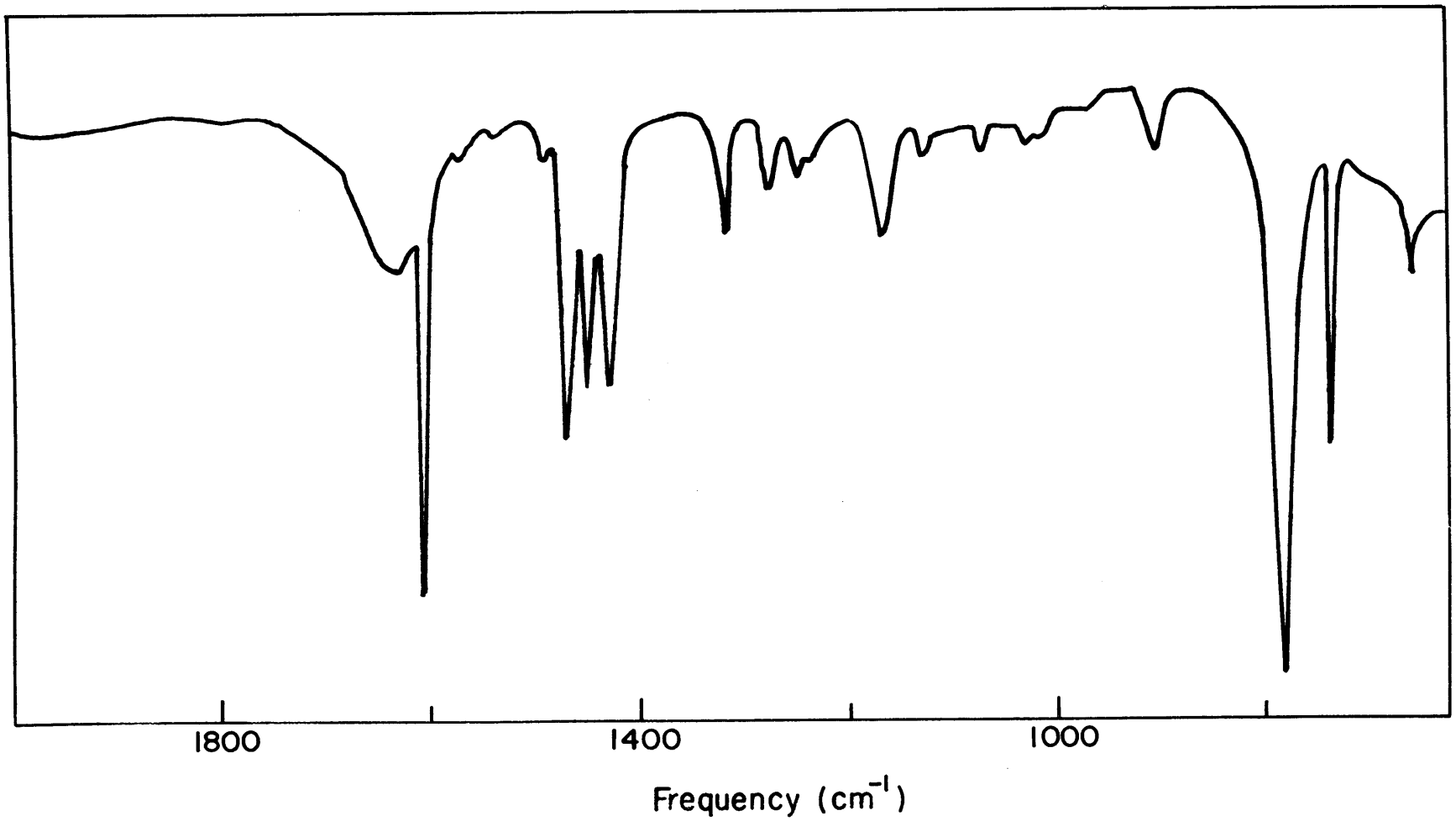
1800
1400
1000
Frequency (cm⁻¹)

FIGURE IV-7

Dependence of the $Ru(bipyr)_3Cl_2$ Lifetime on Temperature

Key

●●●●● Ethanol:methanol (5:1).

ΔΔΔΔΔ 50% H_2SO_4 .

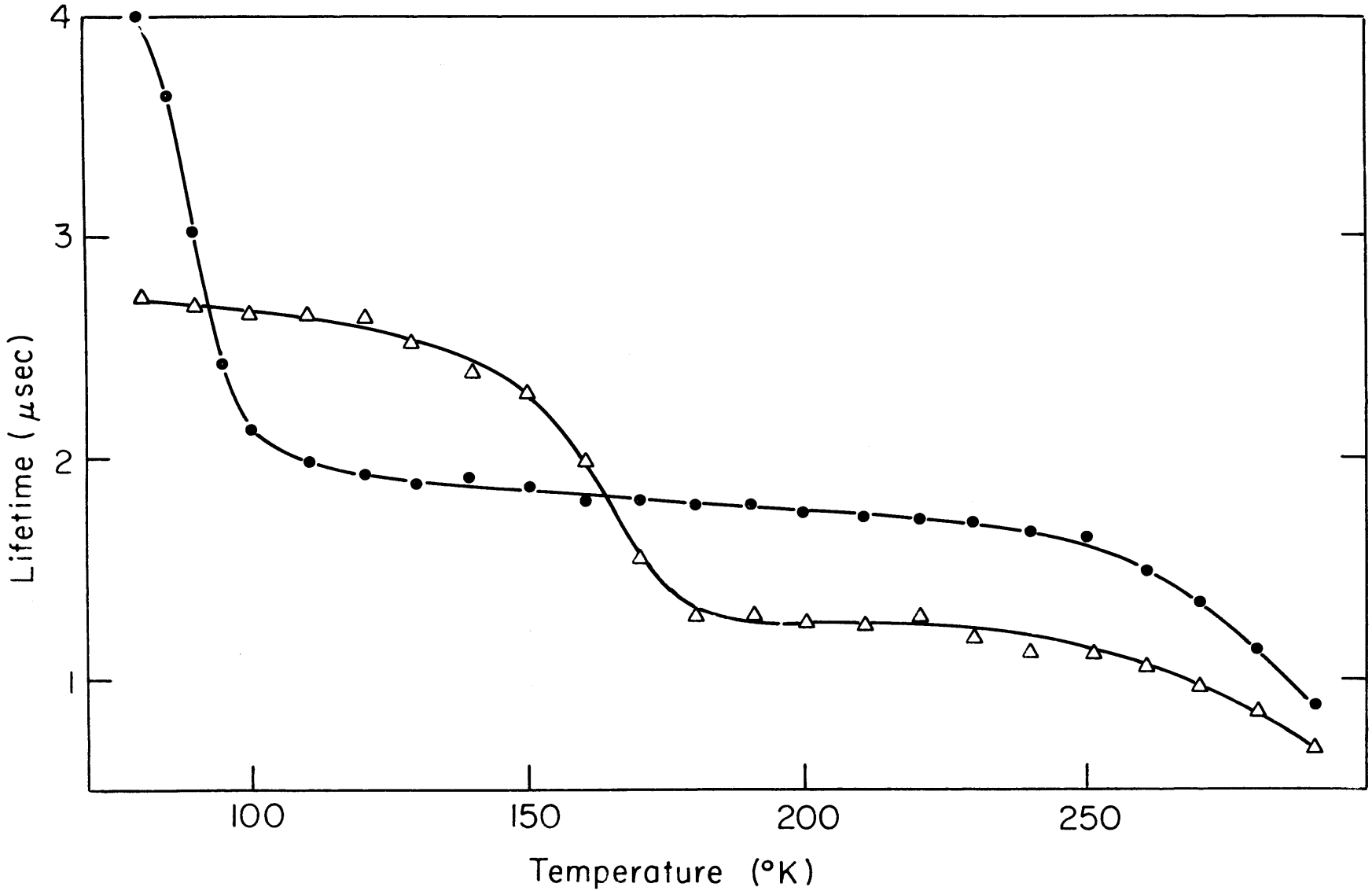
4
3
2
1
Lifetime (μsec)
100
150
200
250
Temperature (°K)

FIGURE IV-8

Dependence of the $Ru(bipyr)_3Cl_2$ Quantum Yield and Lifetime on Temperature

Key

ooooo Quantum yield.

ΔΔΔΔΔ Lifetime.

Both in EPA solvent.

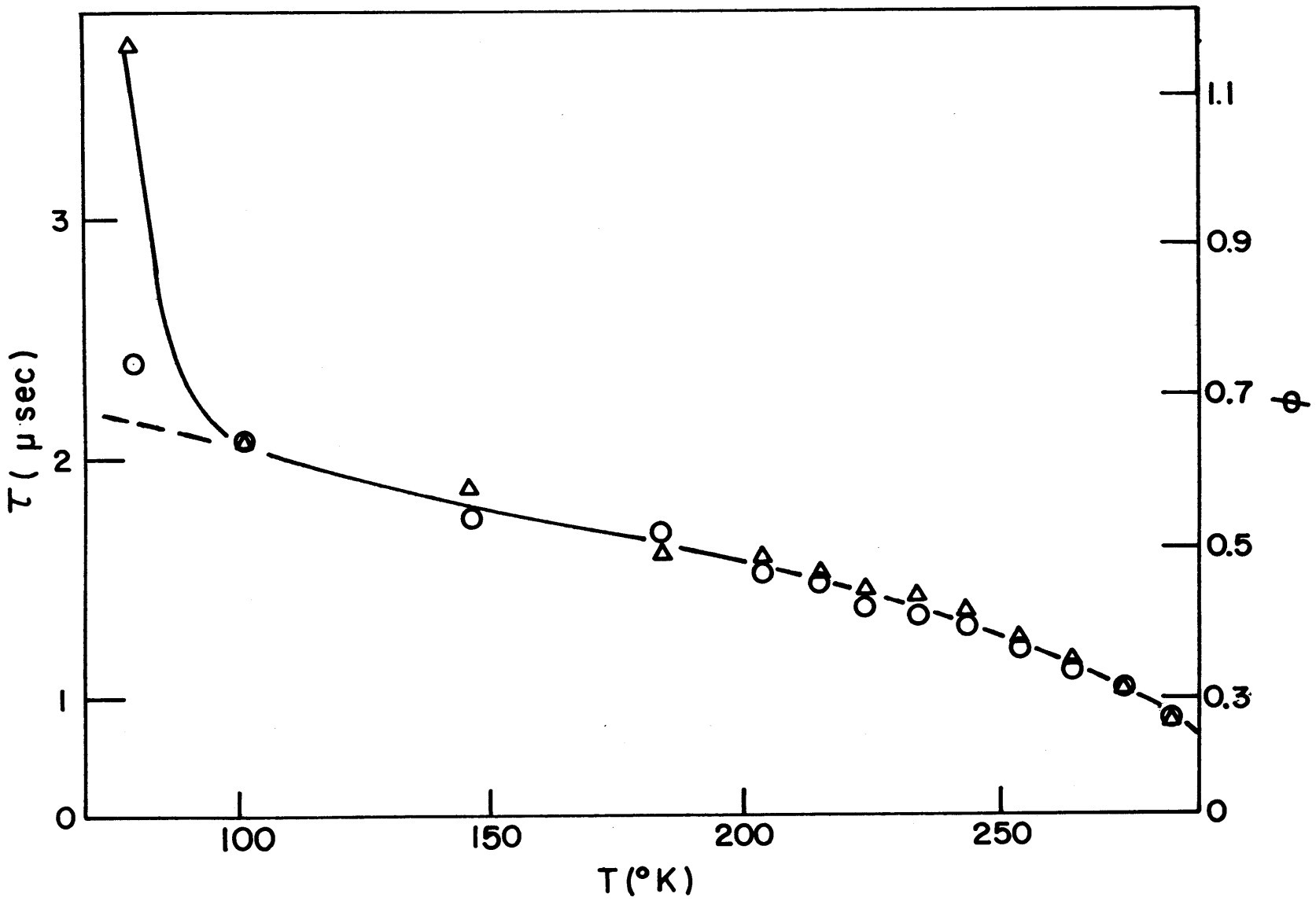
τ (μsec)
T (°K)
θ
0
1
2
3
100
150
200
250
0
0.3
0.5
0.7
0.9
1.1

Mathematical Treatment-The temperature dependence of the luminescence quantum yield and lifetime, at temperature above glass formation, is treated mathematically in a manner analogous to that outlined by other workers (2, 28). The reciprocal of the lifetime can be defined as the sum of all rate constants for reactions depleating the concentration of the excited state responsible for emission. This can be formulated as,

$$1/\tau = k_e + \Sigma_n k'_{dn} + \Sigma_m k_{dm} \exp(-\Delta H_m/RT) \qquad \text{IV-1}$$

where k_e is the rate constant for the emission process; k'_{dn} is the rate constant for the nth temperature independent non-emissive process; k_{dm} is the frequency factor for the mth temperature dependent non-emissive process; and ΔH_m is the activation energy for the mth temperature dependent process. The quantum yield can be defined in a similar manner.

If the above mathematical analysis is correct, the value of k_e should be determinable at any temperature by dividing the luminescence quantum yield, ϕ, by the lifetime. The values of τ, ϕ and k_e are shown in Table IV-2 for an EPA solvent. The value of k_e is constant at 2.9×10^5 sec^{-1}, except for 80°K where the solvent glass formation has started.

If it is assumed that only one temperature dependent process is operative, and if we define $1/\tau' \equiv k_e + \Sigma k'_{dn}$, then the Arrhenius equation can be derived from Equation IV-1, as,

TABLE IV-2

Temperature Dependance of the Luminescence Quantum Yield and Lifetime*

T(K°)	ϕ	τ (μ sec)	k_e ($sec^{-1} \times 10^{-5}$)
285	0.270	0.926	2.9
275	0.316	1.07	3.0
265	0.333	1.14	2.9
255	0.360	1.24	2.9
245	0.388	1.36	2.9
235	0.407	1.42	2.9
225	0.418	1.46	2.9
215	0.452	1.53	3.0
205	0.467	1.57	3.0
185	0.515	1.60	3.2
148	0.543	1.87	2.9
103	0.637	2.11	3.0
80	0.746	3.75	2.0

*$Ru(bipyr)_3Cl_2$ in EPA, 5×10^{-5} M

$$\log(1/\tau-1/\tau') = \frac{-\Delta H}{RT} + k_d \qquad \text{IV-2}$$

An analogous procedure yields the equation

$$\log(1/\phi-1/\phi') = \frac{-\Delta H}{RT} + \frac{k_d}{k_e} \qquad \text{IV-3}$$

where ϕ is the overall quantum yield of luminescence; and $\phi' \equiv k_e/(k_e+\Sigma k'_{dn})$.

Arrhenius Plots-An Arrhenius plot of the lifetimes using Equation IV-2, yields both the energies of activation and the frequency factors found in Table IV-3. All of the data in this table, except that for EPA, were obtained at temperatures above ambient, where the rates of the temperature independent processes were comparatively small. Figure IV-9 shows a sample plot for a DMF solvent.

For EPA, the data were obtained at temperatures below ambient, and the values of the temperature independent parameters (τ' or ϕ') were emperically established so that the data best fit a linear plot. Figure IV-10 shows a plot of the corrected data for the EPA solvent.

3. Wavelength Dependence of the Quantum Yield

The quantum yield luminescence for the $Ru(bipyr)_3CL_2$ complex was measured as a function of exciting wavelength at 77°K. Figure IV-11 shows the Quartz-Iodine lamp output and excitation spectra for a concentrated solution of the chelate in an ethanol: Methanol glass. Three separate curves are shown:

a) the capillary masked in a front surface excitation configuration. This spectrum matches the lamp output quite well.

TABLE IV-3

Arrhenius Constants from Lifetime Data*

Constants	H_2O	EPA	DMF	EtOH: MeOH
ΔH (cm^{-1})	885	1,400	1,600	3,100
k_d (sec^{-1})	1.2×10^8	5.0×10^8	2.4×10^4	5.4×10^{12}

*for $Ru(bipyr)_3Cl_2$ at 5×10^{-5} M.

FIGURE IV-9

Arrhenius Plot for $Ru(bipyr)_3Cl_2$ in DMF

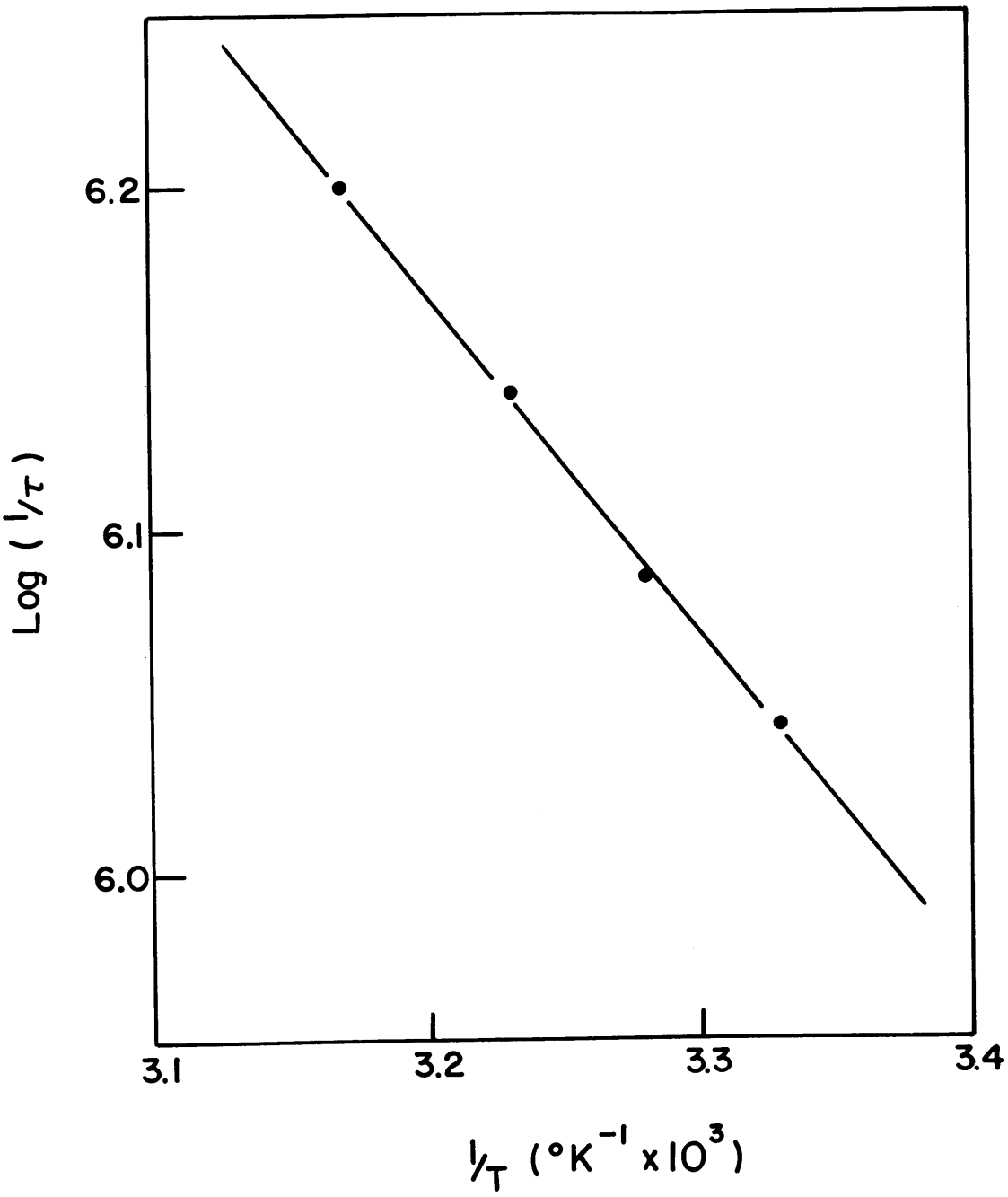
6.2
6.1
6.0
Log (1/τ)
3.1
3.2
3.3
3.4
1/T (°K⁻¹ x 10³)

FIGURE IV-10

Arrhenius Plots for EPA

Key

ΔΔΔΔΔ Quantum yield with $\phi'=0.480$.

ooooo Lifetime, with $\tau'=1.67$ sec.

$\Delta H=1,400\ cm^{-1}$, lifetime intercept is 8.70, quantum yield intercept is 3.22.

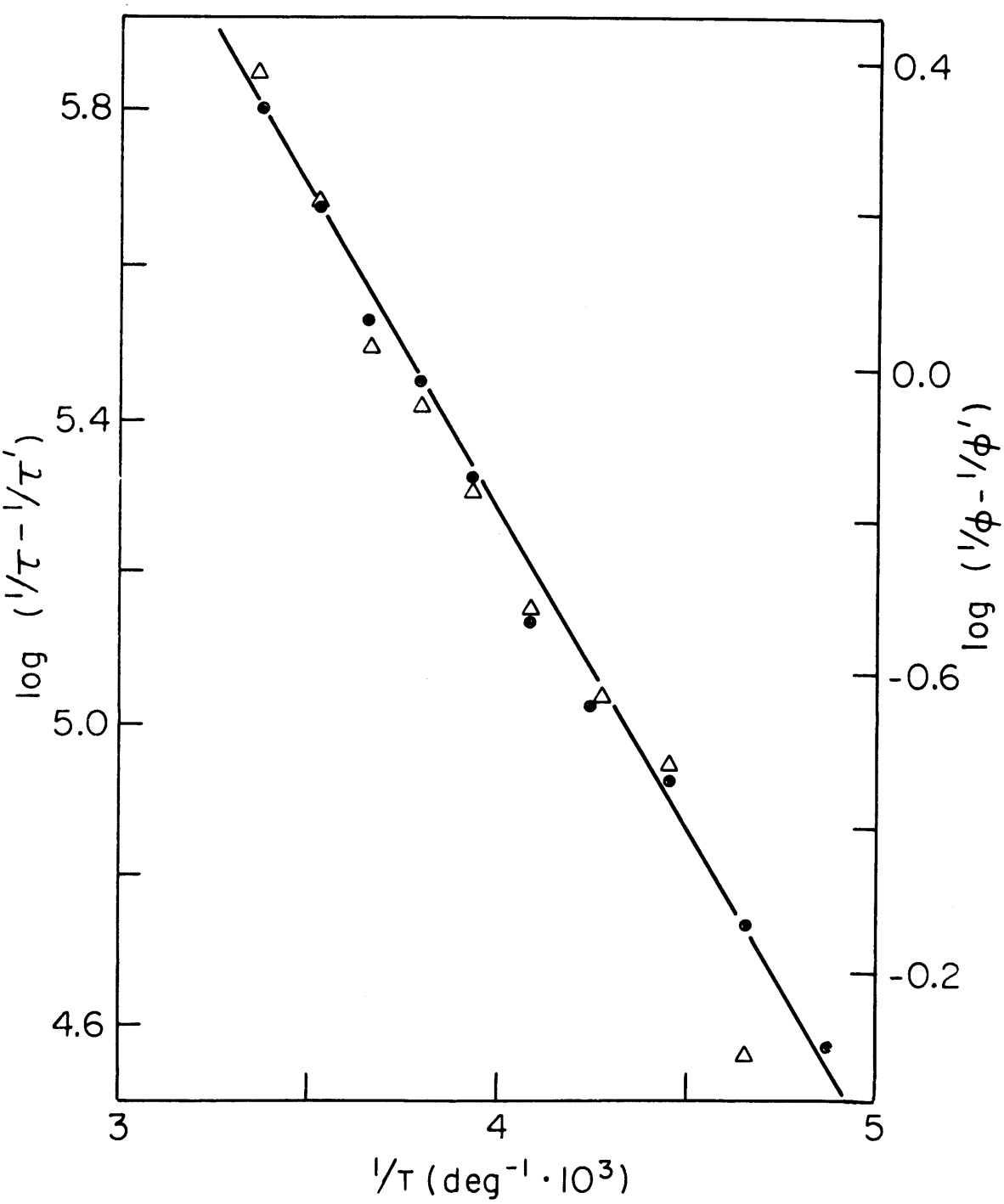
5.8
5.4
5.0
4.6
log (1/τ - 1/τ')
0.4
0.0
-0.6
-0.2
log (1/φ - 1/φ')
3
4
5
1/T (deg⁻¹ · 10³)

FIGURE IV-11

Excitation Spectra of $Ru(bipyr)_3Cl_2$

Key

——— Lamp output.

----- Front surface excitation spectrum.

°°°°° Normal 90° excitation spectrum.

-·-·- Unmasked cell.

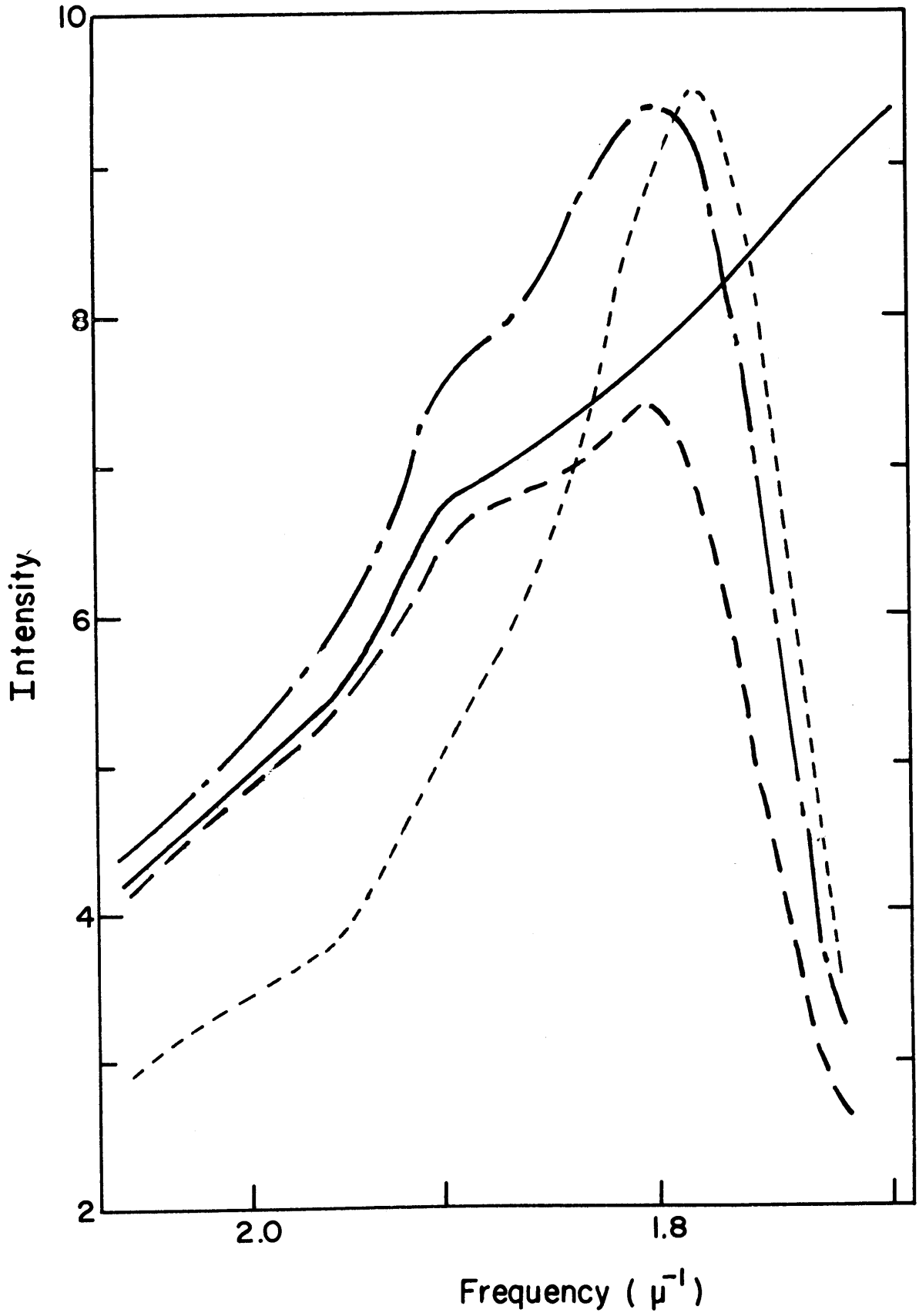
10
8
6
4
2
Intensity
2.0
1.8
Frequency (μ⁻¹)

b) the capillary masked in a normal 90° excitation configuration. This spectrum shows a large discrepancy, probably due to changes in the emission-intensity-distance profile across the tube diameter. This profile change would be caused by relatively small increases in T (λ').

c) the capillary in an unmasked configuration. This spectrum is some linear combination of excitation curves (a) and (b). The shape varies considerably as a function of the position of the quartz capillary tube.

This particular set of spectra indicates that great care must be taken to properly determine the wavelength dependency of the quantum yield under the necessary experimental conditions. For $Ru(bipyr)_3Cl_2$ it is thus evident that no change in the quantum yield is observed.

4. Wavelength Dependence of the Emission Lifetime

The emission lifetime, for the $Ru(bipyr)_3Cl_2$ complex in an ethanol: methanol glass at 77°K, was measured as a function of exciting wavelength. The lamp used, provided by E. Meserve of TRW, had spectral lines in the wavelength region 300 to 600 mμ. Figure IV-12 shows the log intensity vs. time plots for both "blue" and "red" excitation. To the accuracy of the experiment no difference in the lifetime was observed.

B. Discussion

1. Transition types

Figure IV-13 shows the orbital diagram for $Ru(bipyr)_3Cl_2$,

FIGURE IV-12

Log Intensity vs. Time Plots for

$Ru(bipyr)_3Cl_2$ Emission

Key

ooooo Excitation with frequencies smaller than 1.95 μ^{-1}.

+++++ Excitation with frequencies larger than 2.04 μ^{-1}.

Measured in an ethanol:methanol glass at 77°K.

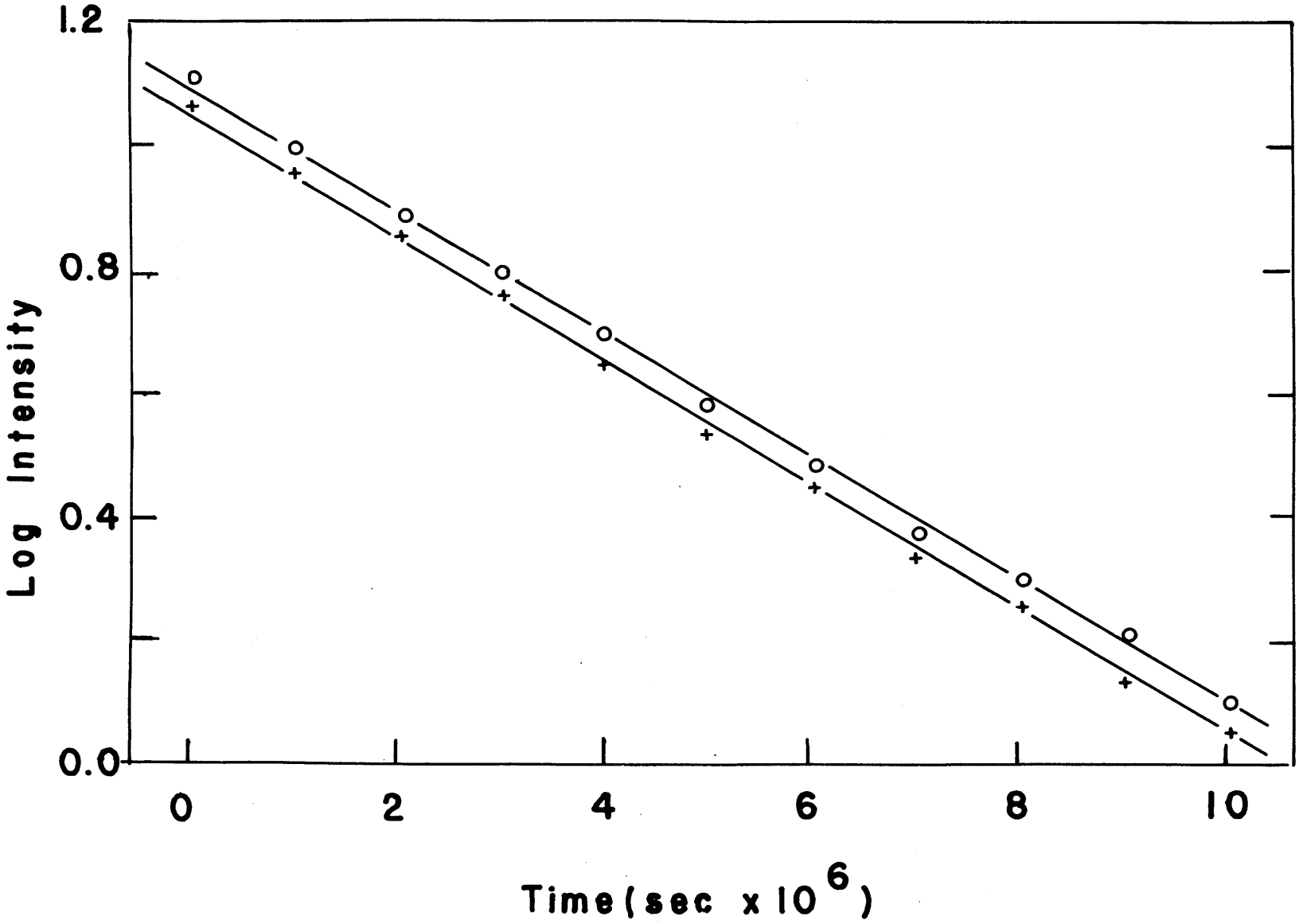
1.2
0.8
0.4
0.0
Log Intensity
0
2
4
6
8
10
Time (sec x 10^6)

FIGURE IV-13

Orbital Diagram for $Ru(bipyr)_3Cl_2$

The diagram is consistent with D_3 symmetry. The metal ion has a $[Kr]4d^6$ low-spin configuration. The ligands have all of the σ and π orbitals filled. Δ is the trigonal splitting.

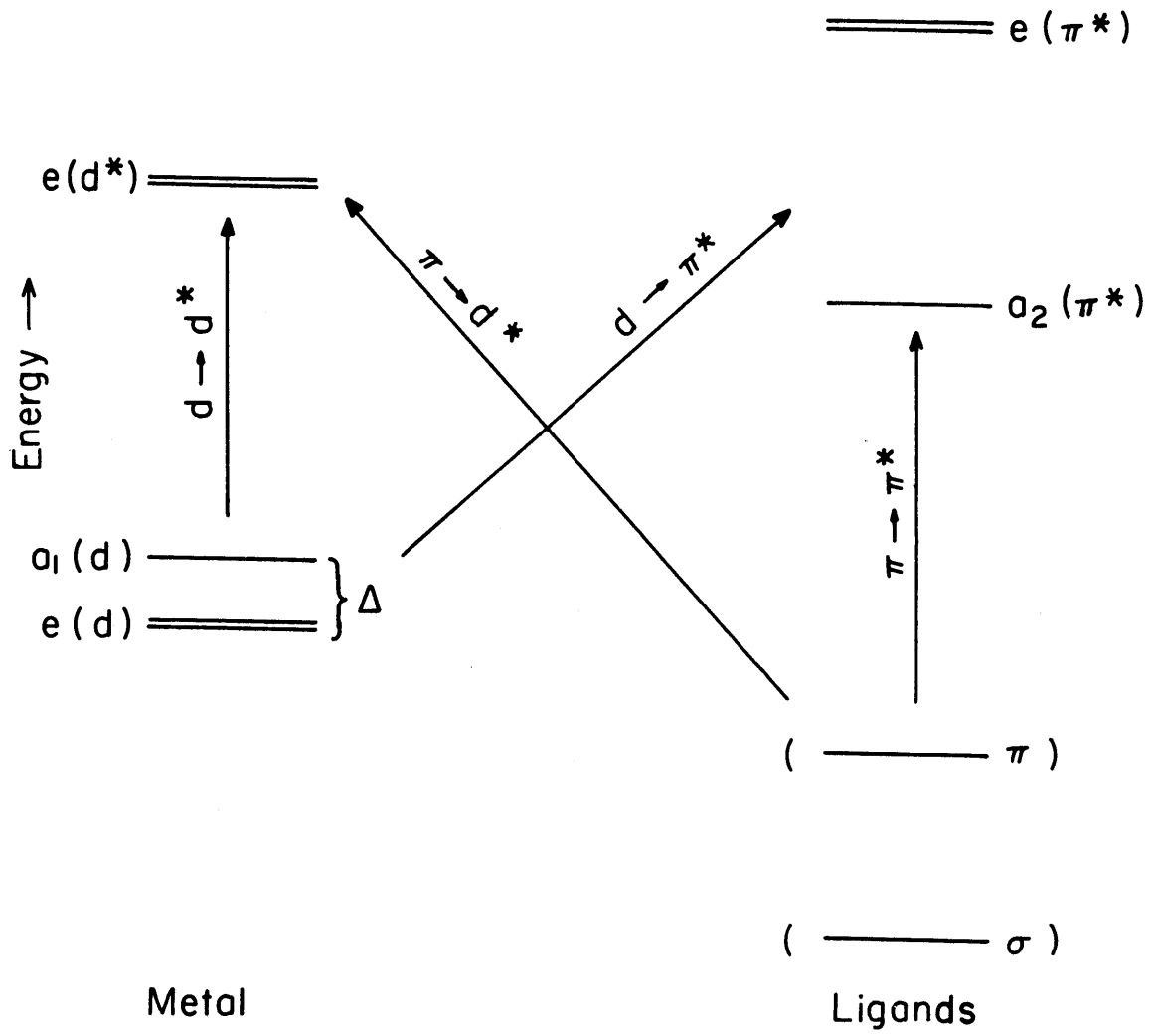
e (π*)
e(d*)
Energy
d → d*
π → d*
d → π*
a2 (π*)
π → π*
a1 (d)
e (d)
Δ
(π)
(σ)
Metal
Ligands

consistent with D_3 symmetry, used in this paper for the classification of transition types. Most discussion of the electronic properties of $Ru(bipyr)_3Cl_2$ have assumed an orbital diagram compatible with octahedral microsymmetry of the ruthenium-nitrogen skeleton, even though the overall symmetry of the complex is D_3. The only significant difference between the two symmetries is the separation of the t_{2g} (d) orbitals into $a_1(d)$ and e(d) components (†). The energy separation ,Δ, of these components will depend upon the amount of trigonal splitting, which has been determined to be $0.20\mu^{-1}$ for this complex. As Palmer and Piper have shown (33) this splitting is not necessarily related to a geometric distortion from the O_h microsymmetry, but may also be due to a degree of covalency in the bonding. Calculations in our laboratory (16) have shown that sigma bonding alone can yield the trigonal splitting observed in both this bipyridine complex and those discussed by Palmer and Piper (33).

The electronic transitions of $Ru(bipyr)_3Cl_2$ can be separated into four general categories as shown in Figure IV-13. The first are the ligand $\pi \rightarrow \pi^*$ transitions; $\pi \rightarrow a_2(\pi^*)$ and $\pi \rightarrow e(\pi^*)$. The second are the $d \rightarrow d^*$ metal transitions; $e(d) \rightarrow e(d^*)$ and $a_1(d) \rightarrow e(\pi^*)$. The third are the charge-transfer $d \rightarrow \pi^*$ transitions; $e(d) \rightarrow a_2(\pi^*)$ and $a_1(d) \rightarrow a_2(\pi^*)$, and $e(d) \rightarrow e(\pi^*)$ and $a_1(d) \rightarrow e(\pi^*)$. The fourth is the charge-transfer $\pi \rightarrow d^*$

† In the notation used in this thesis (d) indicates a metal orbital and (π) indicates a ligand orbital.

transition, $\pi \rightarrow e(d^*)$. Since the electronic states will be strongly mixed, it is not proper, other than for classification, to treat the ligand and metal orbitals as two separate manifolds.

The two low energy charge-transfer $d \rightarrow \pi^*$ transitions are both electronically allowed. The $e(d) \rightarrow a_2(\pi^*)$ transition, designated $\perp$CT, is polarized perpendicular to the C_3 axis of the complex, while the $a_1(d) \rightarrow a_2(\pi^*)$ transition, designated $\parallel$CT, is polarized parallel to the C_3 axis. This agrees with the single crystal absorption data of Palmer and Piper(33). According to their data the $\parallel$CT band has a low intensity. This is probably due to a lack of overlap of the $a_1(d)$ orbital with the $a_2(\pi)$ orbitals.

2. Absorption and Emission

A comparison of the chelate and protonated ligand absorption spectra, Figure IV-1 and IV-3 respectively, aids in the identification of the chelate $\pi \rightarrow \pi^*$ transitions. The bands in the chelate spectrum at 3.50 μ^{-1} and 5.40 μ^{-1} can thus be assigned as those derived from the ligand $\pi \rightarrow a_2(\pi^*)$ and $\pi \rightarrow e(\pi^*)$ transitions, respectively, according to the nomenclature of Figure IV-13.

The unusual broadness of the ligand 3.45μ^{-1} band in comparison to the chelate 3.50μ^{-1} band is due to rotation about the 2,2'-carbon bond. This is substantiated by the half-width data. At 77°K, the 3.45μ^{-1} ligand band halfwidth is the same as that for the 3.50μ^{-1} chelate band at room temperature.

The two remaining intense bands, at ca. $2.3\mu^{-1}$ and $4.1\mu^{-1}$, in the chelate spectrum have been assigned as charge-transfer $d\rightarrow\pi^*$ transitions on the basis of Jørgensen's (23) assignments for similar complexes. Both of these charge-transfer bands have two vibronic components resolved at room temperature, $4.20\mu^{-1}$ and $4.00\mu^{-1}$ for the high energy transition and $2.37\mu^{-1}$ and $2.20\mu^{-1}$ for the low energy transition. There is a reversal in the intensitites of the vibronic components of the ca. $4.1\mu^{-1}$ band in comparison to those of the ca. $2.3\mu^{-1}$ band. This difference is probably caused by a $\pi\rightarrow e(d^*)$ charge-transfer transition. Assignment of the bands of lower intensity cannot be made with certainty. The shoulder at $4.80\mu^{-1}$ can be attributed to a $\pi\rightarrow\pi^*$ transition, since it also appears in the ligand spectrum. The bands at $2.90\mu^{-1}$ and $3.10\mu^{-1}$ could be the metal $a_1(d)\rightarrow e(d^*)$ and $e(d)\rightarrow e(d^*)$ transitions.

Crosby and Klassen (25) attributed the low temperature absorption and emission progressions to a perturbed vibration of the aromatic ring.

Some doubt concerning this conclusion is found in the paper by Schilt and Taylor (40), which compares the infra-red spectrum of 2,2'-bipyridine with several of its metal chelates. The ring frequencies of the free 2,2'-bipyridine were assigned to bands at 1450 cm^{-1} and 1600 cm^{-1}. In all cases it was observed that the ring frequencies were increased upon coordination. Thus it is improbable that the $0.13\mu^{-1}$ emission progression is due to a perturbed virbration of the aromatic ring.

Shilt and Taylor (40) obliterated a large segment of the spectral region by measuring the infra-red spectra of the perchlorate salts of the metal chelates in Nujol mulls. This precluded their commenting on the frequencies of interest to this study.

From the infrared spectra in Figures IV-5 and IV-6 it was noted that at least two new bands are present in the chelate spectrum, those at 1450 cm^{-1} and 1310 cm^{-1}. With the amount of experimental data presently available, it is impossible to determine with certainty the origin of these bands. However, it is possible that both the emission progression and the new infra-red bands are due to ruthenium-nitrogen skeletal vibrations from structures such as:

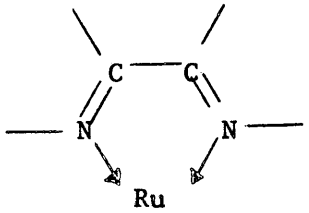

3. Long-Wavelength Absorption Band

The long-wavelength absorption tail in the vicinity of 1.8 - 1.9μ^{-1} cannot be due to the normal tailing of an electronic transition because of the large frequency difference of 0.50μ^{-1} between the emission and the absorption peaks. Crosby et al. (10) suggested that this absorption tail was due to a d→ d* transition. However, Palmer and Piper (33) demonstrated that the d-orbital split (10 Dq) would be very large for the $Ru(bipyr)_3Cl_2$ complex, and any d →d* spin-allowed transitions would appear at energies higher than the

charge-transfer band at ca. $2.3\mu^{-1}$.

Crosby and Klassen (25) later assumed that the long-wavelength tail was due to vibronic components of the $\perp$CT band. This assumption leads to unresolvable difficulties. First, it can be demonstrated that the emission observed cannot arise from a spin-allowed transition associated with the CT band at ca. $2.3\ \mu^{-1}$. Using the equations given by Suzuki (46) for determining intrinsic lifetimes from absorption data, and the integrated band intensity (†) given by Palmer and Piper (33), a value of 87 nanoseconds can be calculated if the emission came from the excited state associated with the $\perp$CT band. The experimental lifetime at 80°K is about four microseconds, inconsistent with such an interpretation.

Second, Crosby and Demas (11), in assigning the emission as phosphorescence, indicated that there is no gap between the end of the absorption band and the start of the emission. If the singlet-triplet energy split were very small, at room temperature the lifetime of the emission would be equal to that for the spin-allowed transition, because of the thermal equilibrium established between the lowest triplet and the lowest excited singlet states. This is not experimentally observed.

---

† Divided by three since there are three legands.

If the long-wavelength absorption tail were due to the || CT transition, the emission could then be due to fluorescence from the excited state associated with this transition. The polarization data of Palmer and Piper (33) show that the $\perp$CT transition is 26.5 times more intense than the ||CT transition. This yields a calculated fluorescence lifetime of 2.3μsecs for emission from the ||CT state. However, if the emission were fluorescence, the absence of phosphorescence cannot be explained. The extent of spin-orbit coupling in a molecule containing ruthenium, should yield a large rate of intersystem crossing, thus significantly populating the lowest triplet level and partially removing the spin-forbiddenness of phosphorescence. This would result in a high population of the lowest triplet level and both fluorescence and phosphorescence would be expected at 77°K. Such is not observed.

Paris (34) suggested that the absorption tail on the ||CT band was a singlet-triplet transition. Normally this type of transition would be forbidden, but the spin-orbit coupling will partially remove the applicability of the spin selection rules. An increase in the strength of singlet-triplet transitions would also shorten the lifetime of phosphorescnece. It will be shown that Paris' interpretation is consistent with all of our experimental data, that the long wavelength absorption tail is most probably a singlet-triplet transition and that the emission is the phosphorescence associated with this transition.

4. Tempreature Dependent Spectral Properties

Figure IV-7 shows the lifetime of $Ru(bipyr)_3Cl_2$ as a function of temperature. This curve can be resolved into three sections. The first is the large change occuring with glass formation. As shown in Figure IV-8, this change does not occur in the quantum yield. This indicates that the excited state rate constants important at these temperatures are changed by a multiplicative factor which divides out in the quantum yield expression. Assuming that the observed emission is phosphorescence, this multiplicative factor can probably be associated with a decrease in spin-orbit coupling resulting from the rigidity of the glass.

The second section of the lifetime-temperature curve is that at temperatures from about 200°K and lower to the glass formation point. In this region, there seems to be a process occuring that involves a small energy of activation. Again assuming phosphorescence, this can be tentatively assigned as due to an internal conversion between an excited vibrational level of the lowest triplet state and the ground state. The energy of activation would then be that energy necessary to promote the molecule to the coupled vibrational level of the triplet responsible for this internal conversion process. The data are not sufficiently precise to determine ΔH or k_d.

The last segment of the curve is that at temperatures above 200°K. Here the assumption of only one important temperature dependent process is valid. The nature of this process will be discussed in the next section. The Arrhenius data in Table IV-3 obtained for several solvents are reasonably similar. However, all mixed solvents, except EPA, yielded anomalously large activation energies and frequency factors. In Table IV-3, the ethanol: methanol solvent is shown as typical example. The cause of the increased Arrhenius constants has not yet been determined.

5. State Diagram

A state diagram corresponding to a phosphorescence mechanism of luminescence for $Ru(bipyr)_3Cl_2$ is shown schematically in Figure IV-14. All of the singlet state energies shown in the diagram were determined directly from absorption spectra except that the ^{1}CT state. The only triplet state energy directly determined from absorption and emission spectra was the lowest triplet level.

The transition assignments for the triplet charge-transfer states are consistent with the spectral data. A fluorescence life-time of 2.3 μsecs has been calculated in this paper for the ^{1}CT transition. If the emission were phosphorescence associated with this transition, spin selection rules would have to be completely removed in order to yield the measured lifetime of 4 μsecs. If these selection rules were removed, singlet-triplet absorption bands would occur with the

FIGURE IV-14

$Ru(bipyr)_3Cl_2$ State Diagram

Key

_____ Measured energy levels.

----- Estimated energy levels.

All rate constants are in units of sec^{-1}.

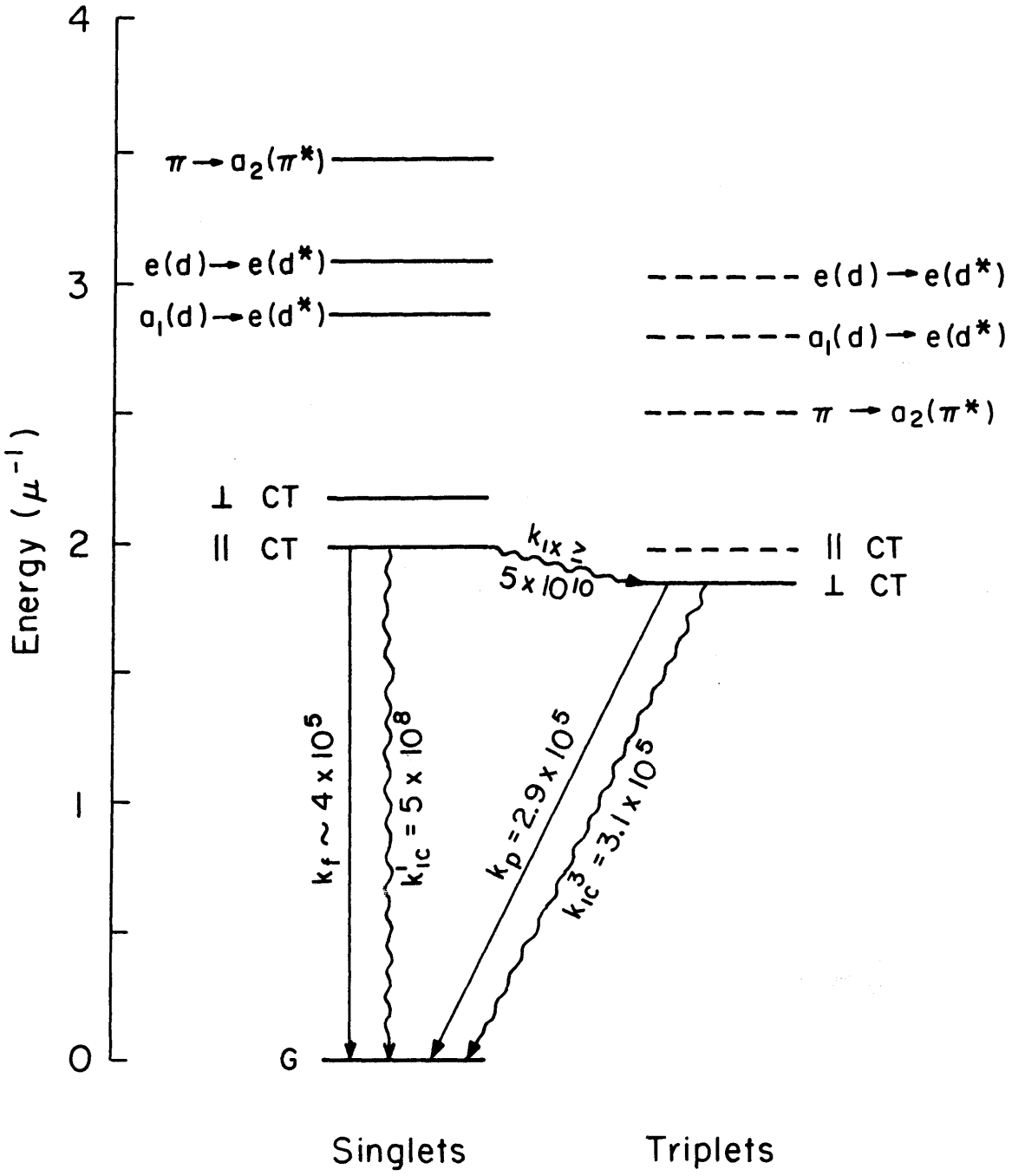
4
3
2
1
0
Energy (μ^{-1})
$\pi \rightarrow a_2(\pi^*)$
$e(d) \rightarrow e(d^*)$
$a_1(d) \rightarrow e(d^*)$
$e(d) \rightarrow e(d^*)$
$a_1(d) \rightarrow e(d^*)$
$\pi \rightarrow a_2(\pi^*)$
$\perp$ CT
$\parallel$ CT
$k_{1x} \geq 5 \times 10^{10}$
$\parallel$ CT
$\perp$ CT
$k_f \sim 4 \times 10^5$
$k_{ic}' = 5 \times 10^8$
$k_p = 2.9 \times 10^5$
$k_{ic}^3 = 3.1 \times 10^5$
G
Singlets
Triplets

same intensity as singlet-singlet absorption bands. The data do not indicate that this is true, therefore we have assigned the lowest triplet level to the $\perp$CT transition.

In pure solvents the Arrhenius data probably represent the deactivation of the lowest excited triplet state by the thermal population of the $\parallel$CT band. Since the energy of activation from the Arrhenius plots would respresent the lowest triplet to lowest excited singlet energy difference, the energy of the $\parallel$CT singlet is thus established.

Using the transition energies shown in Figure IV-14, the value of 10 Dq can be calculated to be $2.96\mu^{-1}$, while the value of the trigonal splitting can be calculated to be 0.20_{μ}^{-1}. The magnitude of this trigonal splitting is in agreement with that found by Palmer and Piper (33) for the tris-bipyridine nickel(II) complex, and the magnitude of 10 Dq is in agreement with the discussion in their footnote 88.

The intrinsic fluorescence lifetime associated with the $\perp$CT transition has been calculated, in this paper, to be 87 nanoseconds. Using the rule that spin-forbidden transitions occur at rates of 10^6 less than those processes spin-allowed, a phosphorescence rate constant (k_p) of 12 sec^{-1} is predicted for the $\perp$CT transition. If the emission rate constants (K_e) in Table VI-1 were taken to be that of phosphorescence, then the spin-orbit coupling must enhance

spin-forbidden processes by a factor of about 10^4. This enhancement would also increase the magnitude of the intersystem crossing rate constant (k_{ix}) to about 10^{11} to 10^{12}, since molecules with no large amounts of spin-orbit coupling have corresponding rates of 10^7 to 10^8.

Two consecutive excited state processes are involved in the thermal deactivation of the excited triplet. Thus a complex mathematical relationship will be necessary to evaluate the Arrhenius data, unless one of the rate constants associated with these two processes is much larger than the other. Since the frequency factors in Table II are of the magnitude of 10^8 to 10^9 sec^{-1} and the intersystem crossing rates are expected to be of the magnitude of 10^{11} and 10^{12}, the frequency factors can be identified with the singlet internal conversion rate constant (k^1_{ic}) and Equations IV-2 and IV-3 can be considered valid.

The assignment of the frequency factors as k^1_{ic} is in agreement with the data in two respects. First, the calculations performed in this paper predict an emission rate constant from the ^{1}CT singlet of 4.3×10^5 sec^{-1}. Since the values of k^1_{ic} are at least one thousand times larger than the emission rate constant, only 10^{-3} of the thermally populated singlets should emit. To the limit of the instrumentation used, no luminescence to the blue of the phosphorescence could be detected. Second, the quantum yield of phosphorescence should vary with the exciting wavelength to the extent

of $k_{ix}/(k_{ix}+k_{ic}^{1})$, depending on whether the excitation were on the ^{1}CT singlet or the ^{1}CT triplet band. With the previously mentioned value of k_{ix} and k_{ic}^{1}, the ratio should be unity. Experimentally it was determined that k_{ix} must be at least one hundred times larger than k_{ic}^{1}.

The value of the rate constant for internal conversion between the lowest excited triplet andthe ground state (k_{ic}^{3}) can be determined from the measured lifetime and k_{p}, at any temperature where the thermal population of the excited singlet is negligible. For EPA the lifetime chosen was τ' and the value of k_{ic}^{3} determined was 3.1×10^{5} sec^{-1}.

V. Chemiluminescence Studies

A. Qualitative Observations

1. Chelate reactions

Two different types of systems producing chemiluminescence by electron transfer to a potential emitter have been investigated. The overall reaction for the first type of system studied can be written as

$$ML_x^{+m} + \text{reductant} \rightarrow ML_x^{+n} + h\nu$$

where M represents a metal ion and L a suitable ligand.

The tetra-chloro complexes of lead(IV), thallium(III) and tin (IV) were reduced to the fluorescent lower stable oxidation state. None of the reactions chemiluminesced. The lack of emission could be due to a change in the ligand number or a geometric reorientation, both of which would drain away the energy of any excited states produced.

Attemps to chemiluminesce the tris-bipyridine complex of iridium(IV) were unsuccessful. The complex was synthesised in the plus-three oxidation state. Most probably the strong oxidizing conditions necessary to produce the higher oxidation state decomposed the chelate.

One successful group of complexes was that containing ruthenium (III) as the central metal ion. The ligands were 2,2'-bipyridine, 5-methyl -1,10-phenanthroline, 5,6-dimethyl -1,10-phenanthroline, and 3,5,6,8-tetramethyl -1,10-phenanthroline . The corresponding1,10-phenanthroline complex did not chemiluminesce. This is probably due to

the reactive 5,6 position on the phenanthroline ring. It would not be difficult for one of the reagents involved in either oxidation or reduction to chemically attack these positions.

Experimentally, an acidic, aqueous solution millimolar in the ruthenium(II) complex was treated with solid lead dioxide. The lead dioxide was subsequently separated by centrifugation from the resulting solution of the ruthenium(III) complex. The ruthenium(III) solution was then added to aqueous base and light emission was observed. Subsequent spectroscopic examination of the reacted solution showed that the ruthenium complex had been reduced to its initial oxidation state. The intensity of the emitted light depended upon the strength of the base used. When a solution of the Ru(III) $(bipyr)_3Cl_3$ complex in 0.1N sulfuric acid was allowed to react with 9N NaOH, the orange chemiluminescence was clearly visible in a dimly lighted room. The duration of light emission was very short, generally less than one second.

One other reducing agent gave a chemiluminescent reaction. If the ruthenium(III) complex was generated in 0.1N H_2SO_4 and 0.1N N_2H_4 in the same solvent was added, the emitted light was quite intense. By choosing different ratios of chelate to reducer, the chemiluminescence could be made to behave differently. At low ratios, i.e. 10^{-3}M chelate and 1M N_2H_4, the light emission occured only where the two solutions first met. The intensity of the light was very high. At higher ratios,

i.e. 5 x 10^{-3}M chelate and 10^{-2}M N_2H_4, the light emission lasted for ten to twenty minutes. However, the intensity was very low.

Other oxidizing and reducing agents were tried with little success. Solid PbO_2 is advantageous because it leaves nothing in the solution to interfer with the reducing agent. Gaseous chlorine was successfully employed as an oxidant, however, it had a tendency to remain in the aqueous acidic solutions and react with most of the reducers subsequently added. A survey of many oxidizers indicated that most would produce the ruthenium(III) chelate but interfer later in the chemiluminescence procedure. Hydrogen peroxide would not even oxidize the ruthenium(II) chelate to the plus-three oxidation state. Many reducing agents would not yield light. Examples from this group are $TiCl_3$, Na_2SO_3, $Na_2S_2O_3$, and $SnCl_2$.

The reversability of the reaction was demonstrated with a sodium hydroxide reducing agent. A millimolar solution of the ruthenium(II) chelate in 0.1N H_2SO_4 was oxidized with PbO_2. The resultant solution was centrifuged and added to an equal volumeof 0.1N NaOH producing chemiluminescence. The pH was restored to its initial value by the addition of concentrated H_2SO_4. The whole procedure was repeated five times. At the end of the series of reactions the solution was spectroscopically examined. No chelate has been decomposed, and the spectral data did not indicate the presence of any compound other than the chelate.

None of the ruthenium(III) complexes could be generated in non-aqueous solvents and none could be isolated in the solid form. In attempting to generate the ruthenium(III) complexes in nonagueous media, all of the combinations of the solvents dimethylformamide acetonitrite, absolute ethanol and dioxame with the [illegible] oxidizers gaseous chlorine, solid lead dioxide and sodium bismuthate were used. Several attmepts, under different conditions, were made to isolate the ruthenium(III) chelates as solids. The chelate would always revert to the plus-two oxidation state just as the last trace of aqueous solvent was removed. The electrochemistry of the ruthenium (II) chelate in ultra-dry dimethylformamide and acetonitrite indicated that no electrode process corresponding to the ruthenium(II)-ruthenium (III) chelate couple was occuring.

2. Aromatic Radical-cation reaction

The over-all reaction for the second type of system studied can be written as

$$RNH_2^{+m} + \text{reductant} \rightarrow RNH_2 + h\nu$$

where RNH_2 represents an aromatic amine. The compound used in the present study was 1,6-diamimopyrene.

Experimentally there are two procedures leading to light emission for 1,6-diaminopyrene. The first was analogous to the ruthenium system. A dimethylformamide solution, millimolar in the

diamine, was oxidized with solid lead dioxide or chlorine gas. The lead dioxide was separated by centrifugation or the chlorine was separated by bubbling with nitrogen gas. The resulting solution was added to a DMF solution 0.1M in hydrazine hydrate and light emission was observed. The second procedure involved preparing the radical bromide salt. The salt was added to a dimethylformamide solution 0.1M in hydrazine hydrate, and light was produced. In both cases the blue luminescence was visible in a darkened room to the non-dark-adapted eye. The duration of light emission was about five to ten seconds.

The naphthalene radical-anion could be used as a reducing agent if the solvent employed was tetrahydrofuran. Experimentally, solid 1,6-diaminopyrene and solid lead dioxide were added to a few milliliters of tetrahydrofuran, stirred for several minutes and then filtered. The resultant solution contained an oxidized form of the diamine. The radical-anion of naphthalene was generated by reacting sodium with naphthalene in a tetrahydrofuran solvent. The two solutions were reacted in the absence of oxygen.

Reaction of the 1,6-diaminopyrene-bromide radical salt with the pyrene radical-anion did not yield light. No other radical-anions were tested.

B. Results

1. Spectra

Using the experimental arrangement described in Section III-C, chemiluminescence spectra were obtained for two systems.

Figure V-1 shows a comparison between the chemiluminescence and phosphorescence spectra of $Ru(bipyr)_3Cl_2$. Both spectra are uncorrected for monochromator-photomultiplier response characteristics. The same chemiluminescence spectrum was produced using either hydroxyl ion or hydrazine as the reducing agent. The only chelate having sufficient intensity so that a spectrum could be obtained was that with 2,2'-bipyridine as the ligand.

Figure V-2 shows a comparison between the chemiluminescence and fluorescence spectra of 1,6-diaminopyrene. Both spectra are uncorrected for monochromator-photomultiplier response characteristics. The only chemiluminescence reaction sufficiently intense to measure was that using N_2H_4 as the reducing agent.

2. Electrochemistry

According to Schilt's data, the potential of the Ru(III) $(bipyr)_3Cl_3 \leftrightarrows$ Ru(II) $(bipyr)_3Cl_2$ couple crosses that for the oxygen-water couple at a pH of about zero. His data cover the range from pH = 2 to pH = 1 and indicate a gradual lowering of the chelate potential toward high acidities. Since some of the chemiluminescence work described in this thesis was done at pH's higher than 2, it was

FIGURE V-1

Chemiluminescence and Phosphorescence Spectra of

$Ru(bipyr)_3Cl_2$

Key

———— Phosphorescence.

o o o o o o Chemiluminescence.

Both spectra are uncorrected for photomultiplier-momochromator response characteristics.

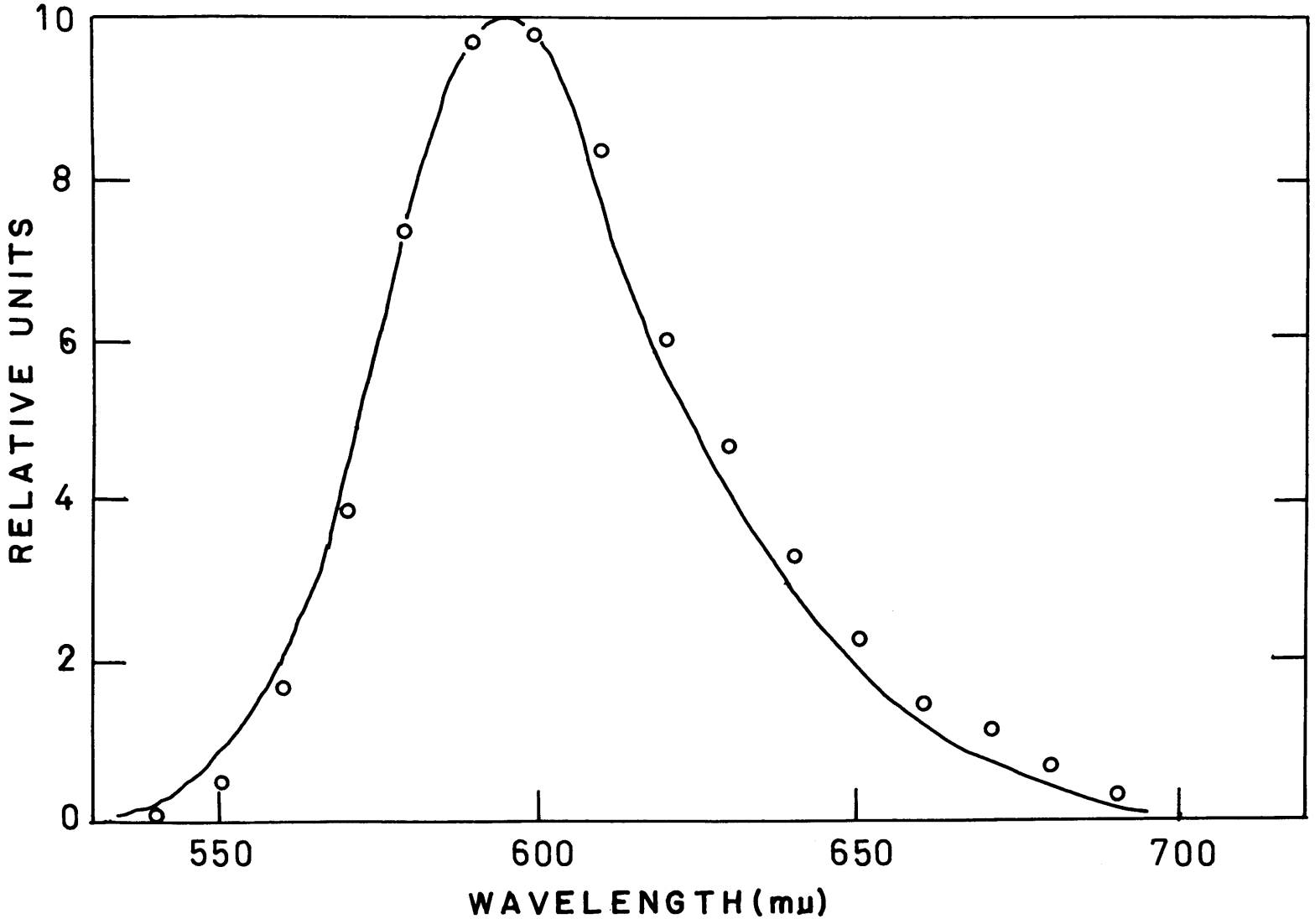
10
8
6
4
2
0
RELATIVE UNITS
550
600
650
700
WAVELENGTH (mμ)

FIGURE V-2

Chemiluminescence and Fluorescence Spectra of

1,6-Diaminopyrene

Key

——— Chemiluminescence.

o o o o Fluorescence.

Both spectra are uncorrected for photomultiplier-monochromator response characteristics.

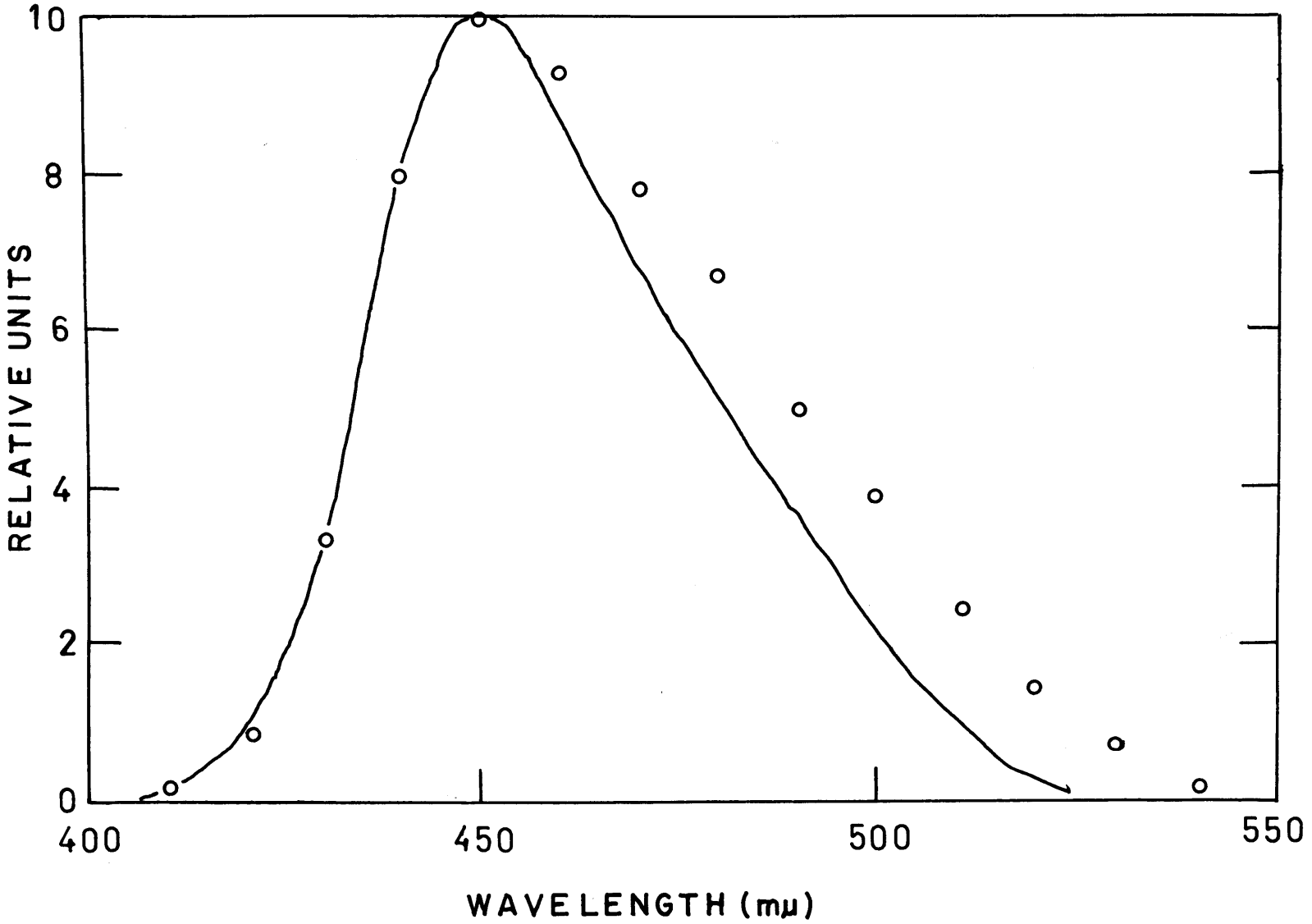
10
8
6
4
2
0
RELATIVE UNITS
400
450
500
550
WAVELENGTH (mμ)

considered desireable to determine the chelate oxidation-reduction potential in this range. By utilizing a wax impregnated graphite electrode having a high oxygen overvoltage, the chelate potential could be measured at pHs as high as 7. It was found that the half-wave potential for the chelate couple remained constant at +1.270 volts vs. N.H.E. from pH=2 to pH=7. Figure V-3 shows the current voltage curve for 10^{-3}M $Ru(bipyr)_3Cl_2$ in 1N HNO_3. At this pH the potential of the chelate couple is +1.238 volts vs. N.H.E.

The current voltage curve for 1,6-diaminopyrene is shown in Figure V-4(†). Both the oxidation of the parent diamine and the radical cation are indicated. The half wave potential for the 1,6-diaminopyrene ⇆ radical cation couple is +0.546 volts vs. N.H.E., while the half wave potential for the radical cation⇆dication couple is +0.766 volts vs. N.H.E. The 1,6-diaminopyrene was millimolar in dimethylformamide and the supporting electrolyte was 0.1M tetrabutyl ammonium perchlorate.

3. Electron Paramagnetic Resonance

Figure V-5 shows the electron paramagnetic resonance spectrum of the 1,6-diaminopyrene-bromide radical salt, millimolar in dimethyl formamide. The center of the sweep is at 3420 gauss and the sweep width is 25 gauss.

The solid radical salt gave a signal at the same sweep center

---

† This data was obtained by Jack Chang.

FIGURE V-3

Current-voltage Curve for Millimolar

$Ru(bipyr)_3Cl_2$ in 1N HNO_3

Key

A - Solvent.

B - Chelate.

Reference electrode is saturate calomel. The scan rate is 2 volts/min.

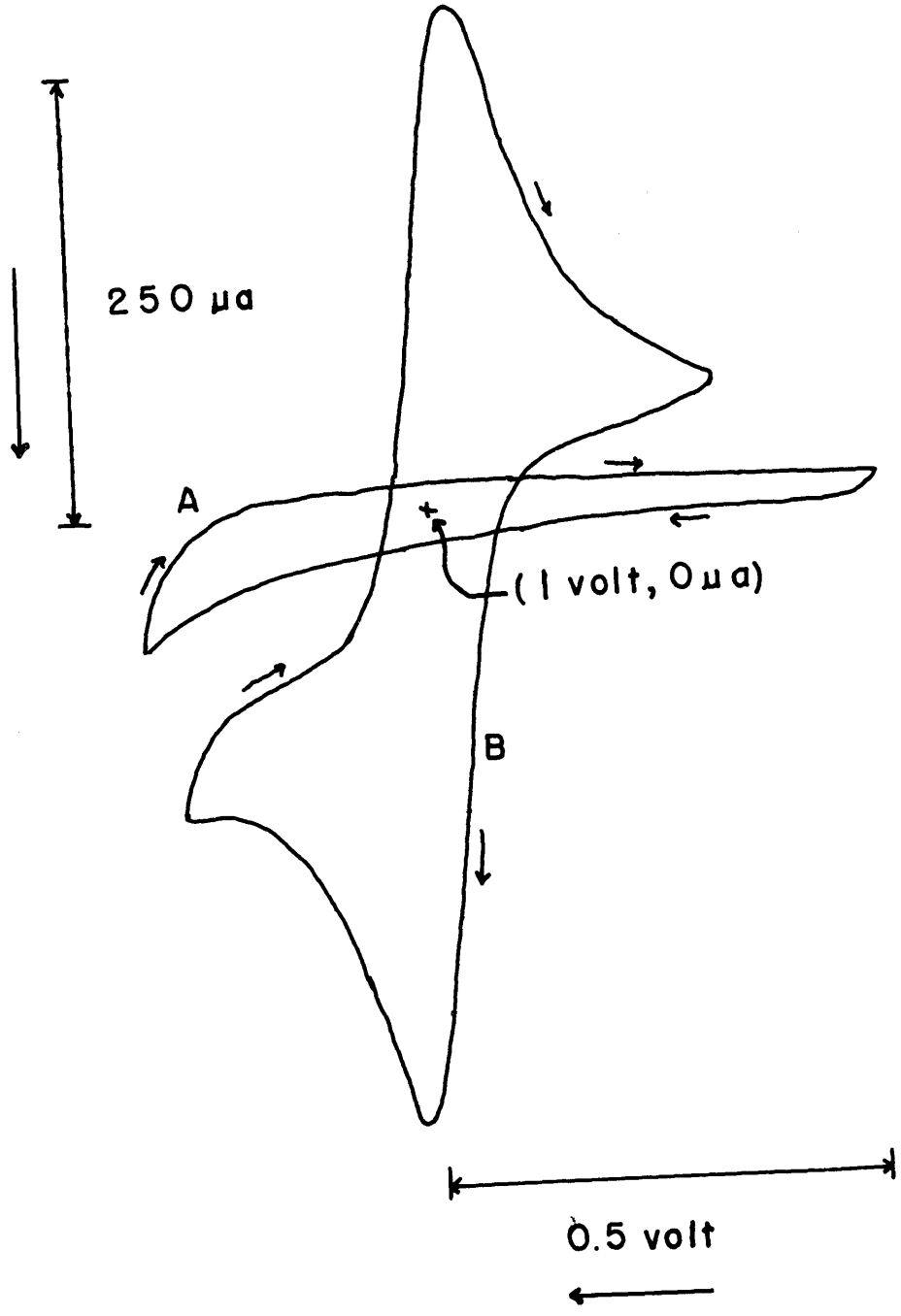
250 μa
A
(1 volt, 0 μa)
B
0.5 volt

FIGURE V-4

Current-voltage Curve for Millimolar
1,6-Diaminopyrene in Dimethylformamide

Reference electrode is Ag/AgCL with E_{ref} = +0.241 volts vs. N.H.E. The scan rate is 2 volts/min.

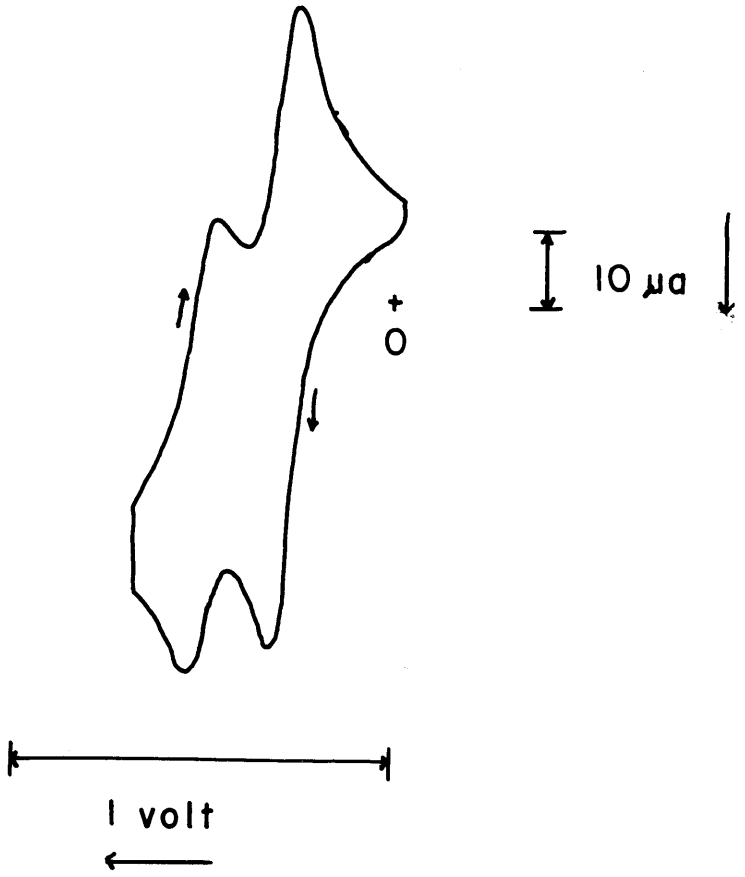
+
0
10 μa
1 volt

FIGURE V-5

Electron Paramagnetic Resonance Spectra for the

1,6-Diaminopyrene Radical Cation in Dimethylformimide

The center of the sweep is at 3420 gauss.

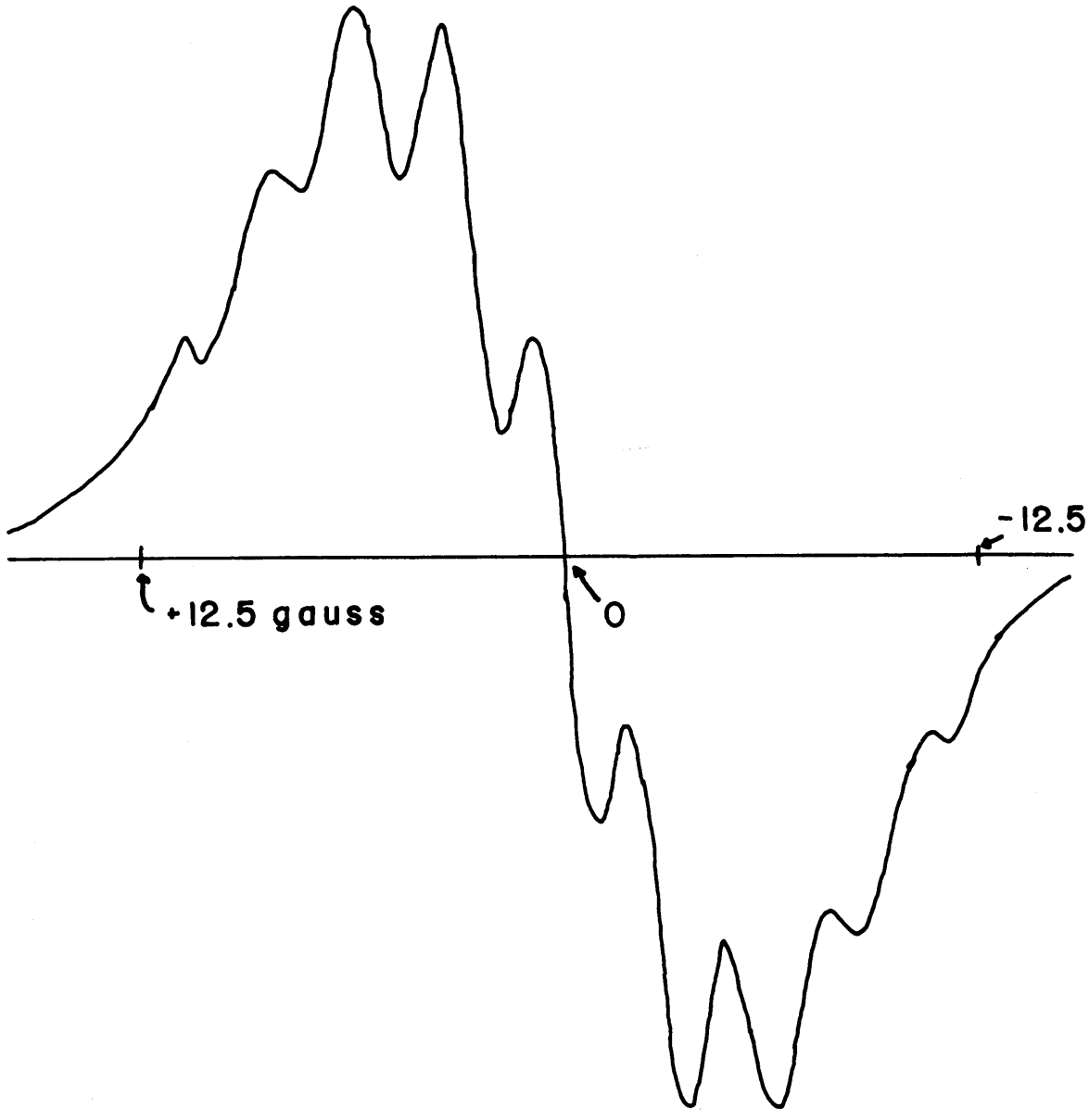
-12.5
+12.5 gauss
0

but exhibited a structureless spectrum.

A solution of 1,6-diminopyrene in dimethyl formamide, when oxidized with lead dioxide, did not have a measureable resonance signal. This demonstrates that the lead dioxide oxidized 1,6-diaminopyrene is not the radical cation but more probably the dication or some other oxidized form of the diamine.

4. Chelate Auto-reduction Kinetics

As stated earlier, the cross-over point for the chelate and oxygen-water oxidation-reduction couples is in the vicinity of pH=0. As a result of this cross-over, in 50% sulfuric acid the Ru(II) $(bipyr)_3Cl_2$ species is unstable and will slowly oxidize to the plus three oxidation state.

In acid media with the proton concentration tenth normal or greater, the Ru(III) $(bipyr)_3Cl_3$ species is reasonably stable, i.e. it has a half-time of disappearance of about seven hours. As the pH is increased above pH=1, it would be expected that the Ru(III) $(bipyr)_3Cl_3$ species would become less stable and would react with the solvent in an auto-reduction reaction. This reaction does occur, however it must have a high activation energy since the reaction half-time is two to three hours at pH=3. Figure V-6 shows both the th absorption of Ru(III) $(bipyr)_3Cl_3$ and the log of the absorption as a function of time for the auto-reduction reaction at pH=3. Note the non-linearity of the log plot at short times. This feature of

FIGURE V-6

Auto-reduction of $Ru(III)(bipyr)_3Cl_3$ at pH = 3

Key

———— $Ru(III)(bipyr)_3Cl_3$ absorption.

o o o o o Log of the absorption.

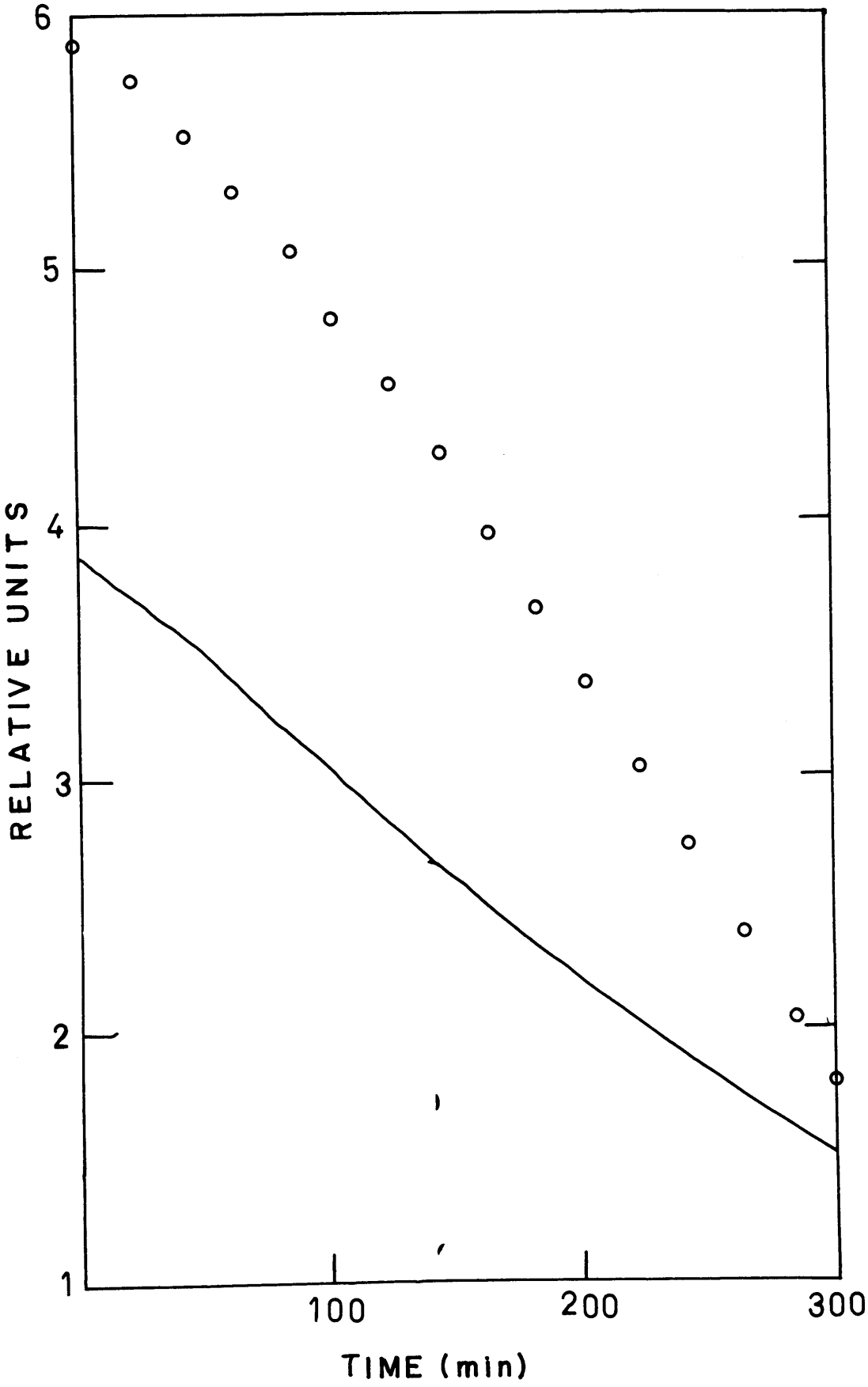
6
5
4
3
2
1
RELATIVE UNITS
100
200
300
TIME (min)

the reaction kinetics only appears at high pHs and could not be explained with the available experimental data.

5. Chelate-Hydrazine Kinetics

The reaction kinetics of the Ru(III) $(bipyr)_3Cl_3$-hydrazine chemiluminescence system in 0.1N H_2SO_4 were studied by use of the instrument described in Section III-E. It was possible to monitor two properties of the chemiluminescing system, the Ru (III) $(bipyr)_3Cl_3$ absorption and the chemiluninescence emission. It was impossible to measure the Ru(II) $(bipyr)_3Cl_2$ absorption because of its high concentration and high molar absorptivity.

For this system there are essentially three different shapes of stopped-flow curves. Figure V-7 shows the stopped-flow curve for chemiluminescence when the concentrations of reactants are 5×10^{-4}M Ru(III) $(bipyr)_3Cl_3$ and 0.1M hydrazine. This curve is typical of those formed at hydrazine to chelate ratios of about 1000:1. At no place on the curve is the decay a simple exponential. At these high ratios of hydrazine to chelate it was nearly impossible to follow the Ru(III) $(bipyr)_3Cl_3$ absorption.

Figure V-8 shows the stopped-flow curves for chemiluminescence and Ru(III) $(bipyr)_3Cl_3$ absorption when the concentrations of reactants are 5×10^{-4}M Ru(III) $(bipyr)_3Cl_3$and 2.5×10^{-2}M hydrazine. This curve is typical of those formed at hydrazine to chelate ratios of about 100:1. The spike in the chemiluminescence at the start of the reaction is probably much higher than indicated, because

FIGURE V-7

Chelate-Hydrazine Stopped-flow Curves

Key

———— Chemiluminescence emission intensity.

5×10^{-4}M $Ru(III)(bipyr)_3Cl_3$, 0.1M Hydrazine

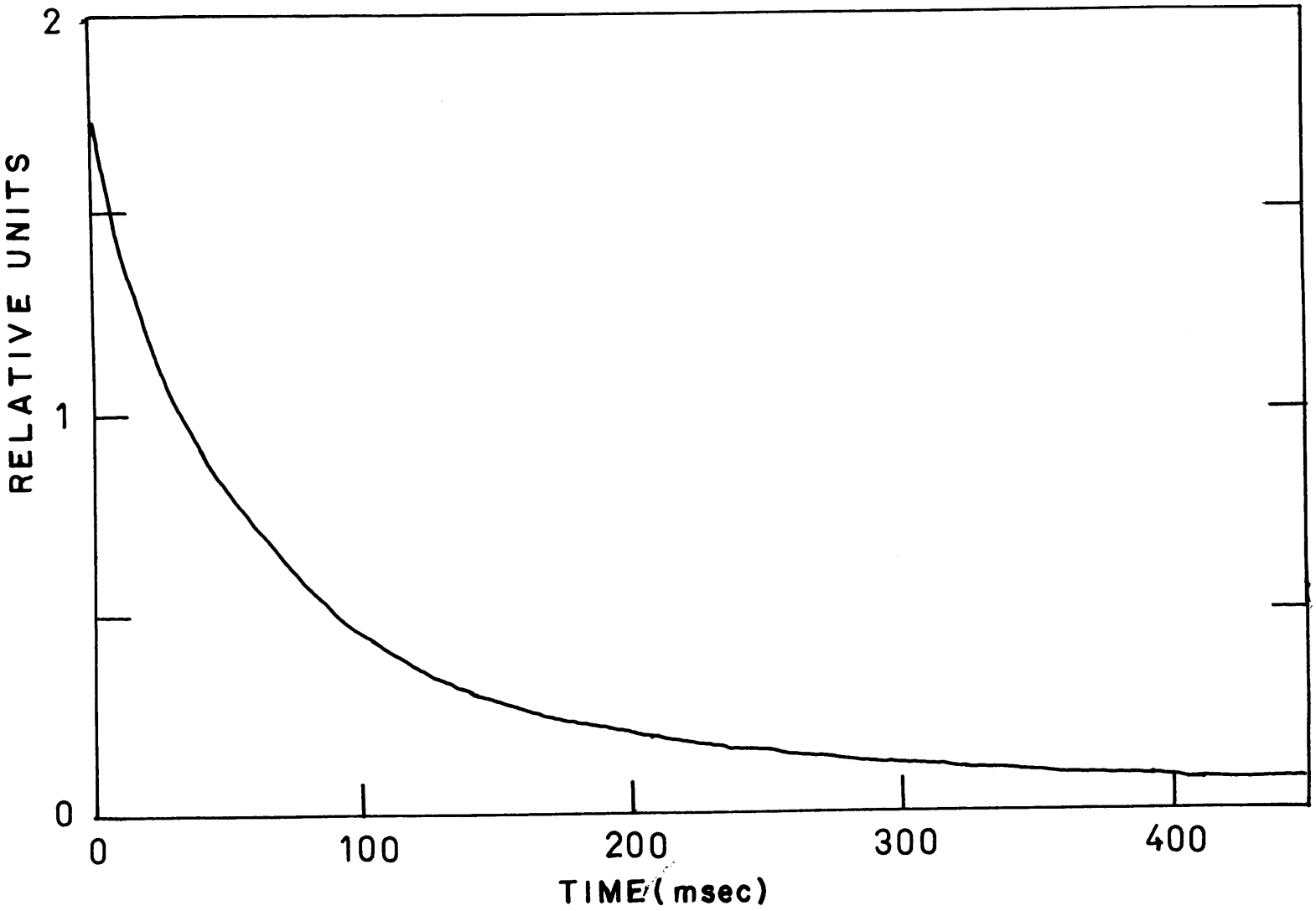
2
1
0
RELATIVE UNITS
0
100
200
300
400
TIME (msec)

FIGURE V-8

Chelate-Hydrazine Stopped-flow Curves

Key

——— Chemiluminescence emission intensity.

- - - - $Ru(III)(bipyr)_3Cl_3$ absorption.

o o o o Computer predicted chemiluminescence.

● ● ● ● Computer predicted absorption.

5×10^{-4}M $Ru(III)(bipyr)_3Cl_3$, 2.5×10^{-2}M Hydrazine

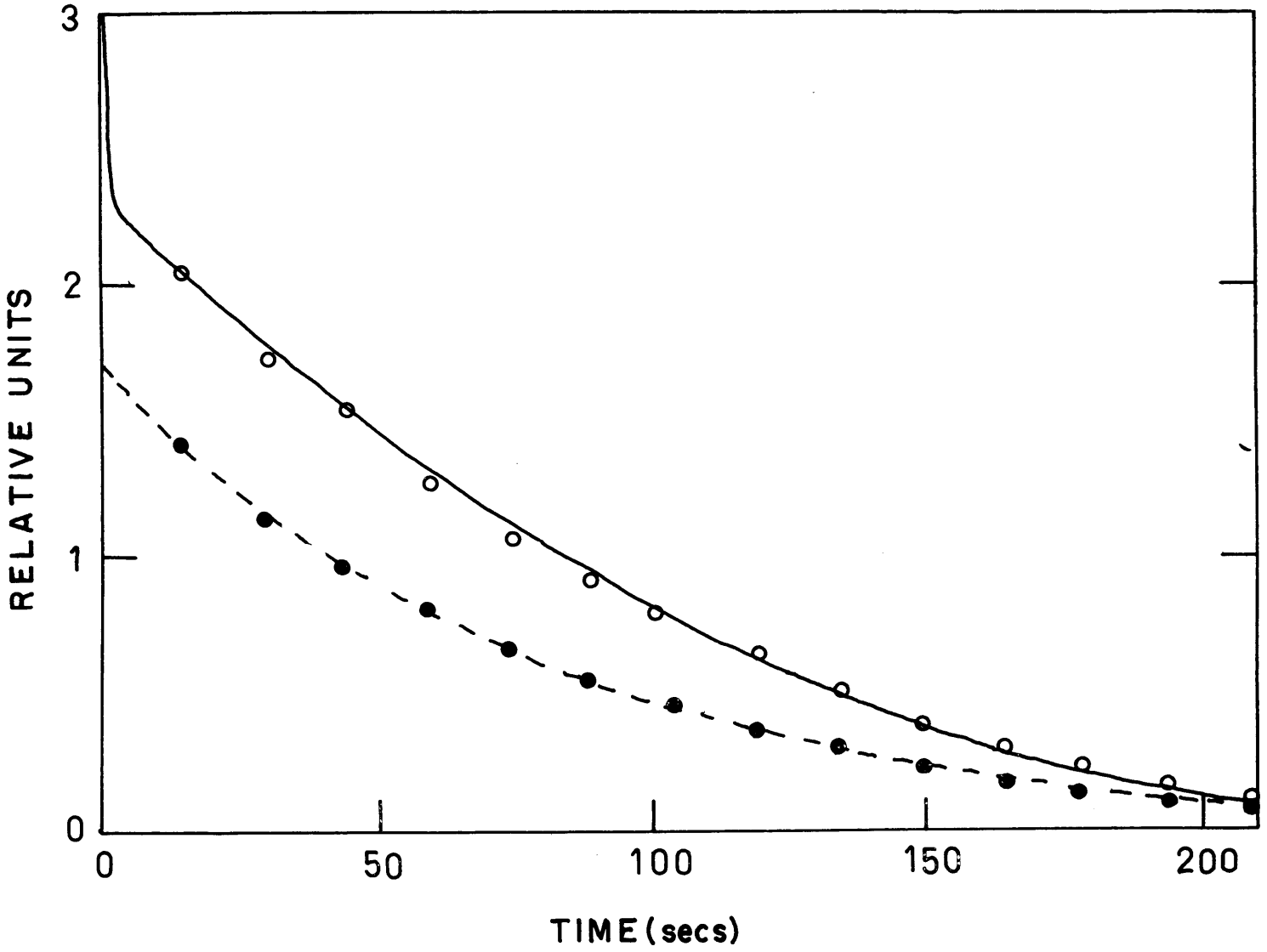
RELATIVE UNITS
3
2
1
0
0
50
100
150
200
TIME (secs)

of slow instrumental response time. The chemiluminescence decay was definitely not exponential, and for several ratios of concentration had a definite "hump" immediately following the spike. Under all of the conditions where the absorption could be measured, its shape was constant. Within one second the absorption would drop by about a factor of two and then would exponentially fall to a value of zero in essentially the same period of time that it took the chemiluminescence emission intensity to reach zero.

Figure V-9 shows the stopped-flow curves for chemiluminescence and Ru(III) $(bipyr)_3Cl_3$ absorption when the concentrations of the reactants are 1×10^{-3}M Ru(III) $(bipyr)_3Cl_3$ and 1×10^{-2}M hydrazine. This curve is typical of those formed at hydrazine to chelate ratios of about 10:1. Both the chemiluminescence emission intensity and the Ru(III) $(bipyr)_3Cl_3$ absorption exponentially fall to zero.

The intensity of the chemiluminescence emission varies considerably as a function of the reactant ratios. At low ratios, the integrated emission intensity was about one-fourth of that at intermediate ratios. At high ratios the intensity again drops. For example, a mixture of 5×10^{-4}M Ru(III) $(bipyr)_3Cl_3$ and 1M hydrazine yielded a very low level of light emission and had a reaction with a half-time of less than five milliseconds.

FIGURE V-9

Chelate-Hydrazine Stopped-flow Curves

Key

———— Chemiluminescence emission intensity.

- - - - $Ru(III)(bipyr)_3Cl_3$ absorption.

1×10^{-3}M $Ru(III)(bipyr)_3Cl_3$, 1×10^{-2}M Hydrazine

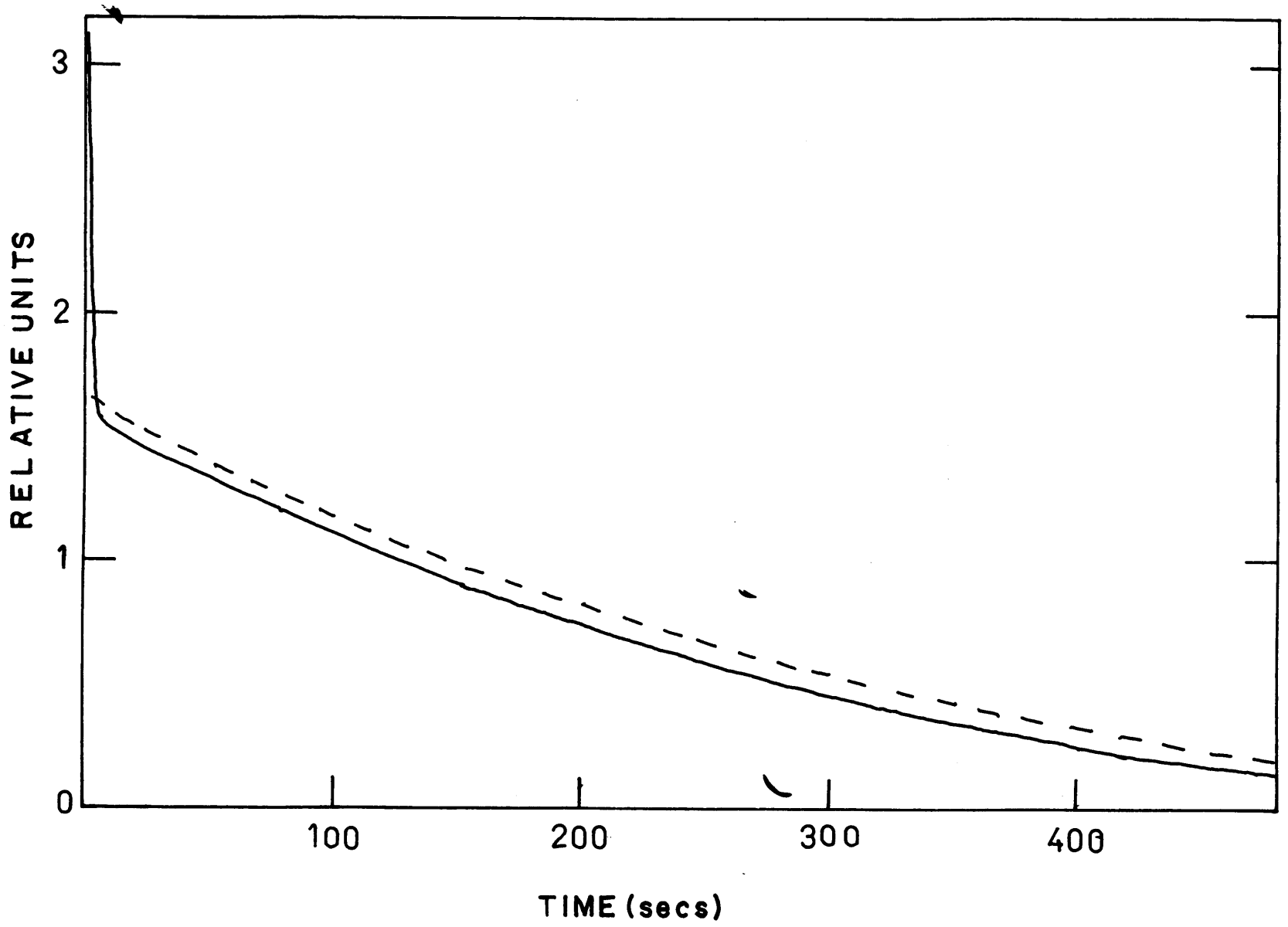
RELATIVE UNITS
3
2
1
0
100
200
300
400
TIME (secs)

C. Discussion

1. Identification of Emitting Species

It is evident from Figure V-1 that the emitting species in the Ru(III) $(bipyr)_3Cl_3$ reduction reaction is the Ru(II) $(bipyr)_3Cl_2$ chelate.

As can be seen in Figure V-2, the chemiluminescence spectrum of the 1,6-diaminopyrene radical cation reduction reaction does not exactly match the fluorescence spectrum of 1,6-diaminopyrene. The difference cannot be attributed to self absorption since the rising portions of the curves are identical. Most probably the long wavelength component is due to the chemiluminescence from an impurity produced by the lead dioxide oxidation procedure. It is evident, however, that a significant percentage of the emission in the chemiluminescence reaction comes from the parent diamine fluorescence.

2. Energy Considerations

It would be of interest to examine the various oxidation-reduction potentials involved in the chemiluminescence reactions to determine whether enough energy is available from a simple one-electron transfer between the donor and acceptor to leave the acceptor in an excited electronic state. The average energy necessary to form an excited state can be expressed in volts by converting the emission 0-0 band from μ^{-1} to volts. The conversion factor is 1 μ^{-1} = 1.24 volts.

From the Ru(II) $(bipyr)_3Cl_2$ emission spectrum a value of 2.23 volts is determined for the energy required by the reduction reaction to leave the chelate in the lowest excited triplet state. The entropy term, T ΔS, should also be considered. For the ruthenium chelate, the entropy should have a value very nearly zero for the change from the plus three to the plus two oxidation states. The potential of the Ru(III) $(bipyr)_3Cl_3 \leftrightharpoons$ Ru(II)$(bipyr)_3Cl_2$ couple has been determined to be 1.270 volts vs. N.H.E. The potentials of the hydroxide and hydrazine oxidation couples are given by Latimer (27) as +0.401 and -0.23 volts vs. N.H.E. respectively. Using these values, 0.8 to 0.9 volts of available energy are calculated for hydroxyl ion as a reducing agent and 1.4 to 1.5 volts of available energy are calculated for hydrazine as reducing agent. Both of these values are considerably below the energy required to produce an excited state. Use of the hydroxyl and hydrazine potentials, as given by Latimer, is probably not valid since these reactions are not reversible and subsequently may have highly energetic intermediate steps.

The average energy needed to form an excited singlet state of 1,6-diaminopyrene can be determined as 2.75 volts. The entropy term, TΔS, for aromatic compounds has been determined by Chandross(50)

as +0.2 ±0.2 volts. This would make the overall energy needed to produce an excited state 2.95 ±0.2 volt. The potential of the 1,6-diaminopyrene $\rightleftharpoons$ radical cation couple has been determined as +0.546 volts vs. N.H.E. One reducing agent yielding a chemiluminescence reaction with the 1,6-diaminopyrene radical cation was the napthalene radical anion. The potential of the reversible naphthalene $\rightleftharpoons$ radical anion couple is -2.254 volts vs. N.H.E. This yields an energy of 2.80 volts which is sufficient to produce an excited singlet state of 1,6-diaminopyrene.

One reducing agent not yielding a chemiluminescence reaction with the 1,6-diaminopyrene radical cation was the pyrene radical anion. The potential of the reversible pyrene $\rightleftharpoons$ radical anion couple is -1.854 volts vs. N.H.E. This yields an available energy of 2.40 volts which is significantly below the required energy.

3. Reaction Kinetics

The kinetics of the $Ru(III)(bipyr)_3Cl_3$-hydrazine chemiluminescence system was chosen for a detailed study for several reasons: the $Ru(III)(bipyr)_3Cl_3 \rightleftharpoons Ru(II)(bipyr)_3Cl_2$ couple is reversible; there is no apparent degradating of the chelate to other products; and the oxidation of hydrazine has been studied in detail in the literature.

The Fe(III) oxidation of hydrazine has been discussed by Higginson and Sutton (20, 21), Cahn and Powell (5), Higginson and

Wright (22), and Roseninsky (39). The mechanism proposed by these authors can be written as:

$$Fe(III) + N_2H_4 \underset{k_{-1}}{\overset{k_1}{\rightleftharpoons}} Fe(II) + N_2H_3\cdot \qquad (V\text{-}1)$$

$$2N_2H_3\cdot \xrightarrow{k_2} N_4H_6 \xrightarrow{fast} N_2 + 2NH_3 \qquad (V\text{-}2)$$

$$2N_2H_3\cdot \xrightarrow{k_3} N_2H_2 + N_2H_4 \qquad (V\text{-}3)$$

$$Fe(III) + N_2H_3\cdot \xrightarrow{k_4} N_2H_2 + Fe(II) \qquad (V\text{-}4)$$

$$2Fe(III) + N_2H_2 \xrightarrow[fast]{k_5} N_2 + 2Fe(II) \qquad (V\text{-}5)$$

The above mechanism has been substantiated by labeling studies, kinetic observations, and mathematical arguments. The mechanism was described by these authors as generally being valid for many oxidizing agents. Specifically they mentioned the metal ions Ce(IV), Fe(III), Mn(III), Tl(III) and V(V). On the basis of the purported generality it was attempted to determine the rate constants for such a mechanism when the oxidizing agent was $Ru(III)(bipyr)_3Cl_3$.

The experimental data for the $Ru(III)(bipyr)_3Cl_3$ oxidation of hydrazine were presented in Section V-B. It was shown that there are only two pieces of experimental information available for each set of reactant concentrations, chemiluminescence intensity and $Ru(III)(bipyr)_3Cl_3$ absorption rate data.

The computer kinetic modeling program described in Section VI-A

was used to test the applicablity of the reported hydrazine oxidation mechanism to the chelate chemiluminescence system. The computer approach consists of modeling the reported mechanism and varying all of the reaction parameters until the computer output matches the experminental data. The problem was computerized by utilizing the following set of reactions:

$$Ru(III) + N_2H_4 \xrightarrow{k_6} [Ru(II)]_1^{\dagger} + N_2H_3 \qquad (V\text{-}6)$$

$$[Ru(II)]_1^{\dagger} \xrightarrow{k_7} Ru(II) \qquad (V\text{-}7)$$

$$[Ru(II)]_1^{\dagger} \xrightarrow{k_8} [Ru(II)]^* \qquad (V\text{-}8)$$

$$2N_2H_3\cdot \xrightarrow{k_9} N_2 + 2NH_3 \qquad (V\text{-}9)$$

$$Ru(III) + N_2H_3\cdot \xrightarrow{k_{10}} N_2H_2 \qquad (V\text{-}10)$$

$$Ru(III) + N_2H_2 \xrightarrow{k_{11}} I \qquad (V\text{-}11)$$

$$Ru(III) + I \xrightarrow{k_{12}} [Ru(II)]_{12}^{\dagger} + N_2 \qquad (V\text{-}12)$$

$$[Ru(II)]_{12}^{\dagger} \xrightarrow{k_{13}} Ru(II) \qquad (V\text{-}13)$$

$$[Ru(II)]_{12}^{\dagger} \xrightarrow{k_{14}} [Ru(II)]^* \qquad (V\text{-}14)$$

$$[Ru(II)]^* \xrightarrow{k_{15}} Ru(II) + h\nu \qquad (V\text{-}15)$$

where the ligands are omitted in the molecular formulas for the chelate; the notation [ ]† indicates an activated complex produced by the ith reaction; [ ]* indicates an excited electronic state; I is an intermediate in the N_2H_2 oxidation reaction; and hν is the light produced by the reaction sequence.

In the computer treatment of the mechanism, the activated complexes are created simply for mathematical reasons. Each reaction yielding products in an excited state will also yield products in the ground state. The ratio of excited states produced to the total amount of excited and ground states produced is defined as the chemiluminescence yield. The activated complex allows a chemiluminescence yield to be assigned to a reaction. For example, the ratio $k_8/(k_7 + k_8)$ is the chemiluminescence yield for the first reaction. The rate constants associated with the disappearance of the activated complexes are always made much larger than the rate constants for the reactions producing the activated complexes. This assures that the activated complexes will always have a steady state concentration near zero.

The reaction,

$$2Fe(III) + N_2H_2 \rightarrow 2Fe(II) + N_2$$

appearing in the Fe(III) oxidation of hydrazine is most probably a sequence of two second order processes. For the Ru(III) oxidation of hydrazine this reaction has been written with I as the hydrazine intermediate between N_2H_2 and N_2.

The dismutation reaction

$$2NH_3^{\cdot} \rightarrow N_2H_2 + N_2H_6$$

has been ignored in the Ru(III) mechanism since it has been shown to be about 100 times slower than the dimerization reaction(39).

By using second order rate constants of $k_6 = 8$, $k_9 = 1 \times 10^4$, $k_{10} = 5 \times 10^4$, $k_{11} = 5 \times 10^5$ and $k_{12} = 1 \times 10^{10}$; quantum yields of $k_8/(k_7+k_8) = 1\%$ and $k_{14}/(k_{13}+k_{14}) = 99\%$; and using a first order excited state phosphorescence rate constant of $k_{10} = 1 \times 10^7$, the stopped flow data for the chemiluminescence reaction with reactant concentrations of 5×10^{-4}M Ru(III) and 2.5×10^{-2}M N_2H_4 could be exactly matched. The computer data are shown in Figure V-8, along with the experimental results.

The use of this set of reaction parameters yielded computer data that were in qualitative agreement with the measured stopped-flow experimental data. The shape of the chemiluminescence emission curves was always correctly predicted, including the sharp spike before the main portion of emission. The shape of the absorption curves was matched even better than those for chemiluminescence. The absorption would drop very rapidly and then exponentially decay within the same time that it took the chemiluminescence emission intensity to go to zero. However, it was impossible to find one set of parameters that would yield the correct data for all of the experimental results.

It is apparent that the reaction scheme outlined by the other

workers is not directly applicable to the oxidation of hydrazine by the ruthenium chelate. It is felt that the general mechanism is correct for dilute hydrazine solutions but is missing one or more important processes that appear at high hydrazine concentrations.

VI. Appendices

A. Kinetic Modeling Computer Program

1. Object

The object of the program is to aid in the identification of the mechanism of an experimental reaction by the controlled simulation of a kinetic scheme utilizing digital computing techniques. Necessary experimental data are one or more curves of concentration as a function of time, initial starting concentrations as a function of time. Operationally, the mechanism and its associated rate constants are varied until the computer data matches the experimental values.

Similar programs have been reported by DeTar(12). The program discussed here is much more general in scope and consumes less computer time.

2. Method of Calculation

For a general reaction where any number of species react to form any number of products, the rate of the reaction can be mathematically defined as the product of the rate constant times all of the reactants taken individually to the power of their stoichiometry. This can be written as

$$R_j = k_j \prod_i C_i^{s_{i,j}} \qquad \text{VI-1}$$

where C_i is the concentration of the ith species; R_j and k_j are the rate and rate constant, respectively, for the jth reaction; and $s_{i,j}$

is the stoichiometry of the ith species in the jth reaction.

The rate of appearance of each individual species will be defined as,

$$R_j = -\frac{1}{s_{i,j}} \cdot \frac{dC_i}{dt} \qquad \text{VI-2a}$$

for reactants, and

$$R_j = \frac{1}{s_{i,j}} \cdot \frac{dC_i}{dt} \qquad \text{VI-2b}$$

The computer approach consists of making the time interval under consideration small enough so that

$$\frac{\Delta C_i}{\Delta t} \sim \frac{dC_i}{dt} \qquad \text{VI-3}$$

Assuming that this is possible, the change in concentration for each species involved in the reaction can be calculated for the time interval Δt. If $\Delta_{i,j}$ is defined as the change in concentration for the ith species in the jth reaction, this can be written as

$$\Delta_{i,j} = -R_j \cdot s_{i,j} \cdot \Delta t \qquad \text{VI-4a}$$

for reactants and

$$\Delta_{i,j} = R_j \cdot s_{i,j} \cdot \Delta t \qquad \text{VI-4b}$$

for products.

The concentration of each species at the start of the next time interval is simply

$$C_i^{t'} = C_i^t + \Delta_{i,j} \qquad \text{VI-5}$$

where $t'-t = \Delta t$. If more than one reaction occurs in the kinetic scheme, the calculations are performed for all of the reactions before a new time interval begins. Equation VI-5 then changes to

$$C_i^{t'} = C_i^t + \sum_j \Delta_{i,j} \qquad \text{VI-6}$$

where the summation is only carried out for those j reactions where species i is a reactant or product.

3. Program Description

Main-Figure VI-1 shows the flow diagram for the main routine, MAIN. Besides controlling the flow of the program, the major job accomplished by MAIN is the recognition of data sets.

The Fortran IV source deck listing for all of the routines is shown in Table VI-1.

Input-Figure VI-2 shows the flow diagram for the input routine, INPUT. The major job accomplished by INPUT is reading the data necessary to define and run the kinetic scheme. The variable JDATA allows some flexability in the type of input to be read. If JDATA equals 1, a complete set of data is read; if JDATA equals 2, trial constants and concentrations are read; if JDATA equals 3, trial rate constants are read; and if JDATA equals 4, starting concentrations are read. The exact meaning of the undefined terms in Figure VI-2 will be discussed later.

TABLE VI-1

Fortran Source Deck Listing

```
0001            COMMON NAME(13),NCOEF(12,12),NSP(5),NDER(4),TRC(12),SC(12)
0002            COMMON COEF(12,12),C(12),NSPE(12),CP(501,12),DELC(501,12)
0003            COMMON TIME(501),NDELTA(12),TDELTA(12),RATE(12),DELTA(12,12)
0004            COMMON FRAC(12),CSAVE(12),L(12)
0005            COMMON MAXC(12),MAXD(12),TIMEC(12),TIMED(12)
0006            COMMON Y(9,501),YMAX(12),MAGC(5),MAGD(4),MAGY(9)
0007            REAL*4 MAXC,MAXD
0008          200 READ(5,100) NCON
0009          100 FORMAT(I2)
0010            IF(NCON) 99,99,1
0011            1 CONTINUE
0012            CALL INPUT(NS,NR,SCALE,NL,JJJJ,NSP,NDER)
0013            DO 88 I=1,NR
0014            DO 88 J=1,NS
0015           88 COEF(I,J)=NCOEF(I,J)
0016            NCT=0
0017            III=1
0018            IIII=JJJJ
0019            DO 2 I=1,NS
0020            NSPE(I)=0
0021            2 C(I)=SC(I)
0022            CALL CALC(NL,NR,NS,SCALE,NCT,IIII,JJJJ,III)
0023            CALL OUTPUT(NCT,NS,NR,NL,SCALE,JJJJ,III)
0024            CALL PLOT(NSP,III,NDER)
0025            GO TO 200
0026           99 CONTINUE
0027            CALL EXIT
0028            END
```

```
0001              SUBROUTINE INPUT(NS,NR,SCALE,NL,JJJJ,NSP,NDER)
0002              COMMON NAME(13),NCOEF(12,12),MSP(5),MDER(4),TRC(12),SC(12)
0003              COMMON COEF(12,12),C(12),NSPE(12),CP(501,12),CELC(501,12)
0004              COMMON TIME(501),NDELTA(12),IDELTA(12),RATE(12),DELTA(12,12)
0005              COMMON FRAC(12),CSAVE(12),L(12)
0006              COMMON MAXC(12),MAXD(12),TIMEC(12),TIMED(12)
0007              COMMON Y(9,501),YMAX(12),MAGC(5),MAGD(4),MAGY(5)
0008              REAL*4 MAXC,MAXD
0009              READ(5,400) JDATA
0010          400 FORMAT(I1)
0011              GO TO (41,42,45,46), JDATA
0012           41 READ(5,401) (NAME(I),I=1,13)
0013          401 FORMAT(13A4)
0014              READ(5,402) NS,NR
0015          402 FORMAT(2I2)
0016              DO44 I=1,NR
0017           44 READ(5,403) (NCOEF(I,J),J=1,NS)
0018          403 FORMAT(12I2)
0019              READ(5,405) SCALE,NL,JJJJ
0020          405 FORMAT(E10.4,I5,I3)
0021              READ(5,500) NSP,(MSP(I),MAGC(I),I=1,5),NDER,(MDER(J),MAGD(J),J=1,4
                 1)
0022          500 FORMAT(11I2,3X,9I2)
0023           42 READ(5,404) (TRC(I),I=1,NR)
0024          404 FORMAT(6E10.4)
0025              READ(5,404) (SC(I),I=1,NS)
0026              GO TO47
0027           45 READ(5,404) (TRC(I),I=1,NR)
0028              GO TO47
0029           46 READ(5,404) (SC(I),I=1,NS)
0030           47 CONTINUE
0031              RETURN
0032              END
```

```
0001            SUBROUTINE CALC(NL,NR,NS,SCALE,NCT,IIII,JJJJ,III)
0002            COMMON NAME(13),NCOEF(12,12),MSP(5),MCER(4),TRC(12),SC(12)
0003            COMMON CCEF(12,12),C(12),NSPE(12),CP(501,12),CELC(501,12)
0004            COMMON TIME(501),NDELTA(12),TDELTA(12),RATE(12),DELTA(12,12)
0005            COMMON FRAC(12),CSAVE(12),L(12)
0006            COMMON MAXC(12),MAXD(12),TIMEC(12),TIMED(12)
0007            COMMON Y(9,501),YMAX(12),MAGC(5),MAGD(4),MAGY(9)
0008            REAL*4 MAXC,MAXD
0009            REAL*4 NDELTA
0010            DO 3 I=1,NL
0011            DO 5 J=1,NR
0012            RATE(J)=TRC(J)
0013            DO 5 JJ=1,NS
0014            IF(COEF(J,JJ)) 5,5,6
0015          6 RATE(J)=RATE(J)*(C(JJ)**COEF(J,JJ))
0016          5 CONTINUE
0017            DO 7 J=1,NR
0018            DO 7 JJ=1,NS
0019          7 DELTA(J,JJ)=-1.0*RATE(J)*SCALE*CCEF(J,JJ)
0020          8 CONTINUE
0021            DO 11 JJ=1,NS
0022            NDELTA(JJ)=0.0
0023            TDELTA(JJ)=0.0
0024            DO 11 J=1,NR
0025            IF(DELTA(J,JJ)) 2003,11,2004
0026       2003 NDELTA(JJ)=NDELTA(JJ)+DELTA(J,JJ)
0027       2004 TDELTA(JJ)=TDELTA(JJ)+DELTA(J,JJ)
0028         11 CONTINUE
0029            CALL NEGC(NS,NCT,NR,&8)
0030            DO 24 JJ=1,NS
0031            IF(C(JJ)+TDELTA(JJ)-1E-30) 2021,2021,2022
0032       2021 C(JJ)=0.0
0033            GO TO 24
0034       2022 C(JJ)=C(JJ)+TDELTA(JJ)
0035         24 CONTINUE
0036            CALL PRINTP(I,NS,SCALE,IIII,III,JJJJ)
0037          3 CONTINUE
0038            RETURN
0039            END
```

```
0001            SUBROUTINE NEGC(NS,NCT,NR,*)
0002            COMMON NAME(13),NCOEF(12,12),MSP(5),MDER(4),TRC(12),SC(12)
0003            COMMON COEF(12,12),C(12),NSPE(12),CP(501,12),DELC(501,12)
0004            COMMON TIME(501),NDELTA(12),TDELTA(12),RATE(12),DELTA(12,12)
0005            COMMON FRAC(12),CSAVE(12),L(12)
0006            COMMON MAXC(12),MAXD(12),TIMEC(12),TIMED(12)
0007            COMMON Y(9,501),YMAX(12),MAGC(5),MAGD(4),MAGY(9)
0008            REAL*4 MAXC,MAXD
0009            REAL*4 NDELTA
0010            DO 2018 JJ=1,NS
0011            IF(C(JJ)+NDELTA(JJ)) 23,22,22
0012          23 IF(C(JJ)+NDELTA(JJ)+1E-06*C(JJ)) 2020,22,22
0013       2020 NCT=1
0014            NSPE(JJ)=NSPE(JJ)+1
0015            SRATE=0.0
0016            DO 2005 J=1,NR
0017            IF(COEF(J,JJ)) 2005,2005,2015
0018       2015 SRATE=SRATE+RATE(J)
0019       2005 CONTINUE
0020            DO 2006 J=1,NR
0021            IF(COEF(J,JJ)) 2006,2006,2016
0022       2016 FRAC(J)=RATE(J)/SRATE
0023       2006 CONTINUE
0024            DO 2011 J=1,NR
0025            IF(COEF(J,JJ)) 2011,2011,2014
0026       2014 DO 2017 IJ=1,NS
0027            IF(COEF(J,IJ)) 2012,2017,2012
0028       2012 DELTA(J,IJ)=(-1.0*C(JJ)*FRAC(J)*COEF(J,IJ))/COEF(J,JJ)
0029       2017 CONTINUE
0030       2011 CONTINUE
0031            RETURN 1
0032          22 CONTINUE
0033       2018 CONTINUE
0034            RETURN
0035            END
```

```
0001            SUBROUTINE PRINTP(I,NS,SCALE,IIII,III,JJJJ)
0002            COMMON NAME(13),NCOEF(12,12),NSP(5),NDER(4),IRC(12),SC(12)
0003            COMMON COEF(12,12),C(12),NSPE(12),CP(501,12),DELC(501,12)
0004            COMMON TIME(501),NDELTA(12),IDELTA(12),RATE(12),DELTA(12,12)
0005            COMMON FRAC(12),CSAVE(12),L(12)
0006            COMMON MAXC(12),MAXD(12),TIMEC(12),TIMED(12)
0007            COMMON Y(9,501),YMAX(12),MAGC(5),MAGD(4),MAGY(9)
0008            DIMENSION SLOPE(12)
0009            REAL*4 MAXC,MAXD
0010            IF(I-1) 1003,1003,1004
0011       1003 DO 19 JK=1,NS
0012            MAXC(JK)=SC(JK)
0013            TIMEC(JK)=0.0
0014            CP(1,JK)=SC(JK)
0015            CSAVE(JK)=SC(JK)
0016            DELC(1,JK)=(C(JK)-SC(JK))/SCALE
0017            MAXD(JK)=DELC(1,JK)
0018         19 TIMED(JK)=0.0
0019            TIME(1)=0.0
0020       1004 DO 1006 JK=1,NS
0021            SLOPE(JK)=(C(JK)-CSAVE(JK))/SCALE
0022            IF(SLOPE(JK)-MAXD(JK)) 1002,1002,1005
0023       1005 MAXD(JK)=SLOPE(JK)
0024            TIMED(JK)=SCALE*I
0025       1002 IF(C(JK)-MAXC(JK)) 1006,1006,1007
0026       1007 MAXC(JK)=C(JK)
0027            TIMEC(JK)=SCALE*I
0028       1006 CSAVE(JK)=C(JK)
0029            IF(I-IIII) 2019,77,77
0030         77 IIII=IIII+JJJJ
0031            III=III+1
0032            DO 55 JK=1,NS
0033            CP(III,JK)=C(JK)
0034         55 DELC(III,JK)=SLOPE(JK)
0035            TIME(III)=SCALE*I
0036       2019 CONTINUE
0037            RETURN
0038            END
```

```
0001            SUBROUTINE OUTPUT(NCT,NS,NR,NL,SCALE,JJJJ,III)
0002            COMMON NAME(13),NCOEF(12,12),MSP(5),MDER(4),TRC(12),SC(12)
0003            COMMON COEF(12,12),C(12),NSPE(12),CP(501,12),DELC(501,12)
0004            COMMON TIME(501),NDELTA(12),TDELTA(12),RATE(12),DELTA(12,12)
0005            COMMON FRAC(12),CSAVE(12),L(12)
0006            COMMON MAXC(12),MAXD(12),TIMEC(12),TIMED(12)
0007            COMMON Y(9,501),YMAX(12),MAGC(5),MAGD(4),MAGY(9)
0008            REAL*4 MAXC,MAXD
0009            IF(NCT) 1005,1006,1005
0010         1005 WRITE(6,1007)
0011         1007 FORMAT(1H1,37HNEGATIVE CONCENTRATIONS WERE PRODUCED)
0012            WRITE(6,1008)
0013         1008 FORMAT(1HO,7HSPECIES,13X,14HTIMES NEGATIVE)
0014            DO 1009  JJ=1,NS
0015            IF(NSPE(JJ)) 1010,1009,1010
0016         1010 WRITE(6,1012) JJ,NSPE(JJ)
0017         1012 FORMAT(1H ,3X,I2,19X,I5)
0018         1009 CONTINUE
0019         1006 CONTINUE
0020            WRITE(6,423)
0021          423 FORMAT(1H1,50X,30HGENERAL KINETIC PROGRAM FL0300)
0022            WRITE(6,101) (NAME(I),I=1,13)
0023          101 FORMAT(1HO,15X,29HSYSTEM UNDER CONSIDERATION = ,13A4)
0024            WRITE(6,102)
0025          102 FORMAT(1HO,60X,10HINPUT DATA)
0026            WRITE(6,103) NS
0027          103 FORMAT(1HO,20X,20HNUMBER OF SPECIES = ,I2)
0028            WRITE(6,104) NR
0029          104 FORMAT(1HO,20X,22HNUMBER OF REACTIONS = ,I2)
0030            WRITE(6,105) NL
0031          105 FORMAT(1HO,20X,25HMAXIMUM PROGRAM PASSES = ,1X,I5)
0032            WRITE(6,106) SCALE
0033          106 FORMAT(1HO,20X,25HEACH PROGRAM PASS EQUALS ,1PE10.3,7HSECONDS)
0034            WRITE(6,107) JJJJ
0035          107 FORMAT(1HO,20X,6HEVERY ,I3,47H PROGRAM PASSES, VALUES ARE RETAINED
                   1 FOR OUTPUT)
0036            WRITE(6,555)
0037          555 FORMAT(1HO)
0038            WRITE(6,108)
0039          108 FORMAT(1HO,25X,20HTRIAL RATE CONSTANTS,25X,22HINITIAL CONCENTRATIO
                   1NS)
0040            DO 301 I=1,20
0041            IF(I-NR) 302,302,303
0042         302 IF(I-NS) 4,4,305
0043            4 WRITE(6,109) I,TRC(I),I,SC(I)
0044          109 FORMAT(1H ,23X,5HRATE(,I2,2H) ,4X,1PE10.3,19X,6HSPECIES(,I2,2H) ,5
                   1X,E10.3)
0045            GO TO 301
0046          303 IF(I-NS) 306,306,301
0047          306 WRITE(6,110) I,SC(I)
0048          110 FORMAT(1H ,65X,8HSPECIES(,I2,2H) ,5X,1PE10.3)
0049            GO TO 301
0050          305 WRITE(6,111) I,TRC(I)
0051          111 FORMAT(1H ,23X,5HRATE(,I2,2H) ,4X,1PE10.3)
0052          301 CONTINUE
0053            WRITE(6,555)
0054            WRITE(6,112)
0055          112 FORMAT(1HO,44X,45HCOEFFICIENT MATRIX DESCRIBING REACTION SCHEME)
0056            WRITE(6,113)
0057          113 FORMAT(1HO,21HCOLUMNS EQUAL SPECIES)
0058            WRITE(6,114)
0059          114 FORMAT(1H ,20HROWS EQUAL REACTIONS)
0060            DO 37 I=1,12
0061           37 L(I)=I
0062            WRITE(6,115)(L(I),I=1,12)
0063          115 FORMAT(1HO,10X,12(1H(,I2,1H),1X))
0064            DO38 I=1,NR
0065           38 WRITE(6,116) L(I),(NCOEF(I,J),J=1,NS)
0066          116 FORMAT(1H ,3X,1H(,I2,1H),3X,12(1X,I2,2X))
0067            WRITE(6,117)
0068          117 FORMAT(1H1,59X,14HPROGRAM OUTPUT)
0069            9 WRITE(6,118)
0070          118 FORMAT(1HO,50X,35HCONCENTRATION AS A FUNCTION OF TIME)
0071            WRITE(6,119) (L(I),I=1,12)
0072          119 FORMAT(1HO,3X,4HTIME,4X,12(1X,5HSPEC(,I2,1H),1X))
0073            DO 13 I=1,III
0074           13 WRITE(6,120) TIME(I),(CP(I,JJ),JJ=1,NS)
0075          120 FORMAT(1H ,13(1PE10.3))
0076            WRITE(6,121)
0077          121 FORMAT(1H1,50X,33HDERIVATIVES AS A FUNCTION OF TIME)
0078            WRITE(6,122) (L(I),I=1,12)
0079          122 FORMAT(1HO,3X,4HTIME,4X,12(1X,5HDERV(,I2,1H),1X))
0080            DO 14 I=1,III
0081           14 WRITE(6,120) TIME(I),(DELC(I,JJ),JJ=1,NS)
0082            RETURN
0083            END
```

```
0001              SUBROUTINE PLOT(NSP,III,NDER)
0002              COMMON NAME(13),NCOEF(12,12),MSP(5),MDER(4),TRC(12),SC(12)
0003              COMMON COEF(12,12),C(12),NSPE(12),CP(501,12),DELC(501,12)
0004              COMMON TIME(501),NDELTA(12),TDELTA(12),RATE(12),DELTA(12,12)
0005              COMMON FRAC(12),CSAVE(12),L(12)
0006              COMMON MAXC(12),MAXD(12),TIMEC(12),TIMED(12)
0007              COMMON Y(9,501),YMAX(12),MAGC(5),MAGD(4),MAGY(9)
0008              REAL*4 MAXC,MAXD
0009              IF(NSP) 74,71,72
0010           72 DO 73 I=1,NSP
0011              NNN=MSP(I)
0012              MAGY(I)=MAGC(I)
0013              YMAX(I)=MAXC(NNN)
0014              DO 73 J=1,III
0015           73 Y(I,J)=CP(J,NNN)
0016           71 IF(NDER) 777,777,75
0017           75 DO 76 I=1,NDER
0018              NNN=MDER(I)
0019              INSP=I+NSP
0020              MAGY(INSP)=MAGD(I)
0021              YMAX(INSP)=MAXD(NNN)
0022              DO 76 J=1,III
0023           76 Y(INSP,J)=DELC(J,NNN)
0024          777 NYS=NSP+NDER
0025              NDATA=III
0026              WRITE(6,501)
0027          501 FORMAT(1H1,45X,19HPLOT ROUTINE FL0400)
0028              IF(NSP) 993,993,994
0029          994 CONTINUE
0030              DO 78 I=1,NSP
0031           78 WRITE(6,502) MSP(I),I,TIMEC(MSP(I)),MAXC(MSP(I)),MAGC(I)
0032          502 FORMAT(1H ,5HSPEC(,I2,4H) = ,I1,10X,18HTIME AT MAXIMUM = ,1PE10.3,
                 110X,10HMAXIMUM = ,1PE10.3,10X,17HMAGNIFICATION = X,I3)
0033          993 CONTINUE
0034              IF(NDER) 991,991,992
0035          992 DO 87 I=1,NDER
0036              IDER=I+NSP
0037           87 WRITE(6,503) MDER(I),IDER,TIMED(MDER(I)),MAXD(MDER(I)),MAGD(I)
0038          503 FORMAT(1H ,5HDERV(,I2,4H) = ,I1,10X,18HTIME AT MAXIMUM = ,1PE10.3,
                 110X,10HMAXIMUM = ,1PE10.3,10X,17HMAGNIFICATION = X,I3)
0039          991 CONTINUE
0040              CALL FL0400(NYS,NDATA)
0041           74 CONTINUE
0042              RETURN
0043              END
```

```
0001            SUBROUTINE FL0400(NYS,NDATA)
0002            COMMON NAME(13),NCOEF(12,12),MSP(5),MDER(4),TRC(12),SC(12)
0003            COMMON COEF(12,12),C(12),NSPE(12),CP(501,12),DELC(501,12)
0004            COMMON TIME(501),NDELTA(12),TDELTA(12),RATE(12),DELTA(12,12)
0005            COMMON FRAC(12),CSAVE(12),L(12)
0006            COMMON MAXC(12),MAXD(12),TIMEC(12),TIMED(12)
0007            COMMON Y(9,501),YMAX(12),MAGC(5),MAGD(4),MAGY(9)
0008            DIMENSION N(11),NP(101),NY(9,501)
0009            DATA N/'1111','2222','3333','4444','5555','6666','7777','8888','99
               199','    ','++++'/
0010            DO 33 J=1,NYS
0011            IF(YMAX(J)) 31,31,30
0012         31 DO 32 I=1,NDATA
0013         32 NY(J,I)=1
0014            WRITE(6,34) J
0015         34 FORMAT(1H ,20X,31HYMAX WAS ZERO FOR CURVE NUMBER ,I2)
0016            GO TO 33
0017         30 SCALE=YMAX(J)/100.
0018            DO 5 I=1,NDATA
0019            NY(J,I)=((Y(J,I)*MAGY(J))/SCALE)+1.5
0020            IF(NY(J,I)-101) 5,5,200
0021        200 NY(J,I)=101
0022          5 CONTINUE
0023         33 CONTINUE
0024            NX=0
0025            NH=5
0026            NF=0
0027            DO 45 I=1,101
0028         45 NP(I)=N(10)
0029         11 NX=NX+1
0030            IF(NX-1) 12,13,12
0031         12 IF(NX-NH) 14,15,14
0032         15 NH=NH+10
0033            NP(51)=N(11)
0034            GO TO 16
0035         14 IF(NX-NF) 16,13,16
0036         13 DO 17 I=1,101,10
0037         17 NP(I)=N(11)
0038            NF=NF+10
0039         16 CONTINUE
0040            DO 18 J=1,NYS
0041            NN=NY(J,NX)
0042         18 NP(NN)=N(J)
0043            WRITE(6,102) NX,N(11),(NP(I),I=1,101),N(11),NX
0044        102 FORMAT(1H ,10X,I4,1X,103A1,1X,I4)
0045            DO 19 I=1,101
0046         19 NP(I)=N(10)
0047            IF(NX-NDATA) 11,20,20
0048         20 CONTINUE
0049            RETURN
0050            END
```

FIGURE VI-1

Main Routine, MAIN

Key

START - Program beginning.

STOP - Program end.

NCON - A variable used to determine if any data are present.

INPUT - Input subroutine.

INITIALIZE - Initializes any data before the program starts calculating.

CALC - Calculating subroutine.

NEGC - Negative concentration subroutine.

PRINTP - Print preparation subroutine.

Output - Output subroutine.

PLOT - Plot preparation routine.

FL0400 - A standard printer plotting routine.

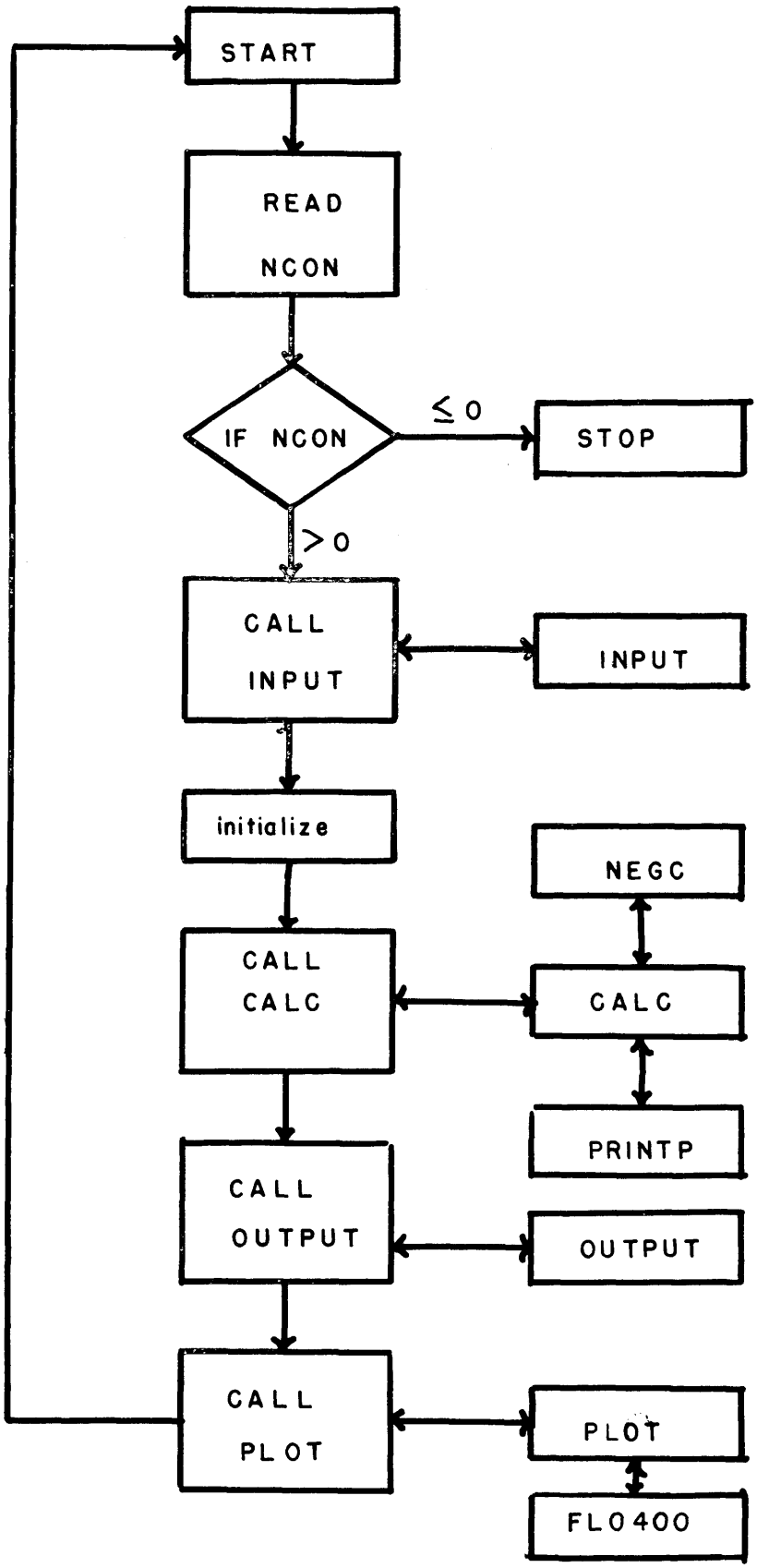
START
READ
NCON
IF NCON
≤ 0
STOP
> 0
CALL
INPUT
INPUT
initialize
NEGC
CALL
CALC
CALC
PRINTP
CALL
OUTPUT
OUTPUT
CALL
PLOT
PLOT
FL0400

FIGURE VI-2

Input Subroutine, INPUT

Key

MAIN - Statement in the main routine calling the subroutine.

JDATA - A variable used to determine the type of input to be read.

RETURN - Statement returning control to the calling routine.

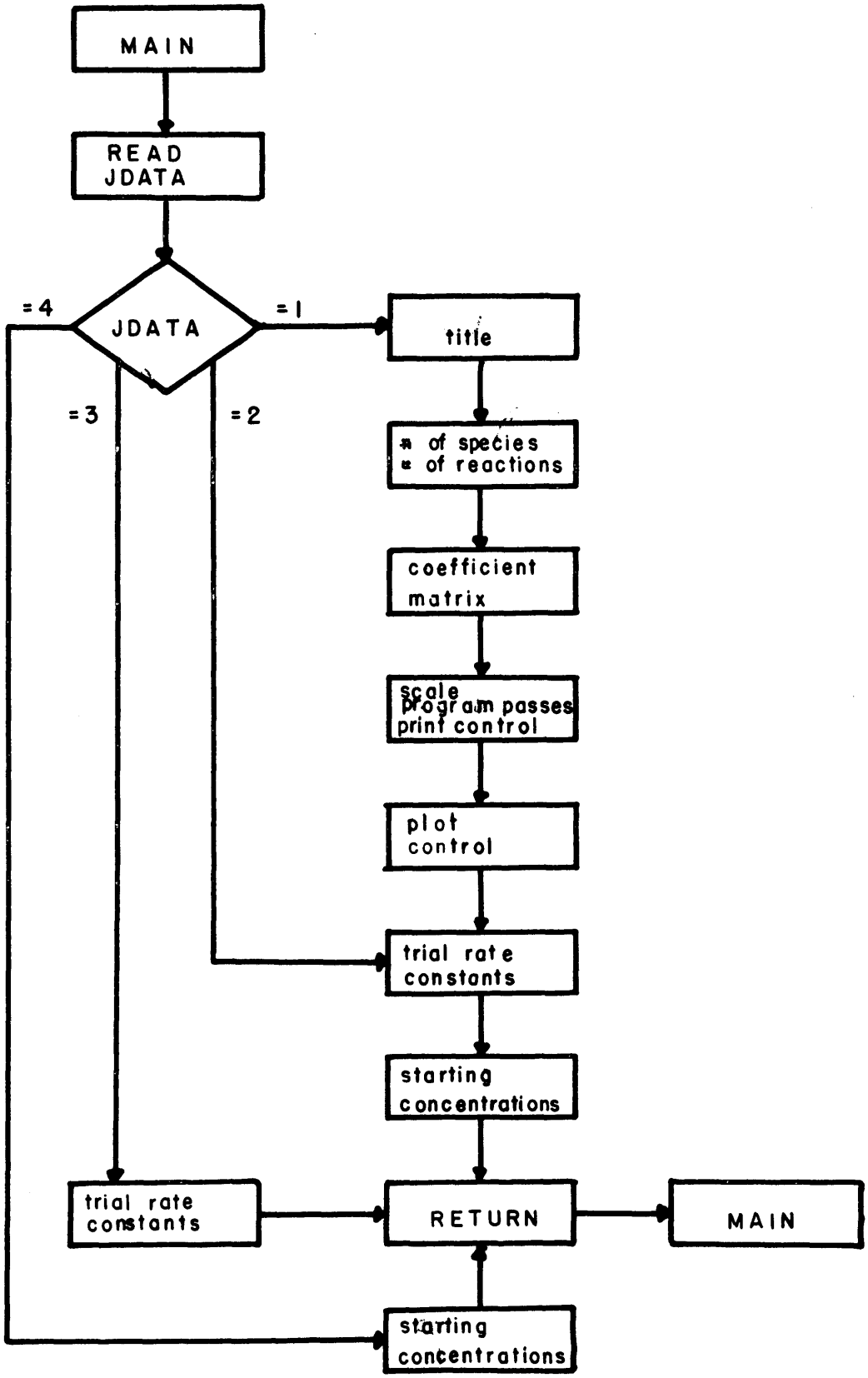
MAIN
READ JDATA
JDATA
=4
=1
=3
=2
title
# of species
# of reactions
coefficient matrix
scale
program passes
print control
plot control
trial rate constants
starting concentrations
trial rate constants
RETURN
MAIN
starting concentrations

Calculation-Figure VI-3 shows the flow diagram for the calculating subroutine, CALC. The major job accomplished by CALC is the generation of concentrations and the derivative of the concentrations as a function of time.

Each pass through the program, from INCREMENT COUNTER to FINISHED, represents a time interval of duration Δt. The program calculates the rates by use of Equation VI-1. Then it calculates, by use of Equations VI-4a, 4b, the changes in concentration, $\Delta_{i,j}$, occuring during the time interval. Equation VI-6 is used to determine the total change in the concentration. When the last time interval has been reached, control is passed back to the main routine.

Negative Concentrations-Figure VI-4 shows the flow diagram for the negative concentration routine, NEGC. The major job accomplished by NEGC is the identification and correction of a negative concentration produced by the calculating routine.

The key approximation in the program is the one concerning the equality or near equality of $\Delta Ci/\Delta t$ and dC_i/dt. Because the time interval Δt is not infinitely small, there exists the chance that the sum of all of the negative $\Delta_{i,j}$ will be greater than the value of C_i at the start of the time interval. This can be corrected.

The first check made by NEGC is the sign of the expression

$$C_i + \sum_j \Delta_{i,j} \qquad \text{VI-7}$$

FIGURE VI-3

Calculating Subroutine, CALC

Key

MAIN - Statement in the main routine calling the subroutine.

INCREMENT COUNTER - Keeps track of the number of time intervals calculated.

ΔC - Represents the change in the concentration of a species during the current time interval.

NEGC - Negative concentration subroutine.

PRINTP - Print preparation subroutine.

FINISHED ? - Stops calculations when the correct number of time intervals has been reached.

RETURN - Statement returning control to the calling routine.

RETURN 1 - Statement returning NEGC control to SUMΔC's operation.

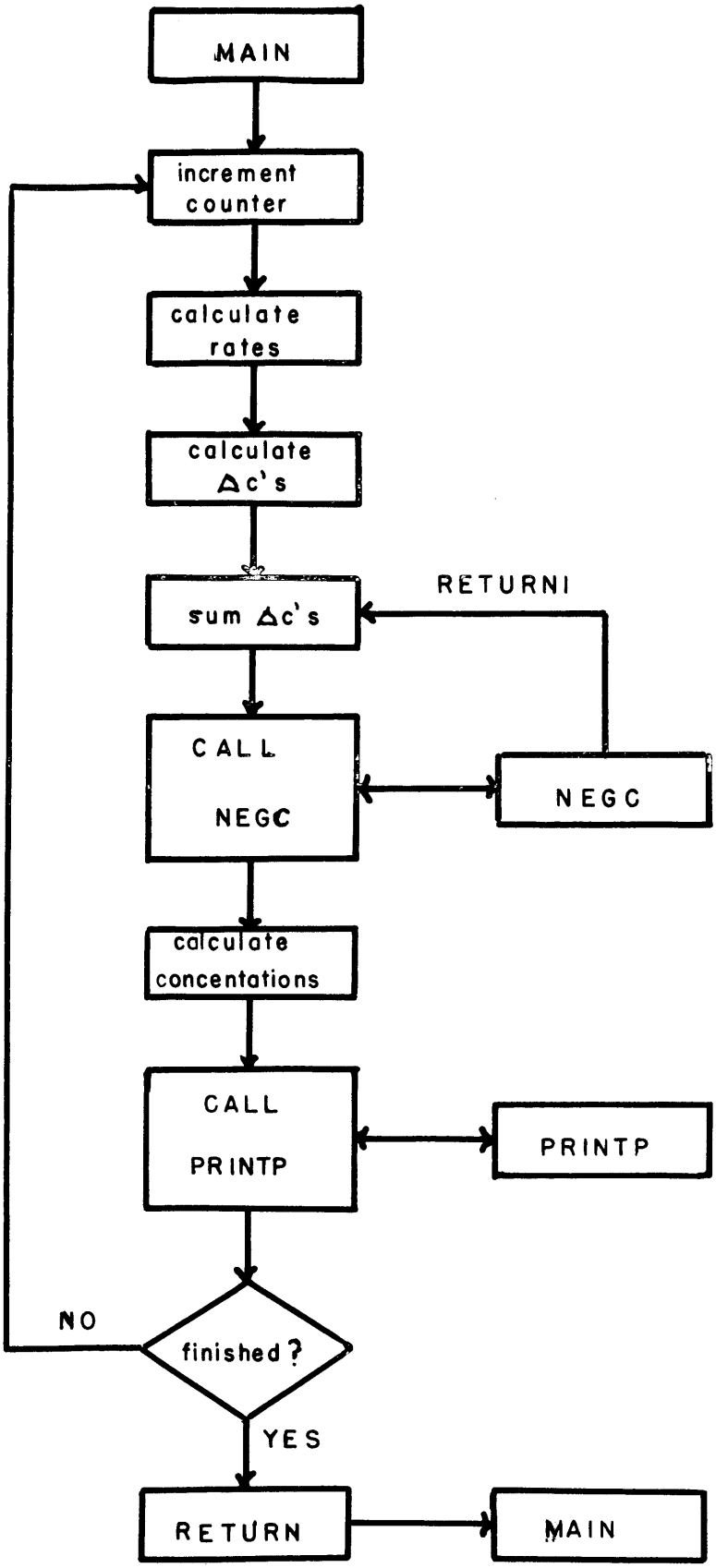
MAIN
increment counter
calculate rates
calculate Δc's
sum Δc's
RETURNI
CALL NEGC
NEGC
calculate concentations
CALL PRINTP
PRINTP
NO
finished ?
YES
RETURN
MAIN

FIGURE VI-4

Negative Concentration Subroutine, NEGC

Key

CALC - Statement in the calculating routine calling the subroutine.

INCREMENT COUNTER - Keeps track of the concentrations checked.

CONC NEGATIVE ? - Enters the correction section if a negative concentration is encountered.

FINISHED ? - Stops calculating when all of the concentrations are positive.

RETURN - Statement returning control to the calculating routine.

RETURN 1 - Statement returning control to the SUMΔC's operation in the calculating routine.

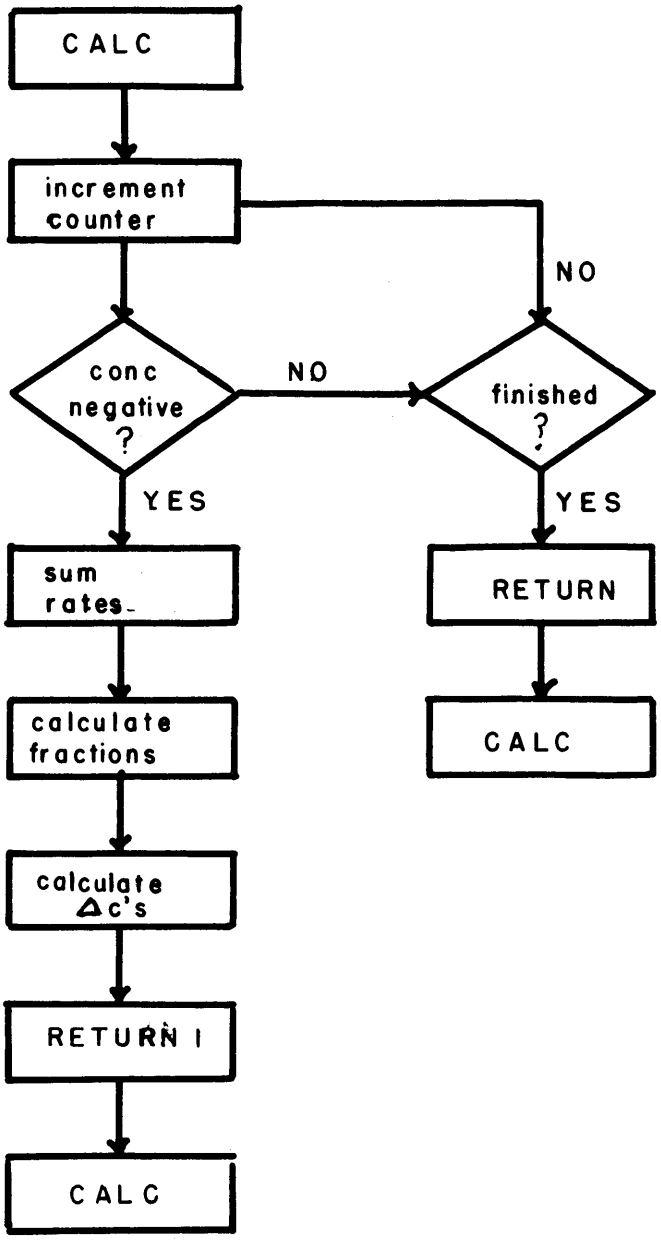
CALC
increment counter
NO
conc negative ?
NO
finished ?
YES
YES
sum rates
RETURN
calculate fractions
CALC
calculate Δc's
RETURN
CALC

where the summation is carried out for all j's where species i is a reactant; and the $\Delta'_{i,j}$'s are the negative set of the $\Delta_{i,j}$. If this expression is found positive, the counter is incremented and the next species is examined. This continues until all of the concentrations are found positive.

If Equation VI-7 is found negative, a correction routine is entered. First, the routine sets the maximum concentration of the offending species, k, available to react, equal to C_k. Then the routine parcels out this concentration to all of the reactions where species k is reactant. This is achieved by calculating the fractions

$$F_j = R_j / \Sigma_j R_j \qquad \text{VI-8}$$

where the summation is carried out for all j where species k is a reactant. The maximum concentration available for each reaction is then $C_k \cdot F_j$.

Also, all of the species appearing in all of the reactions where k is a reactant, must have their values of $\Delta_{i,j}$, adjusted. This is done by the equation

$$\Delta_{i,j} = (- C_k \cdot F_j \cdot s_{i,j}) / s_{k,j} \qquad \text{VI-9}$$

where k is the offending species; j is any reaction where species k appears as a reactant; and i is any species appearing in the jth reaction.

After making the appropriate corrections, the program control is returned to CALC.

Print Preparation-Figure VI-5 shows the flow diagram for the print preparation routine, PRINTP. The major job accomplished by PRINTP is the saving of concentrations and derivatives for printing.

The initializing section performs some preliminary tasks for the derivative calculation and maxima searching sections. The derivatives are calculated by the expression

$$(C_i^{t'} - C_i^{t})/\Delta t \qquad \text{VI-10}$$

The time is calculated by multiplying the number of the particular pass through the calculating routine times the value of Δt.

The maximum values of the concentrations and derivatives, determined here, are used in the plot preparation routine and will be discussed there.

Output-Figure VI-6 shows the flow diagram for the output routine, OUTPUT. The major job accomplished by OUTPUT is the printing of the program results.

If any negative concentrations were produced, information is displayed that shows what species went negative and how many times it did so. The routine then prints out the input data. Next it prints the concentrations as a function of time and then the derivatives as a function of time.

Plot Preparation-Figure VI-7 shows the flow diagram for

FIGURE VI-5

Print Preparation Subroutine, PRINTP

Key

CALC - Statement in the calculating routine calling the subroutine.

FIRST PASS ? - Initializes data needed in the routine on the first pass.

SAVE DATA ? - If data are to be saved for printing during this pass through the calculating routine, the saving section is entered.

RETURN - Statement returning control to the calculating routine.

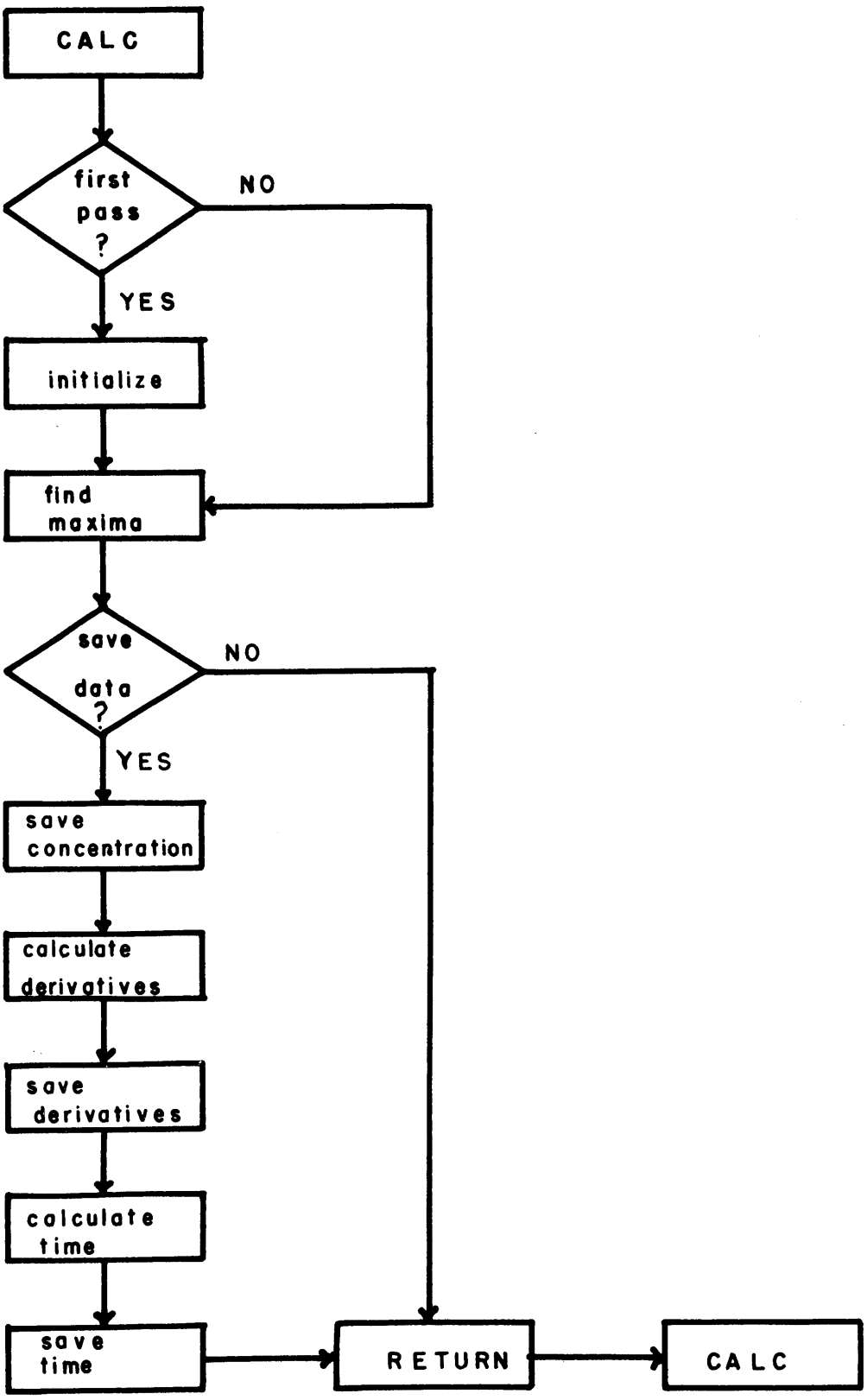
CALC
first pass ?
NO
YES
initialize
find maxima
save data ?
NO
YES
save concentration
calculate derivatives
save derivatives
calculate time
save time
RETURN
CALC

FIGURE VI-6

Output Subroutine, OUTPUT

Key

MAIN - Statement in the main routine calling the subroutine.

CONCS NEGATIVE ? - If any concentrations were ever negative, the related information is printed.

RETURN - Statement returning control to the main routine.

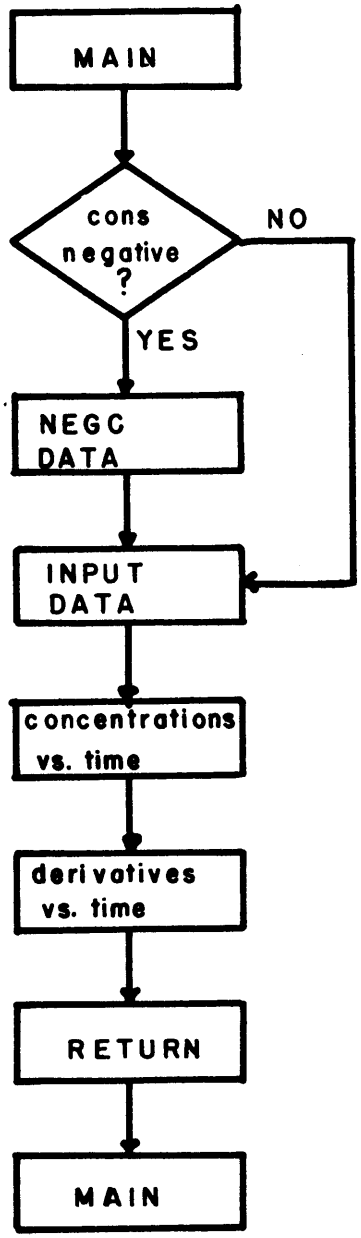
MAIN
cons negative ?
NO
YES
NEGC DATA
INPUT DATA
concentrations vs. time
derivatives vs. time
RETURN
MAIN

FIGURE VI-7

Plot Preparation Subroutine, PLOT

Key

MAIN - Statement in the main routine calling the subroutine.

PLOT ? - If there are no data to be plotted, the routine is bypassed.

FL0400 - The plotting routine.

RETURN - Statement returning control to the main routine.

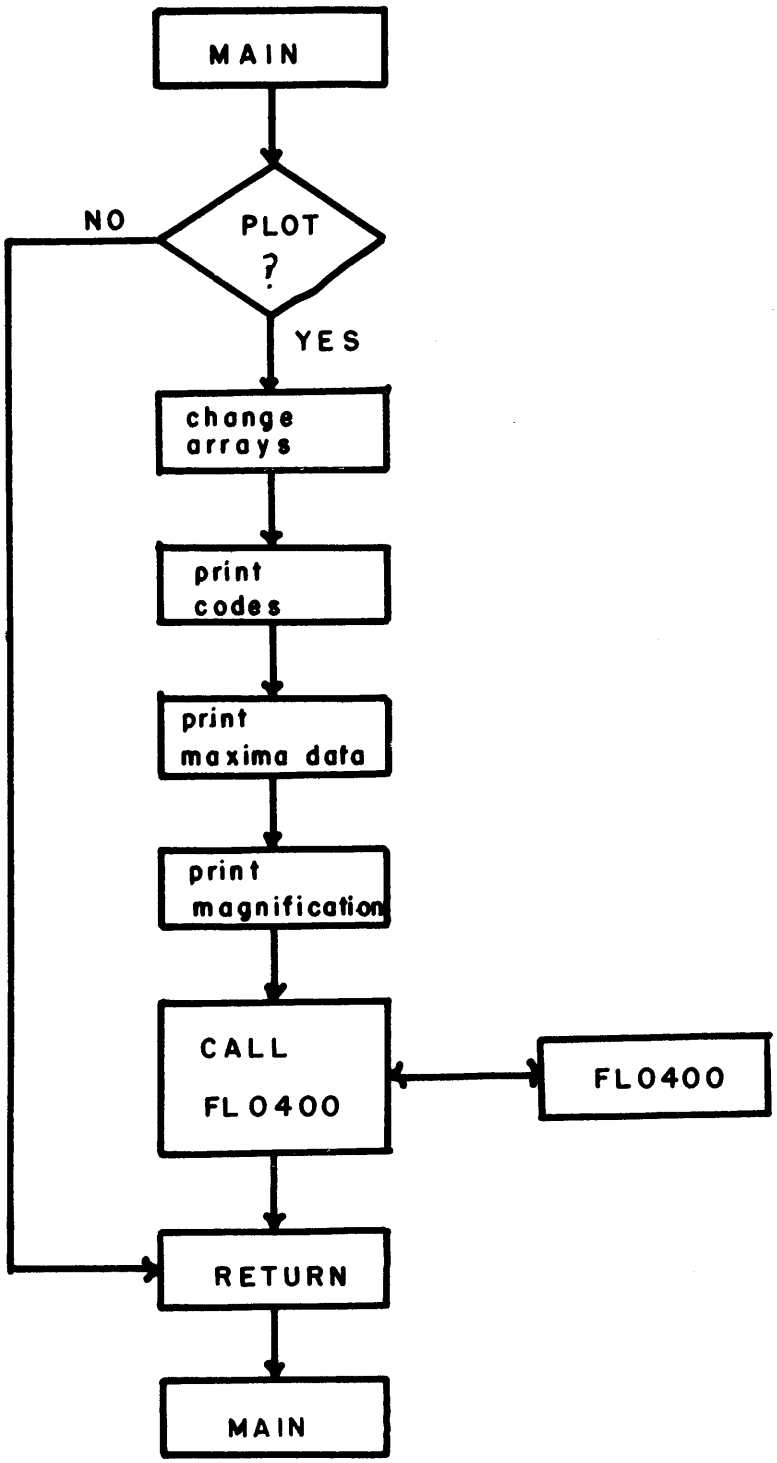
MAIN
PLOT ?
NO
YES
change arrays
print codes
print maxima data
print magnification
CALL FL0400
FL0400
RETURN
MAIN

the plot preparation routine, PLOT. The major job accomplished by PLOT is the arrangement of the data before it is plotted.

First, the concentration and derivative arrays are rearranged into a form compatible with the plotting routine FL0400. Codes are printed which indicate to the programmer how to identify the species or derivatives appearing in the plot. The maxima found in PRINTP are printed along with the time at which they occured. Finally, the magnification of each plot is printed.

PLOT calls FL0400 before returning control to the main routine.

Plotting Routine-No flow diagram is shown for the plotting routine, FL0400, since it is a typical printer plotter.

Nine curves can be simultaneously plotted by FL0400. The data for each curve are normalized by the appropriate maximum found by PRINTP. Each curve can be magnified so that small features in new the data can be examined.

4. Coefficient Matrix

In order to describe a reaction mechanism in a manner that allows the computer to perform the appropriate calculations, a coefficient matrix is necessary. For the purpose of illustration, the for following reaction scheme will be discussed,

$$[1] + 2[2] \xrightarrow{k_1} [3]$$

$$[3] + 3[4] \xrightarrow{k_2} 2[5]$$

$$2[5] \xrightarrow{k_3} [3] + 3[4]$$

$$[5] \xrightarrow{k_4} [6]$$

$$[6] \xrightarrow{k_5} [7]$$

$$3[5] \xrightarrow{k_6} [8]$$

where the numbers in brackets refer to species and the numbers outside of the brackets refer to stoichiometry. For the above scheme the coefficient matrix is

reaction \ species	1	2	3	4	5	6	7	8
1	1	2	-1	0	0	0	0	0
2	0	0	1	3	-2	0	0	0
3	0	0	-1	-3	2	0	0	0
4	0	0	0	0	1	-1	0	0
5	0	0	0	0	0	1	-1	0
6	0	0	0	0	3	0	0	-1

where the stoichiometry is entered as a positive number if the species is a reactant and a negative number if the species is a product. A value of zero is entered whenever a species does not appear in a reaction.

5. Input

Card (1):

a) a(1) punch in column one, if data are present.

b) a blank card, if no data are present.

Note: this means that several sets of data can be processed on the same computer run. The last card of every data deck, must be a blank card.

Card (2):

a) If a non-abbreviated form of the data is to be read in, a (1) punch in column one is used.

b) If only trial rate constants and starting concentrations are to be read in, a (2) punch in column one is used.

c) If only trial rate constants are to be read in, a (3) punch in column one is used.

d) If only starting concentrations are to be read in, a (4) punch in column one is used.

Note: the first set of data must have a (1) punch on this card, since all of the input data are needed to execute the program. However, each successive set of data can retain the key parameters read in on the first set, and simply substitute new operational parameters, i.e. trail rate constants and/or starting concentrations.

Card (3):

The title of the program can be punched in any alphameric form. This field is columns one through seventy-two. This title will be printed with the output to identify the computer run.

Card (4):

a) Columns one and two contain the number of different species appearing in the reaction scheme(NS).

b) Columns three and four contain the number of reactions appearing in the reaction scheme(NR).

Next NR Cards:

These cards contain the coefficient matrix. Each of these cards will have NS coefficients, each taking two columns of card space.

Examples: the coefficient for the reaction labeled (1) and the species labeled (1) will be found in columns one and two of card one. The coefficient for the reaction labeled (3) and the species labeled (7) will be found in columns thirteen and fourteen of card three.

Note: These coefficients must be right adjusted. If the coefficient is negative, a minus sign must appear in the odd numbered column. Zero's do not have to be punched, the columns may be left blank.

Next card:

a) Columns (1) through (10) contain the time scale in the form +x.xxxE±xx, where x is any integer. The time scale is the

unit of time that each program pass represents. For example, each program pass could represent 0.001 seconds, therefore one-thousand passes would give a total simulated time of one second.

b) Columns (11) through (15) contain the maximum number of program passes. This value is right justified. A typical value would be one-thousand as discussed above.

c) Columns (16) through (18) contain a print control. If every pass through the program created data to eventually be printed out, the volume of output would be enormous. The print control allows only certain program passes to create output data. For example, if the maximum number of passes is one-thousand and the print control is ten, then every tenth program pass will create data to be used as output, for a total of 100 pieces of data.

Next Card:

This card is the plot control. Up to five concentrations and four derivatives can be plotted simultaneously.

Columns (1) and (2) contain the main plot control. If these columns contain a (-1), nothing will be plotted; if they contain zero, only derivatives will be plotted; if they contain an integer from 1 to 5, that many concentrations will be plotted. Columns (3) through (22) contain sets of information for five species. The first two columns in each set contain the species code, and the second two columns contain the magnification code.

Columns (26) and (27) contain the derivative plot control. If these columns are zero, no derivatives will be plotted; if they contain an integer from 1 to 4, that many derivatives will be plotted. Columns (28) through (43) contain four sets of information. These sets are arranged in the same fashion as those mentioned above for the concentrations.

For example, the data control card

```
0205011002 . . . . . 010825 . . . .   punch
↑                    ↑
01                   26               column
```

indicates that two concentrations should be plotted, those of species (5) and species (10); that one derivative should be plotted, that of species (8); and that their corresponding curves should be magnified by one, two and twenty-five, respectively.

Next set of Cards:

The next set of cards contains the trial rate constants. The TRC for reaction one will be punched in columns (1) through (10) in the form +x.xxxE+xx. The TRC for reaction two in columns (11) through (20), reaction three in columns (21) through (30), reaction four, etc. Each card contains only six TRC's so the seventh through twelfth will be found on the second card of this set.

Next set of Cards:

The next set of cards contains the starting concentrations. The SC for reaction one will be punched in columns (1) through (10) in

the form +x.xxxE±xx. The remainder of the values follow the format of the trial rate constants.

6. Program Check

The program has been checked for several kinetic schemes and has been found to be suitable for the calculations needed in this thesis. The program yields correct values of reaction half-times for first order, second order and parallel first order reactions. However, it is difficult to find a complex kinetic scheme where the values of the rate constants and the concentrations are known with any degree of accuracy. Equilibrium problems offer a logical program check.

Butler (4) discusses the equilibrium problems associated with the salts of polyprotic acids. His example calculating the pH of and a 0.1M NaH_2PO_4 solution, is easily programmed.

The reactions of interest are

$$H_3PO_4 \underset{k_2}{\overset{k_1}{\rightleftharpoons}} H_2PO_4^- + H^+$$

$$H_2PO_4^- \underset{k_4}{\overset{k_3}{\rightleftharpoons}} HPO_4^{-2} + H^+$$

$$HPO_4^{-2} \underset{k_6}{\overset{k_5}{\rightleftharpoons}} PO_4^{-3} + H^+$$

where k_1=5.90 x 10^{-3}, k_3=6.15 x 10^{-8}, and k_5-4.80x 10^{-13}. All of the back reactions, k_2, k_4 and k_6, are arbitrarily set equal to unity. The starting concentrations are, H_3PO_4=0, $H_2PO_4^-$=0.1M, HPO_4^{-2}=0, and H+= 1 x 10^{-7}M.

Using 20,000 passes through the program with each time interval being equal to 1 second, the reactions came reasonably close to equilibrium. At the end of the program, the computer's values and Butler's values, in parentheses, are; H_3PO_4= 3.098×10^{-4}(3.1×10^{-4}); $H_2PO^-_4$=9.896×10^{-2}(0.10); HPO_4^{-2}= 3.282×10^{-4}(3.3×10^{-4}); PO^{-3}_4= 8.109×10^{-12}(8.6×10^{-12}); and H+ = 1.847×10^{-5}(1.85×10^{-5}). In every case the computers values were "going" in the correct direction. Butler claims that his numbers are good to within 5% of the actual values.

The total computer time involved in running this example was 2.85 minutes. Normally 1,000 passes through the program are sufficient to obtain the degree of accuracy required.

VI. Appendices

B. Nuclear Magnetic Resonance Studies†

1. Introduction

An analytical analysis of $Ru(bipyr)_3Cl_2$ was deemed necessary since many spectral studies are sensitive to impurities that could be present in the chelate preparation. A melting point is not available for this compound since it readily decomposes. Elemental analysis, at best, offers a crude estimation of both purity and composition. Nuclear Magnetic Resonance, NMR, was chosen since it has found use in inorganic chemistry for determining ligand numbers and structural properties of metal complexes(31). Besides its analytical function which parallels the results expected for elemental analysis, NMR studies would also furnish information on charge distribution in the chelated ligand and other special effects such as those caused by the geometrical configuration of the complex.

2. Ligand Spectra

The ligand, 2,2'-bipyridine, I, has four nonequivalent protons on each ring which give an NMR spectrum that can be completely analyzed as repeated AX patterns. Only simple first-order spin-spin splitting theory need be invoked. Kramer and West (26) have reported a detailed interpretation of this spectrum in a dichloromethane solution. Not only are the peak positions for each proton widely

---

† It is to be noted that all of the work described in this section was done by both the author and Steven A. Carlson of our laboratory.

separated; but also the principle splitting constants for H_3 and H_4 are about double these for H_5 and H_6. Thus although

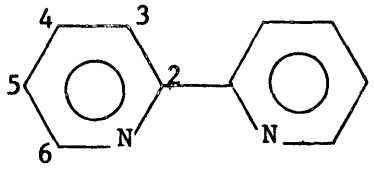

I

H_3 and H_6 appear as doublets in the spectrum, they can be differentiated by their coupling constants. The assignment of H_4 and H_5 is similarly facilitated.

Although dichloromethane was found suitable as a solvent for studying the 2,2'-bipyridine spectrum, for solubiblity reasons a polar solvent, such as ethanol or dimethyl sulfoxide, was required for examining any chelate having this compound as a ligand. To facilitate spectral comparisons, the ligand spectrum was also measured in the same solvents. The spectrum of 2,2'-bipyridine in ethanol is shown in Figure VI-8. It matches that found by Kramer and West in dicholromethane solution so far as peak shape and splitting constants, although the peak positions move slightly downfield as the solvent becomes more polar.

3. Protanted Ligand Spectra

Smith and Schneider (43) studied the effect of protonation on the NMR spectrum of pyridine, II. In trifluoroacetic acid, TFA, solutions, the proton peaks undergo a downfield displacement due to the

FIGURE VI-8

NMR Spectrum of 2,2'-Bipyridine

15% w/w in ethanol, 500 cycle sweep width. Units are cps downfield from tetramethylsilane.

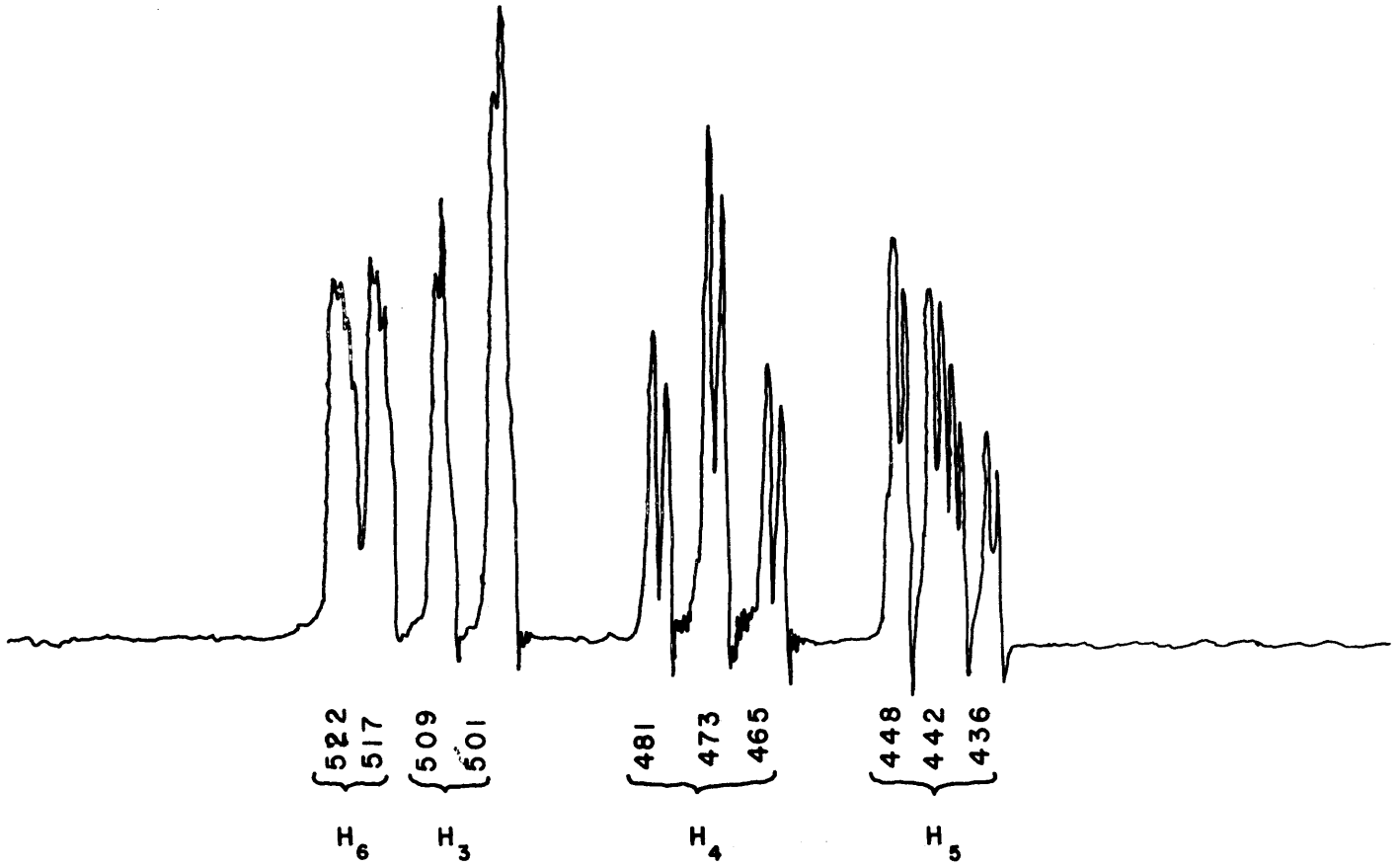
522
517
509
501
481
473
465
448
442
436
H6
H3
H4
H5

decrease in electron charge density at the individual carbon nuclei.

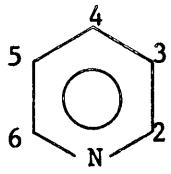

II

Protons 2 and 6 are shifted downfield by 15 cps; proton 3 and 5, by 65 cps; and proton 4 is shifted downfield by 73 cps. The NMR spectrum of 2,2'-bipyridine in TFA is shown in Figure VI-9. This spectrum has downfield shifts similar to those found for acidified pyridine. Protons 4, 5, and 6 shift downfield 54 cps, 51 cps and 25 cps, respectively.

Proton 3 for 2,2'-bipyridine, which differs from that in pyridine by being adjacent to the 2,2' bond, shows a downfield shift on only 10 cps. This small shift gives rise to an interesting phenomenon. As a DMSO solution of 2,2'-bipyridine is acidified with TFA, proton 4 (originally slightly upfield from proton 3) moves downfield faster than proton 3. Between the point of monoprotonation and diprotonation, the two protons become nearly equivalent and give rise to complex AB spectra. An infinite variety of AB spectra can be obtained by changing the solution acidity. Since all of the proton coupling constants are known from spectra in neutral solutions, the complex AB spectra can be interpreted with prior knowledge of the coupling constants.

Figure VI-10 shows the magnitude of the downfield shift as acid is added drop by drop. It resembles a titration curve where the

FIGURE VI-9

NMR Spectrum of Diprotonated 2,2'-Bipyridine

15% w/w in TFA, 500 cycle sweep width. Units are cps downfield from tetramethylsilane.

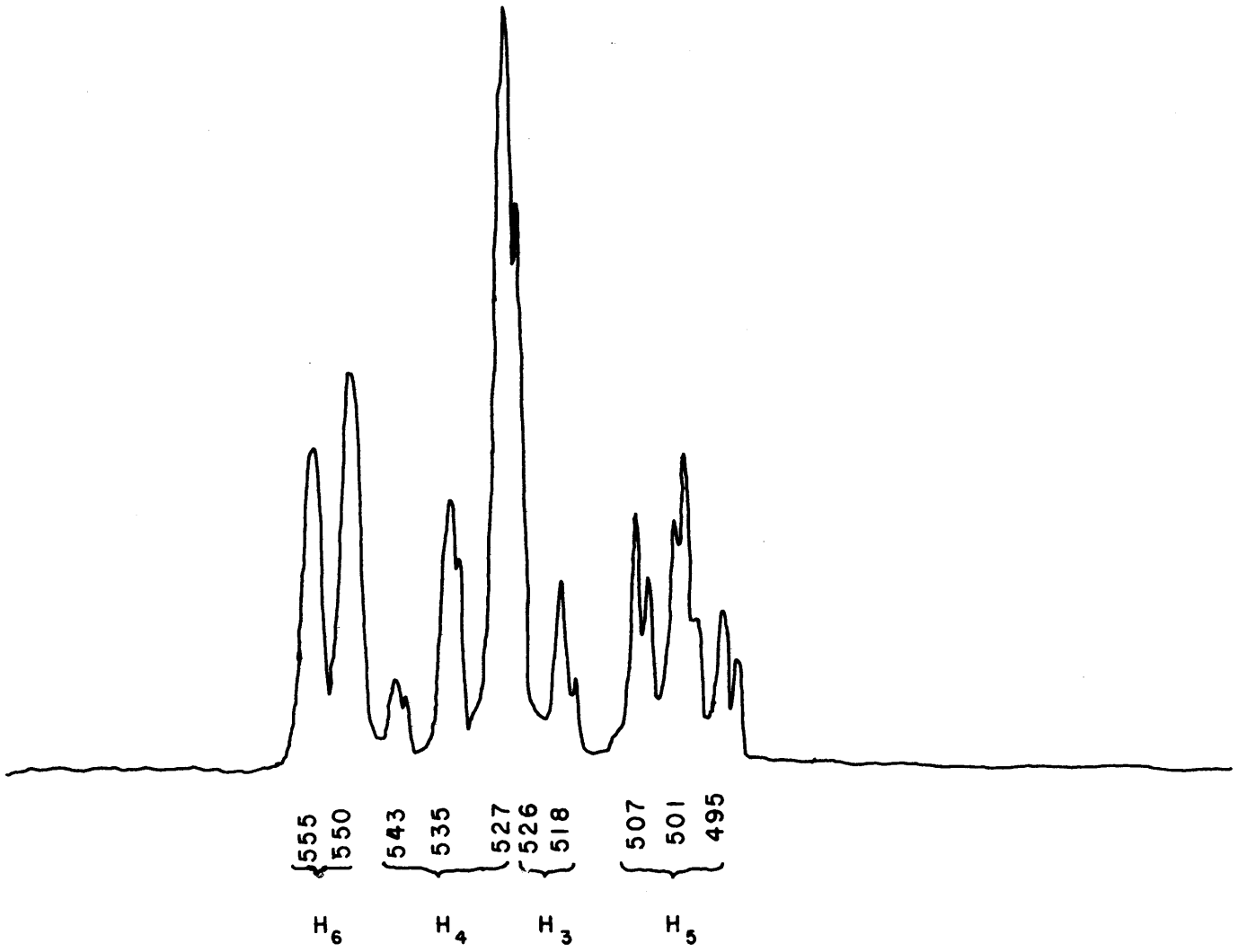
555
550
543
535
527
526
518
507
501
495
H6
H4
H3
H5

FIGURE VI-10

Downfield Shift of the 2,2'-Bipyridine Protons

as a Function of Acidity

Key

● ● ● ● ● Protons 4 and 5.

o o o o o Proton 6.

+ + + + + Proton 3.

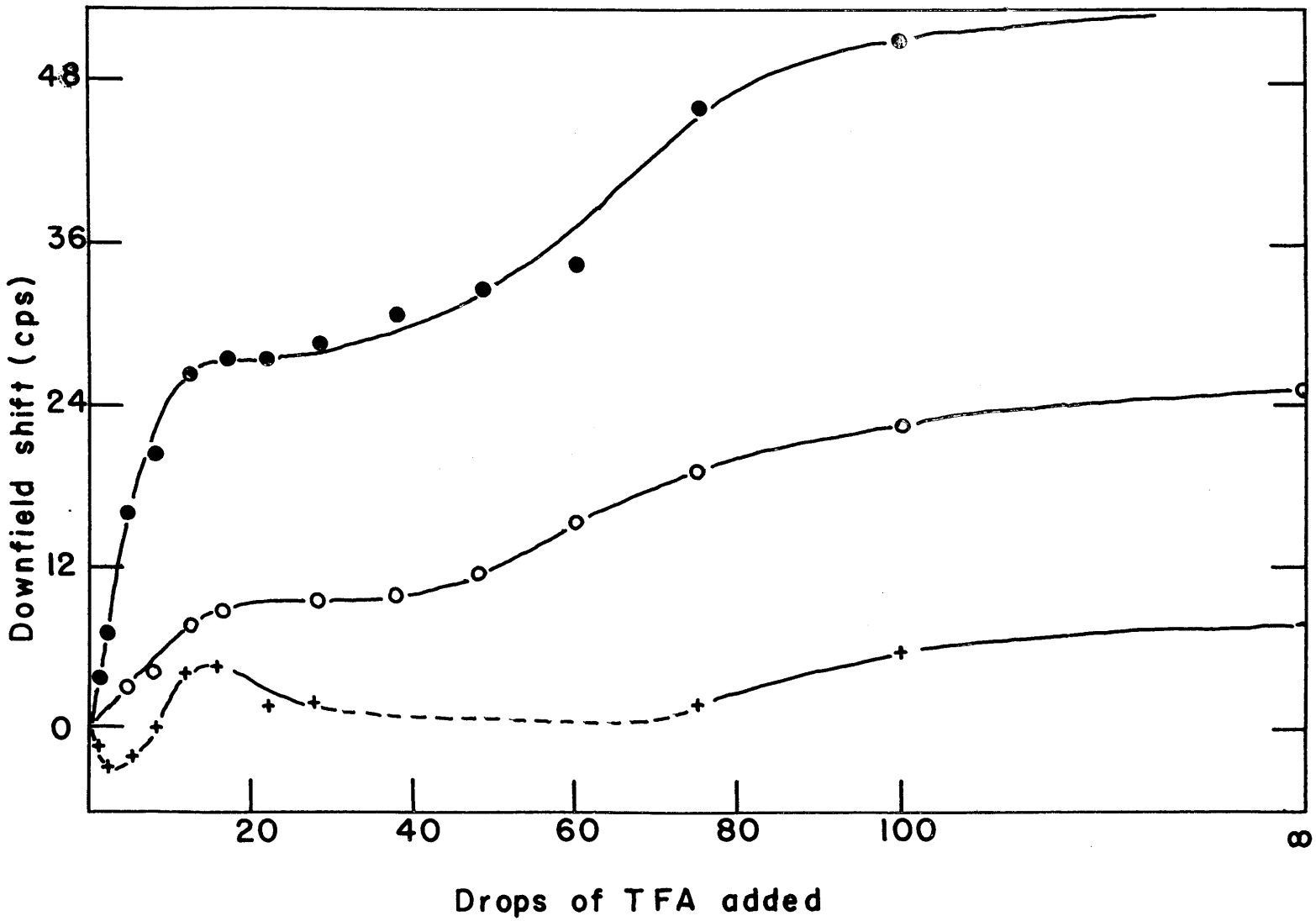
48
36
24
12
0
Downfield shift (cps)
20
40
60
80
100
∞
Drops of TFA added

first plateau represents monoprotonation and the second plateau represents diprotonation. As expected, the downfield change upon monoprotonation is approximately half that for diprotonation. Once again proton 3 shows abnormal behavior. The reason for this is not clear, but it may include steric hindrance between the 3 proton on adjacent rings when the monoprotonated form is held planar.

When 2,2'-bipyridine is bonded to a ruthenium(II) ion in a metal ion complex, a positive charge is introduced at the nitrogens. With three ligands per chelate, each nitrogen experiences a net + 1/3 charge. If the only effect on the ligand upon chelation were that of an increased positive charge, the downfield shifts of the proton would be expected to be about 1/3 of those found for the ligand in TFA. The change would be 3 cps for H-3, 18 cps for H-4, 17 cps for H-5 and 8 cps for H-6.

4. Chelate Spectra

Since the ruthenium(II) complexes of interest are diamagnetic, their NMR spectra are not subject to the large contact shifts found in paramagnetic species. Figure VI-11 shows the NMR spectrum of $Ru(bipyr)_3Cl_2$ in ethanol. Protons 3, 4 and 5 are shifted downfield, from the ligand positions in ethanol, by 35 cps, 18 cps and 17 cps, respectively. Proton 6 was shifted upfield by 56 cps.

The downfield shifts of H-4 and H-5 agree with the value predicted on the basis of a +2/3 charge on each ligand. However, H-3 is shifted 32 cps further downfield than expected. This is not unreasonable when

FIGURE VI-11

NMR Spectrum of $Ru(bipyr)_3Cl_2$

15% w/w in ethanol, 500 cycle sweep width. Units are cps downfield from tetramethylsilane.

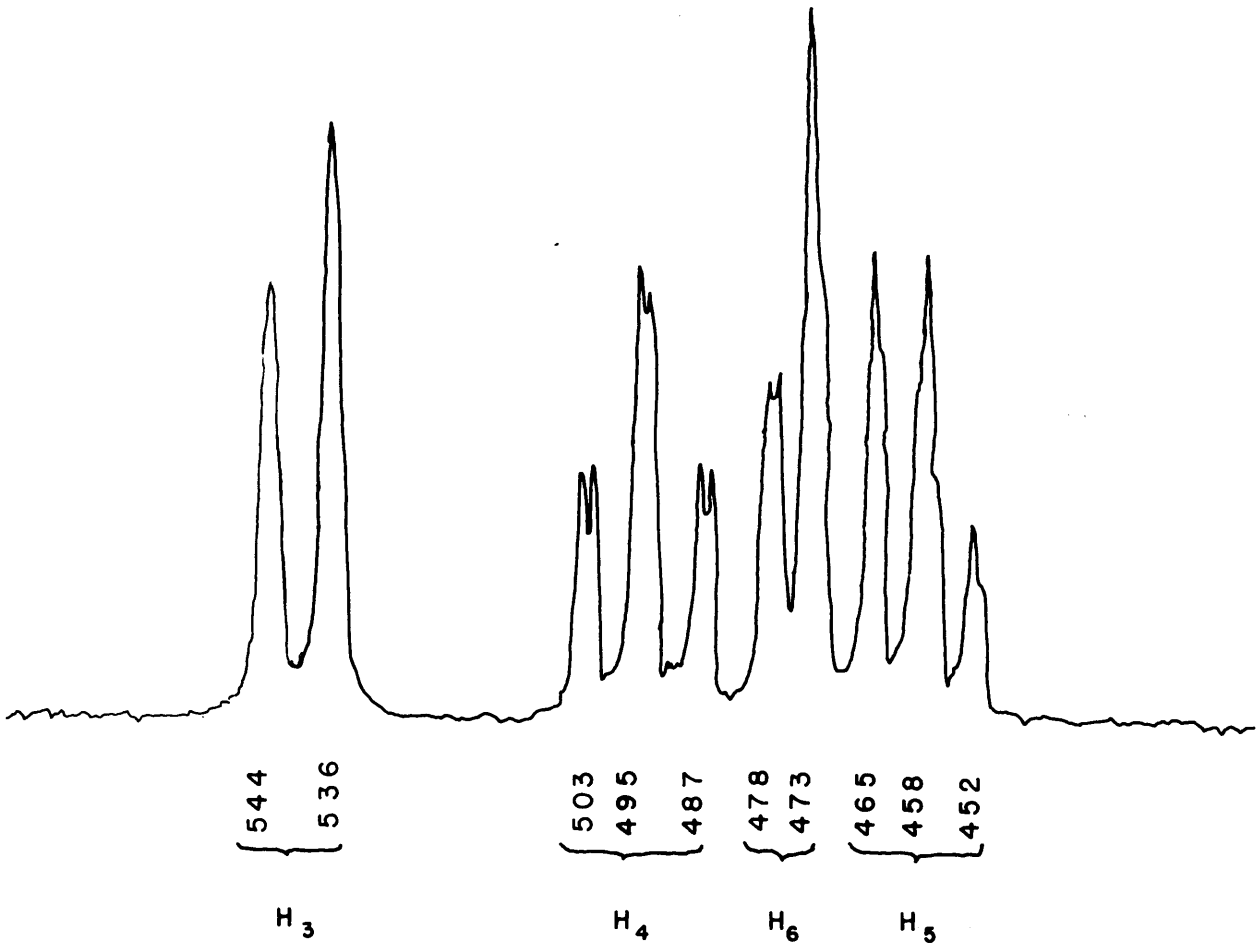
544
536
503
495
487
478
473
465
458
452
H3
H4
H6
H5

the steric requirements of the complex are considered. Upon chelation the ligand is forced into a planar configuration. Molecular models domonstrate the presence of a large steric interaction between the H-3 protons on adjacent rings. This steric hindrance would be expected to cause an additional downfield shift of the H-3 peak position.

Instead of the 8 cps downfield, as expected, H-6 is found 56 cps upfield. This large shift can be ascribed to the geometric position of H-6. A molecular model of the chelate shows that each 6 proton is held closely over one of the aromatic rings on an adjacent ligand. Such protons, for example those in the metacyclophanes, are known to be shifted upfield, and the magnitudes of these shifts are often 60 to 120 cps.

Miller and Prince (30) reported NMR spectra, for chelates similar to $Ru(bipyr)_3Cl_2$. They studied complexes of 1,10-phenanthroline, III, with various metal ions, including ruthenium.

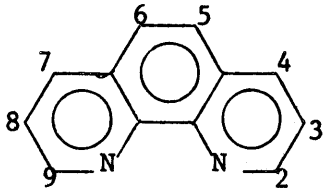

III

Their results and conclusions provide excellent background material for the 2,2'-bipyridine system. Proton 2 and 9 in the 1,10-phenanthroline ligand have the same upfield shift due to chelation as proton 6 in $Ru(bipyr)_3Cl_2$. In fact the magnitude of the change is similar: 58 cps vs. 56 cps for 2,2'-bipyridine. Miller and Prince explained

the shift as resulting from a metal-non-bonded hydrogen interaction such as the type observed in directly bonded transition-metal hydrides. In support of this, they found the magnitude of the upfield shift increased as the size of the central metal ion decreased i.e., as the M-N distance decreases. However, their results are equally compatible with the idea of proton 2 and 9 being shielded by the aromatic rings of the adjacent ligands. This is corroborated by models of the chelate and the numerous examples of aromatic shielding in the literature.

Miller and Prince did their earliest work in aqueous solutions. To gain more information on the large upfield shift of protons 2 and 9, they used a DMSO solvent. They found small changes in protons 3 to 8, and almost no change in position of protons 2 and 9. This is understandable since protons 2 and 9 are buried in the aromatic system of the adjacent ligand where solvent molecules cannot penetrate.

When Miller and Prince examined the NMR spectrum for the neutral complex $Ru(phen)_2(CN)_2$ in DMSO, they observed that the frequency of the 2 and 9 protons was similar to that of the charged ruthenium(II) complex, while the other proton frequencies resembled those of the free ligand. This suggested that the upfield shift is not strongly dependent on the charge of the complex.

5. Analytical Applications

Once the NMR spectrum of the chelate has been properly analyzed, it is possible to state with absolute certainty that the

ligands are 2,2'-bipyridine.

If an equimolar solution of the chelate and 2,2'-bipyridine is prepared and a spectrum recorded it is possible to determine the number of ligands in the chelate. For example, the chelate 3 proton has peaks at 551 and 543 cps while the free ligand proton has peaks at 530 and 526 cps. This allows integration of the area under the peaks. The integration, for this example, gave a value of 3:1 for the chelate: ligand ratios.

Purity can be checked to a certain extent. In the above example the free ligand 6 proton peak occurs in a region of the chelate spectrum that has no peaks. An examination of this area under high sensitivity indicated that there must be less than 1% free ligand in the chelate preparation.

The geometry of the chelate can also be ascertained by NMR. For the tris-complexes of ruthenium this is not exceedingly important but the bis-complexes should be checked since there are different possibilities for their steric arrangement.

Other information is also available. For example, the NMR spectrum of bis-(2,2',2''-terpyridine) ruthenium dichloride had two waters shifted downfield from their normal spectral positions. All indications point to the ligands only being bonded on two of the nitrogens per terpyridine, the other ruthenium coordination sites being occupied by water.

BIBLIOGRAPHY

1. H. O. Albrecht, Z. Phys. Chem., 136, 321 (1928)

2. R. G. Bennett and P. J. McCartin, J. Chem. Phys., 44, 1969 (1966)

3. W. W. Brandt, F. P. Dwyer and E. G. Gyarfas, Chem. Rev., 54, 959 (1954)

4. J. N. Butler, "Ionic Equilibrium", Addison-Wesley, Reading, Mass. (1964), pages 216-217

5. J. W. Cahn and R. E. Powell, J. Amer. Chem Soc., 76, 2568 (1954)

6. B. Chance, R. Eisenhardt, Q. Gibson, K. Lonberg-Holm, "Rapid Mixing and Sampling Techniques in Biochemistry," Academic Press, New York (1964)

7. E. A. Chandross and F. I. Sonntag, J. Amer. Chem. Soc., 86, 3179 (1964)

8. E. A. Chandross and F. I. Sonntag, J. Amer. Chem. Soc. 88, 1089 (1966)

9. G. A. Crosby, J. Chem. Phys., 64, 160 (1967)

10. G. A. Crosby, W. G. Perkins and D. M. Klassen, J. Chem. Phys., 43, 1498 (1965)

11. J. N. Demas and G. A. Crosby, J. Mol. Spectrosc., 26, 72 (1968)

12. D. F. Detar and C. E. Detar, J. Phys. Chem., 70, 3842 (1966).

13. E.M.I. Photomultiplier Tube Catalogue, 20M/6-67/PMT Issue 1, Pg. 37

14. K. Glen and P. Petsch, Angew. Chem., 48,57 (1935)

15. K. D. Gundermann, Angew. Chem. Intern. Ed. Engl., 4, 566 (1935)

16. D. Henrie and D. M. Hercules, unpublished studies, M.I.T., 1968

17. D. M. Hercules, Anal.Chem., 38, 29A(1966)

18. D. M. Hercules, Science, 145, 808 (1964)

19. D. M. Hercules, R. C. Lansbury and D. K. Roe, J. Amer. Chem. Soc., 88, 4578 (1966)

20. W. C. E. Higginson and D. Sutton, J. Chem. Soc., 1380 (1953)

21. W.C.E. Higginson and D. Sutton, J. Chem Soc., 1402 (1953)

22. W.C.E. Higginson and Wright, J. Chem. Soc., 1551 (1955)

23. C. K. Jørgenson, Acta. Chem. Scand., 11, 166 (1957)

24. D. Judd, J. Research Nat. Bur. Stand., 44, RP2053 (1950)

25. D. M. Klassen and G. A. Crosby, J. Chem. Phys., 48, 1853 (1968)

26. F. A. Kramer and R. West, J. Phys. Chem, 69, 673 (1965)

27. W. M. Latimer, "Oxidation Potentials", 2 ed., Prentice-Hall Inc., Englewood Cliffs, New Jersey,(1952)

28. E. C. Lim. J. D. Laposa and J.M.H. Yu, J. Mol. Spectrosc., 19, 412 (1966)

29. F. McCapra, Quar. Rev., 485 (1966)

30. J. D. Miller and R. H. Prince, J. Chem. Soc., 3185(1965)

31. K. Nakamato and P. J. McCarthy, "Spectroscopy and Structure of Metal Chelate Compounds," John Wiley and Sons, New York, New York (1968)

32. W. E. Ohnesorge in "Fluorescence and Phosphorescence Analysis," D. M. Hercules, ed., Interscience, New York, New York (1966), Chapter 4

33. R. A. Palmer and T. S. Piper, Inorg. Chem., 5, 864 (1966)

34 J. P. Paris, Ph.D. Thesis, Purdue University, Lafayette, Ind., 1960

35. J. P. Paris and W. W. Brandt, J. Am. Chem. Soc., 81, 5001 (1959)

36. C. Parker and W. Rees, Analyst, 85, 587(1960)

37. G. B. Porter and H. L Schläfer, Ber. Bunsenges. Physik. Chem., 68, 316 (1964)

38. B. Radziszewski, Ber., 10, 70, 321 (1877)

39. D. R. Roseinsky, J. Chem. Soc., 4685 (1957)

40. A. A. Schilt and R. C. Taylor, J Inong. and Nuclear Chem., 9, 211 (1959)

41. A. A. Schilt, Anal. Chem., 35, 1599 (1963)

42. H. Scott, P. L. Knonick, P. Chairge and M. M. Labes, J. Phys. Chem., 69, 1740 (1965)

43. I. C. Smith and W. G. Schneider, Can. J. Chem., 39, 1158 (1961)

44. K. S. V. Southanam and A. J. Bard, J. Amer. Chem. Soc., 87, 139 (1965)

45. R. Stair, W. Schneider and J. Jackson, Applied Optics, 2, 1151 (1963)

46. H. Suzuki, "Electronic Absorption Spectra and Geometry of Organic Molecules," Academic Press Inc. New York, New York (1967), pp. 58-59

47. F. Teale and G. Weber, Biochemical Journal, 65, 476 (1957)

48. G. K. Turner, personal communication.

49. H. Veening and W. W. Brandt, Anal. Chem., 32, 1426 (1960)

50. R. E. Visco, E. A. Chandross and F. I. Sonntag, Presented at the Boston Meeting of the Electrochemical Society, May (1968), Abstract 205.

51. R. E. Visco and E. A. Chandross, J. Amer. Soc., 86, 5350 (1964)

52. H. Vollman, H. Becker, M. Correll and H. Streeck, Annalen der Chemie, 531, 1 (1937)

53. G. Weber and F. Teale, Trans. Far. Soc., 53, 646 (1957)

54. G. Weber and F. Teale, Trans. Far. Soc. 54, 640 (1958)

55. K. R. Wunschel and W. E. Ohnesorge, J. Amer. Chem. Soc., 89, 2777 (1967)

BIOGRAPHICAL NOTE

The author was born January 13, 1943, in Lewisburg, Pennsylvania. He attended public schools in Sunbury, Pennsylvania, graduating from Sunbury Area High School in 1960. He entered Juniata College, Huntingdon, Pennsylvania in September 1960, from which he received the B.S. degree in Chemistry in June 1964.

After graduation from Juniata College, he was employed by Eastman Kodak Inc. Rochester, New York, during the summer of 1964. He entered M.I.T. in September 1964, as a candidate for the degree of Doctor of Philosophy.

While at M.I.T. he married the former Marsha Kay Jones.

The author is a member of the American Chemical Society.